EASTERN EQUATORIAL PACIFIC OCEAN SEDIMENTATION: INVESTIGATING CONSTANT FLUX PROXIES

A Dissertation

by

AJAY KUMAR SINGH

Submitted to the Office of Graduate Studies of
Texas A&M University
in partial fulfillment of the requirements for the degree of

DOCTOR OF PHILOSOPHY

Approved by:

Chair of Committee,	Franco Marcantonio
Committee Members,	Mitchell Lyle
	Debbie Thomas
	Matthew Schmidt
	Brent Miller
Head of Department,	Rick Giardino

December 2012

Major Subject: Geology

ABSTRACT

Age-model derived sediment mass accumulation rates (MARs) are consistently higher than ^{230}Th-normalized MARs in the Equatorial Pacific Ocean during the past 25 ka. The offset, being highest in the Panama Basin, suggests sediment redistribution in this region is prominent. I test the hypothesis that downslope transport of sediments from topographically highs that surround the Panama Basin is the cause of higher-than-expected xs^{230}Th inventories in the deeper parts of the basin. There is little difference in xs^{230}Th inventories between the highest and lowest reaches of the basin suggesting that the topographic highs did not serve as a source of xs^{230}Th. A spatial analysis suggests that there may be an enhanced scavenging of xs^{230}Th closest to the equator in productive waters.

To examine whether lateral mixing of productive equatorial waters with adjacent waters delivers xs^{230}Th to the Panama Basin, I measured dissolved ^{230}Th in eight deep-water casts within the Guatemala, Panama, and Peru Basins along a meridional transect at ~86°W. Below 1000 m, the Panama Basin shows the highest deficit (~50%) of ^{230}Th in deep waters assuming a reversible exchange of ^{230}Th between dissolved and sinking particulate matter. Peru Basin waters have a larger range of dissolved ^{230}Th concentrations (7.9-16.5 fg/kg) than that within Panama Basin waters (5.7-7.1 fg/kg). There is a progressive decrease, suggesting advection, in average dissolved deep-water (>1000 m) ^{230}Th concentrations from the southernmost sites in the Peru Basin toward the

Panama Basin. My calculations suggest that advected ^{230}Th is between 15-30% of the total ^{230}Th being produced within waters of the Panama Basin itself.

In the Panama Basin, the averaged biogenic barium and opal MARs suggest that productivity was greater during the Holocene (0-13000 years) than that during the last glacial (13000-25000 years) suggesting higher productivity during the Holocene. U_{auth}, however, is higher in sediments deposited during the last glacial than in those deposited during the Holocene, suggesting that low bottom water oxygen contents rather than respiration of organic matter drives U_{auth} enrichment. This oxygen depletion during the last glacial suggests that bottom waters were enriched in respired carbon, which, in turn, could be a driver of lower glacial atmosphere pCO_2 values.

DEDICATION

I dedicate my thesis to my family for their unwavering support throughout the course of this study.

ACKNOWLEDGEMENTS

I am pleased to acknowledge the help and support I received from numerous people during my doctoral studies at Texas A&M University (TAMU). First of all, I would like to thank my advisor Dr. Franco Marcantonio for his enthusiasm and support during the course of my research. His contagious laughter got me through times of stress. I would also like to thank my committee members, Dr. Lyle, Dr. Thomas, Dr. Miller, and Dr. Schmidt, for their guidance and support throughout the course of my graduate student life at TAMU. I also thank Annette, Anna and Julia for their help with opal and carbonate analyses. I would like to thank Luz Romero for keeping the ICP-MS running even after I would clog it with my sticky thorium. I am grateful to the science party and crewmembers for making the cruise enjoyable and successful. I further thank Precious for her help with the boring part, siphoning of seawater, of my lab work.

I also thank my aggie friends, colleagues, department faculty and staff for making my time at TAMU such a great experience. Occasional breaks in the form of new student parties, Christmas parties, American-Italian feasts at Franco's house, fall parties at Debbie/Brent's house and so on were always refreshing.

Finally, I would like to thank my parents and siblings for their steady support and encouragement.

TABLE OF CONTENTS

Page

LIST OF FIGURES

LIST OF TABLES

CHAPTER I
INTRODUCTION TO THE CONSTANT FLUX PROXY AND RESEARCH MOTIVATIONS

1.1 Introduction

Marine sediments provide archives of physical, biological and chemical processes that respond to, or are a response of, climate changes. My research efforts have been focused on understanding marine sedimentation and its relationship with continental aridity, riverine fluxes, ocean circulation, biological productivity and climate change. My doctoral research involves the completion of three different but related projects dealing with aspects of pelagic sedimentation, biological productivity, terrigenous inputs and redox conditions in the eastern tropical Pacific Ocean. Two of my doctoral research projects tackle a long–standing "sediment focusing controversy" in the Panama basin using ^{230}Th as a constant flux proxy (CFP).

Constant flux proxies (such as ^{230}Th, ^{3}He) are useful tool for studying particle fluxes because their fluxes to the ocean floor over time is known, and by comparing (normalizing) their *in-situ* fluxes one can quantitatively evaluate temporal fluxes of other sediments to the ocean (Bacon, 1984; Francois et al., 2004; Henderson and Anderson, 1999). The controversy has arisen because of inconsistencies found between CFP derived sediment mass accumulation rates (MARs) and age-model derived MARs. The age-model MARs are estimated by multiplying linear sedimentation rate, which is based on dated (oxygen-isotope- or radiocarbon-derived) horizons, with dry bulk density. The age-model derived MARs are consistently higher than the ^{230}Th-normalized MARs in the Panama basin (Lyle et al., 1988; Lyle et al., 2005; Lyle et al., 2007). Proponents of the age-model method explain higher MARs by higher particle fluxes in the productive surface waters off of the Peruvian coast. They further suggest that higher particle fluxes will scavenge more ^{230}Th out of water column and would cause MARs to be

underestimated (Lyle et al., 2005; Lyle et al., 2007). Contrarily, the proponents of the ^{230}Th-normalizing method suggest that the more-than-expected ^{230}Th (denoted as focusing factor) found ubiquitously in the Panama Basin is due to sediment redistribution (focusing) at the seafloor (Francois et al., 2007; Kienast et al., 2007). Notably most of the sediments analyzed in these previous studies were taken from deeper parts of the basin.

For the first project (Chapter 2), I measured ^{230}Th inventory in shallower sediments sampled near the tops of ridges to see if the *downslope transport of sediments from topographic highs* was responsible for the source of higher-than-expected ^{230}Th inventory in the deeper parts of Panama Basin (Kienast et al., 2007). ^{230}Th inventories from shallow depths were similar to those from deeper depths suggesting that transport of sediments cannot explain the higher inventories of ^{230}Th. Furthermore, the highest inventories of ^{230}Th found in equatorial sediment cores suggest that scavenging and lateral mixing of water masses near equator is a possibility (Broecker, 2008). To test the possibility of enhanced scavenging and the reasons behind higher-than-expected ^{230}Th in Panama basin sediments, it is crucial to understand ^{230}Th systematics in the water column, aspects of which comprise the second chapter (Chapter 3) of my Ph.D. thesis.

For this work, we performed oceanographic surveys (October 17 and November 14, 2010) to collect seawater samples in the eastern tropical Pacific. Since highly reactive ^{230}Th is produced at a uniform rate and is reversibly exchanged between particulate and dissolved phases as particles settle in the water column, it should always display a linear increase with increasing depth. Measured tropical Pacific dissolved ^{230}Th concentrations did not show the hypothesized linear increase. Two important patterns were noted in the dissolved ^{230}Th data: 1) The Panama basin shows the highest deficit (~50%) of dissolved ^{230}Th assuming a linear increase with depth and similar concentrations between stations and 2) a progressive decrease in dissolved ^{230}Th in Peru basin as one move from S to N towards the Panama basin. This decrease suggests that enhanced scavenging within, and

advection of dissolved ^{230}Th towards, the Panama basin is happening. Resuspension of particulate Mn (scavenger of ^{230}Th), most enriched in the top fluff layer of Panama basin sediments, seems to be one potential cause enhanced scavenging of ^{230}Th. Also, calculations based on influxes of Peruvian waters into the Panama Basin suggest that the amount of higher-than-expected ^{230}Th that is being transported is only 30% greater than that which is being produced within Panama Basin waters. This means that MARs may be underestimated by 30% and, consequently, that focusing factors of no greater than 1.3 can be explained by excess scavenging of ^{230}Th in the Panama Basin. Hence, focusing factors greater than 1.3 are real and suggest that syndepositional sediment redistribution in the Panama Basin is likely.

The research objective for Chapter 4 was to evaluate the paleoproductivity and paleoredox conditions in the Panama Basin for the last 25ka. There is growing evidence that the changes in glacial-interglacial CO_2 variation in the atmosphere were related to changes in the nutrient reservoir in the deep ocean and is referred as the "nutrient deepening hypothesis (Boyle, 1988)" or "respired carbon deepening hypothesis (Jaccard et al., 2009)". Changes in water-column nutrient gradient on glacial-interglacial times is important because it suggests the potential for a greater storage of respired CO_2 in the deep ocean reservoir along with a greater withdrawal of atmospheric CO_2 during glacial times. To test the abovementioned hypothesis, I measured two paleoproductivity proxies, i.e., biogenic barium (BioBa) and opal concentrations to better constrain the export of organic carbon from the surface ocean. I also measured authigenic uranium (U_{auth}) concentrations to constrain the redox state of sediments retrieved from 9 cores in the eastern tropical Pacific. Using U_{auth} along with paleoproductivity estimates can help decouple the effect of respiration causing low bottom-water oxygen versus a water mass with lower bottom water oxygen contents. My results show that the redox sensitive U_{auth} concentrations in sediments were greater during the last glacial (compared to the Holocene) with no accompanying change in BioBa and opal fluxes. This suggests that the changes in U_{auth} were not related to changes in biological productivity (and the

resulting rain of organic matter to the seafloor) suggesting that deep waters of the eastern tropical Pacific Ocean were less oxygenated during the last glacial maxima than during the Holocene.

CHAPTER II
SEDIMENT FOCUSING IN THE PANAMA BASIN, EASTERN EQUATORIAL PACIFIC OCEAN*

2.1. Introduction

Essentially all sediments that reach the pelagic ocean floor are either derived from the continents through weathering processes or formed as a result of biological productivity in surface water. Contemporaneous climatic conditions largely affect the processes and mechanisms that bring these sediments to the ocean floor. For example, sediment intervals that record higher biogenic fluxes are often interpreted as being deposited at a time during which export production to the seafloor was increased. Similarly, intervals during which lithogenic particle fluxes are high can represent an intensified transport of continental material via rivers (if close to a continental margin) and/or wind. Thus, reconstruction of particle fluxes from oceanic sedimentary archives can broaden our understanding of past climate conditions.

Historically and to the present, sedimentary mass accumulation rates (MARs) have been estimated by multiplying the linear sedimentation rate (LSR), estimated using dated horizons (oxygen-isotope- or radiocarbon-derived), with sediment dry bulk density. This method measures the amount of sediment preserved at the sea floor but does not discriminate between vertically falling particles and those redistributed by a variety of horizontal advection processes. The $xs^{230}Th$ constant-flux proxy (CFP) method of determining mass accumulation rates is thought to "see through" such sediment redistribution processes and is purported to measure the true vertical flux (Bacon, 1984; Francois et al., 2004). The idea behind this constant-flux proxy lies in the different geochemical behavior of thorium and uranium in the oceanic water column. In seawater, ^{230}Th is produced by the α-decay of ^{234}U. Unlike uranium, which has a constant seawater concentration, thorium is extremely particle reactive, and the decay product,

* Reprinted with permission from "Sediment focusing in the Panama Basin, Eastern Equatorial Pacific Ocean" by Ajay K. Singh, Franco Marcantonio, and Mitchell Lyle, 2011. *Earth and Planetary Science Letters,* 309 (1-2), 33-44, Copyright 2011 Elsevier.

^{230}Th, is rapidly scavenged onto sinking particles so that the flux of ^{230}Th to the ocean floor is identical to its rate of production in the water column (Bacon, 1984). Hence, MARs within an interval of sediment can be calculated by dividing the known production rate of ^{230}Th by the concentration of ^{230}Th within the same interval. Hence, the vertical flux of any component preserved in the sediment, F_i, can be calculated theoretically using the following equation:

$$F_i = \frac{(conc)_i * \beta * Z}{\left[xs\,^{230}Th_o\right]} \qquad [1]$$

in which $(conc)_i$ is the concentration of component i; β is the production rate of ^{230}Th in the water column (0.0267 dpm m^{-3} year^{-1}); Z is the water depth in m; and $[xs^{230}Th_o]$ is the measured sedimentary ^{230}Th activity corrected for decay, *in situ* production of ^{230}Th from authigenic ^{234}U, and detrital ^{230}Th. The elegance of equation 1 is that the derived sedimentary flux is, by definition, solely the vertical component of the preserved sedimentary flux. Furthermore, one can solve for the 'normalized' sedimentary flux by measuring the concentration of xs^{230}Th alone. The extent that such normalization works depends on how realistic the assumption is that the production of ^{230}Th in the water column is equal to the flux of the scavenged ^{230}Th to the underlying sediments (Bacon, 1984; Francois et al., 2004). If the postulated behavior of oceanic ^{230}Th is correct, an added benefit to the constant-flux proxy methodology is that syndepositional sediment redistribution can be quantified by integrating the xs^{230}Th inventory within an interval of sediment and comparing it to the integrated production of ^{230}Th in the overlying water column over the time of accumulation (Suman and Bacon, 1989). Indeed, the ratio of these two parameters has been defined by a physical parameter called the "focusing factor, (Ψ)" (Suman and Bacon, 1989). A Ψ value of one implies that sediment has not been redistributed at the studied site. A Ψ value greater than one implies sediment in excess of what has been delivered vertically has been advected by deep-sea horizontal advection (i.e., focusing) to the studied site, while a Ψ value less than one implies winnowing or removal of sediment from the studied site at the time of sediment deposition (Francois et al., 2004). Model studies have shown that 70% of the ocean floor

receives a ^{230}Th flux within 30% of its production in the water column (Henderson and Anderson, 1999; Siddall et al., 2008), implying a sensitivity of the xs^{230}Th profiling technique that is typically within +/- 30%. This estimate must be considered somewhat tentative given the reliance of this result on the assumption that isopycnal and vertical diffusion is a reasonable approximation of ocean mixing processes inherent in many ocean models (Siddall et al., 2008).

Although age-model-derived and xs^{230}Th-normalized MARs have been widely used in paleoceanographic research, in some cases the differently calculated MARs are significantly different, and, therefore, yield competing interpretations. Perhaps the best known of these discrepancies exists in the equatorial (west, central and east) Pacific Ocean (Broecker, 2008; Higgins et al., 1999; Francois et al., 2007; Kienast et al., 2007; Koutavas et al., 2002; Koutavas and Sachs, 2008; Kowsmann, 1973; Loubere et al., 2004; Lyle et al., 2005; Lyle et al., 2007 Marcantonio et al., 2001a; Marcantonio et al., 1996; Paytan et al., 1996; Thomas et al., 2000). Here, xs^{230}Th-derived focusing factors, suggest that horizontal sediment transport almost always is higher (sometimes several times higher) than the vertical flux. The highest focusing factors (as high as 5.5; Kienast et al., 2007) are observed during the last glacial in the eastern equatorial Pacific (EEP) Ocean in the Panama Basin.

In the Panama Basin, using age-model-derived MARs, many investigators have concluded that particle fluxes during the last glacial were as much as 100% higher than those during the Holocene, and are caused by enhanced primary productivity (Pedersen, 1983; Lyle, 1988; Lyle et al., 2002; Paytan et al., 1996). However, xs^{230}Th normalized MARs for sediments deposited during the last glacial suggest calcite fluxes that are 30-50% *lower* than those during the Holocene (Loubere et al., 2004). These authors contend that the higher glacial age-model-derived fluxes are due to sediment focusing processes in the Panama Basin. In addition, Kienast et al. (2007) reexamined several sites that were studied by others (Loubere et al., 2004; Lyle et al., 2005) in the Panama Basin and came

to a similar conclusion; namely, that xs^{230}Th-normalized MARs are lower and less variable than age-model-derived MARs, indicating varying degrees of sediment focusing.

Lyle et al. (2005) disagree with the interpretation that sediment focusing is widespread in the Panama Basin, and argue that xs^{230}Th normalization overestimates the degree to which sediment redistribution processes are occurring in the EEP. They reason that the observed larger-than-expected inventories of sedimentary xs^{230}Th in the EEP, that are in excess of those expected from a constant water column production rate of ^{230}Th, can be attributed to increased boundary scavenging at the surface due to increased productivity close to the equator, in agreement with an analysis by Broecker (2008). However, within an efficient (low resolution) ocean circulation model, Siddall et al. (2008) found that particle scavenging effects are not sufficient to explain the additional xs^{230}Th inventories measured in the Panama Basin. Using the Bern3D ocean model, they considered particle scavenging over a broad range of particle fluxes reaching up to 10 times higher than actual measurements in the equatorial Pacific region. Even at the highest end of this range of particle fluxes, the model by Siddall et al. (2008) suggests only a two-fold increase in the flux of ^{230}Th over the production of ^{230}Th in water column due to particle scavenging effects.

Kienast et al. (2007) propose that downslope transport of sediment from the east-west trending Carnegie Ridge, which forms the southern boundary of the Panama Basin, might explain the additional xs^{230}Th in sediments of the Panama Basin. In this study, we test this downslope transport hypothesis by measuring xs^{230}Th inventories of sediments deposited on the Cocos and Carnegie Ridges—regional topographic highs that surround the Panama Basin. In general, xs^{230}Th inventories in sediment from the tops of ridges suggest sediment focusing factors that are greater than 1 for both the Holocene and glacial sediments. More importantly, sediment xs^{230}Th inventories on the ridge tops are similar to those in the previously studied deeper cores (Kienast et al., 2007). If ridge tops

were the source of extra xs^{230}Th inventory in the basin, one would expect their focusing factors to be less than one and/or lower than those measured in the basin. We explore the potential causes for the larger-than-expected xs^{230}Th inventories throughout the Panama Basin, including the effects of particle scavenging on ^{230}Th fluxes to the seafloor.

2.2 Methodology

2.2.1 Site selection and sampling strategies

We chose sites to test whether downslope transport from surrounding-ridge and within-basin topographic highs can explain the higher inventories of sedimentary xs^{230}Th in the Panama Basin as suggested by Kienast et al. (2007). Cores were retrieved from the Carnegie and Cocos Ridges that ranged in depth from 712 meters to 2230 meters (Figure 2.1; Table 2.1). We also selected two deeper cores (TR 163-22, just west of the Galapagos platform, and Y69-106P, just south of the Cocos Ridge) to add to the literature data collected from sites in the central basin or from the foot of the Carnegie Ridge. Our philosophy in approaching the sampling of cores here differs from that of previous studies in that we have sampled intervals at a lower resolution in order to obtain a broader spatial sampling of the sedimentary inventory throughout the Panama Basin (a total of 9 cores have been sampled). The consistency between average sediment focusing factors calculated here and those calculated by Kienast et al. (2007) at nearby sites (see Figure 2.1) shows that we are justified in our sampling methodology.

Selected cores, in addition to those studied previously (Kienast et al., 2007; Loubere et al., 2004) at depths greater than 2300 meters, provide for a more complete assessment of the xs^{230}Th inventory in the Panama Basin. Cores in this study were obtained from the core repositories of Lamont-Doherty Earth Observatory, Oregon State University and University of Rhode Island. Six or seven sediment intervals spanning the past 25 ka were sampled from each core. Sample selection for the Holocene and the last glacial was

based on published age models (Benway et al., 2006; Kienast et al., 2007; Koutavas and Lynch-Steiglitz, 2003; Martinez et al., 2003; Lea et al., 2006; Pisias and Mix, 1997) (Table 1). In addition to age models for each core, we also need information on the dry bulk density (DBD) in order to calculate average MARs and focusing factors. DBDs for cores V19-27 and Y69-106P were estimated based on the $CaCO_3$ content in Lyle et al. (2002). For cores RC8-102 and MV0005A-27JC, DBDs were estimated from $CaCO_3$ concentrations in Ruddiman et al. (1992) and Kienast et al. (2007) using the equation in Snoeckx and Rea (1994) (DBD (g cm^{-3}) = 1/(3.6–0.0279 × %CaCO3). DBD for core TR163-22 was estimated in Lea et al. (2006). For cores TR163-11, TR163-33 and ME0005A-43JC, average DBDs are estimated using carbonate content of nearby cores ODP 1241, ME0005A-27JC and ODP 1242, respectively (Mix et al., 2003 [ODP Leg 202 Scientific Results]). For core TR163-38 we averaged the DBD of three nearby cores (TR163-33, V19-27 and ME0005A-27JC) with similar sedimentary lithologies and histories. The average DBD is the least constrained for core V21-29, for which we assumed an average value of 0.6 g cm^{-3}. In order to compare our dataset with that of Kienast et al. (2007) and Loubere et al. (2004), we averaged our xs^{230}Th-derived MARs and age-model-derived MARs similarly for two time slices, one for a specified interval covering the entire Holocene (0-13 ka), and one for a specified interval in the last glacial (13-25 ka). We used broad time intervals in order to reduce errors in sedimentation rates caused by errors from assigned ages.

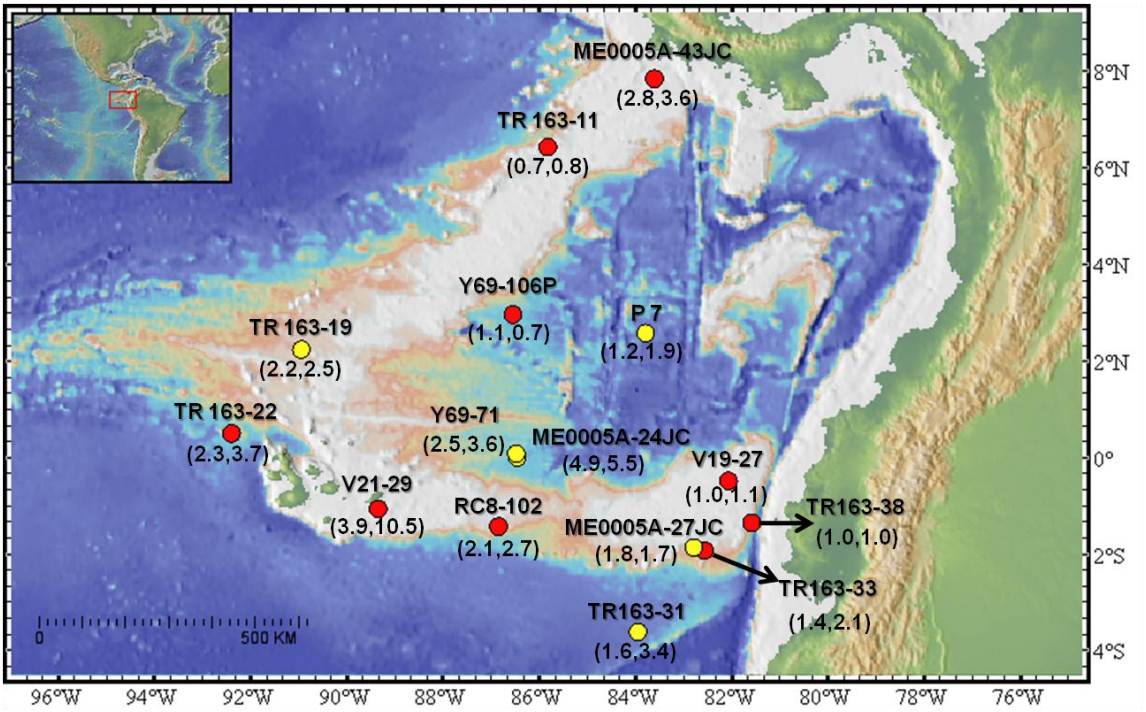

Figure 2.1. Map showing location of studied cores in the Panama Basin. Red circles represent cores analyzed here and yellow circles represent cores studied previously (Kienast et al., 2007; Loubere et al., 2004). Focusing factors are bracketed next to each core identification (first number in bracket represents Holocene (0-13 ka) focusing factor and second number represents focusing factor for sediments deposited during the last glacial (13-25 ka). This map has been generated using GeoMapApp software available at http://www.geomapapp.org.

Table 2.1. ^{230}Th-derived Mass Accumulation Rates (MARs), age-model-derived MARs, and focusing factors in Panama Basin sediments during the Holocene and glacial. Equatorial cores (within ±2º N and S) are shown in bold letters (other cores are non-equatorial). Margin cores are shown in light shade of grey (all other cores are non-margin cores), and deep cores are located at water depths greater than 2300 meters (see text for discussion). Subdivision of these cores into equatorial and non-equatorial, margin and non-margin, and, shallow and deep cores are mutually inclusive. All MAR values have a common unit ($g \cdot cm^{-2} \cdot ka^{-1}$). Data from Kienast et al (2007) are italicized.

				^{230}Th derived MAR		Age-model MAR		Focusing factor		
Core ID	Latitude	Longitude	Water Depth (m)	Holocene	Glacial	Holocene	Glacial	Holocene	Glacial	Age model reference
V19-27	**-0.47**	**-82.07**	**1373**	**2.4**	**1.8**	**2.3**	**2.0**	**1.0**	**1.1**	**Koutavas and Lynch-Stieglitz 2003**
RC8-102	**-1.42**	**-86.85**	**2180**	**1.4**	**2.0**	**3.0**	**5.7**	**2.1**	**2.7**	**Koutavas and Lynch-Stieglitz 2003**
TR163-11	6.45	-85.82	1950	1.4	1.0	0.7	0.8	0.7	0.8	Martinez et al., 2003
V21-29	**-1.05**	**-89.35**	**712**	**1.1**	**1.1**	**4.1**	**11.7**	**3.9**	**10.5**	**Koutavas and Lynch-Stieglitz 2003**
ME0005A-43JC	7.86	-83.61	1368	2.1	2.3	5.7	5.8	2.8	3.6	Benway 2006
TR163-22	**0.52**	**-92.40**	**2830**	**1.3**	**1.4**	**2.9**	**5.2**	**2.3**	**3.7**	**Lea et al., 2006**
Y69-106P	2.98	-86.55	2870	1.2	1.4	1.4	0.9	1.1	0.7	Pisias and Mix 1997
TR163-38	**-1.34**	**-81.58**	**2200**	**2.8**	**2.9**	**2.7**	**2.8**	**1.0**	**1.0**	**Martinez et al., 2003**
TR163-33	**-1.91**	**-82.57**	**2230**	**1.9**	**2.2**	**2.7**	**4.5**	**1.4**	**2.1**	**Martinez et al., 2003**
ME0005-24JC	**0.02**	**-86.46**	**2941**	***1.4***	***1.5***	***8.5***	***8.0***	***4.9***	***5.5***	**Kienast et al., 2007**
Y69-71	**0.10**	**-86.48**	**2740**	***1.3***	***1.5***	***3.8***	***5.3***	***2.5***	***3.6***	**Kienast et al., 2007**
P7	2.60	-83.79	3085	*1.4*	*1.5*	*1.6*	*2.8*	*1.2*	*1.9*	Kienast et al., 2007
ME0005-27JC	**-1.85**	**-82.79**	**2203**	***1.6***	***1.8***	***2.9***	***3.0***	***1.8***	***1.7***	**Kienast et al., 2007**
TR163-19	2.26	-90.95	2348	*1.1*	*1.4*	*2.4*	*3.5*	*2.2*	*2.5*	Kienast et al., 2007
TR163-31	-3.60	-83.95	3209	*1.6*	*1.9*	*2.4*	*7.0*	*1.6*	*3.4*	Kienast et al., 2007

2.2.2 Radionuclide isotope measurement

Radionuclide measurements followed the procedures described in Pourmand et al. (2004). Approximately 0.3-0.5 gram of dried and homogenized sediment was spiked with known amounts of ^{236}U and ^{229}Th (spikes used for isotope dilution analysis of uranium and thorium isotopes). Sample and spike mixtures were digested using HCl, HNO_3, $HClO_4$ and HF acids. After complete sediment digestion Th and U were separated and purified from the digested solution using ion exchange chromatography. Uranium and thorium isotope ratios were measured on an *Element XR* magnetic sector ICP-MS at Texas A&M University (Table 2.2). Th and U were analyzed separately to avoid isotopic interferences during mass spectrometer measurements. ^{238}U abundance sensitivity at lower masses (^{234}U, ^{235}U and ^{236}U) was corrected assuming an exponential decrease in ^{238}U counts toward lower masses. In most cases the ^{238}U abundance sensitivity was about 1.5 ppm at 3 amu and 0.6 ppm at 4 amu. Similarly, the ^{232}Th abundance was approximately 3.2 ppm at 2 amu and 1.3 ppm at 3 amu. Mass bias was determined by measuring the $^{238}U/^{235}U$ in each sample in the case of uranium analyses, and by bracketing thorium analyses with measurements of the $^{238}U/^{235}U$ in the U500 standard and assuming similar fractionation between uranium and thorium. Mass bias corrections ranged from about 0.1 to 0.3‰/amu.

In order to determine the true unsupported sedimentary $^{230}Th_{xs}$, measured concentrations of ^{230}Th (Table 2) were corrected for detrital ^{230}Th and *in situ* growth of ^{230}Th from authigenic ^{234}U using equation 2.

$$^{230}Th_{xs} = {}^{230}Th_{meas} - \left[\left(\frac{^{238}U}{^{232}Th}\right)_{det} \times {}^{232}Th_{meas}\right] - \left[\left\{{}^{238}U_{meas} - \left(\frac{^{238}U}{^{232}Th}\right)_{det} \times {}^{232}Th_{meas}\right\} \times \left\{\left(1 - e^{-\lambda_{230}t}\right) + \frac{\lambda_{230}}{\lambda_{230} - \lambda_{234}} \times \left(e^{-\lambda_{234}t} - e^{-\lambda_{230}t}\right) \times \left(\left(\frac{^{234}U}{^{238}U}\right)_{sw} - 1\right)\right\}\right] \quad [2]$$

The subscripts xs, meas, det and sw refer to excess (unsupported), measured, detrital and seawater, respectively. λ_{230} and λ_{234} are the decay constants for ^{230}Th and ^{234}U,

respectively. For the detrital $^{238}U/^{232}Th$ activity ratio, we assumed a ratio of 0.7, which is the best estimate for the U/Th activity ratio of detrital material delivered to the Pacific Ocean (Henderson and Anderson, 2003). All calculations used a seawater $^{234}U/^{238}U$ activity of 1.146 (Robinson et al., 2004). In all cases, except for Holocene intervals in cores closest to the margin (see our definition of "margin cores" below), the detrital ^{230}Th amounted to less than 5% of the total measured ^{230}Th. Only for one of the Holocene samples of one margin core was the correction significant (~50% in sample from 45-46 cm in core V19-27). Authigenically-produced ^{230}Th made up between 20-30% of the measured ^{230}Th in all samples, similar to the amount found in sediments studied by Kienast et al. (2007). Finally, $xs^{230}Th$ activities were corrected for decay since time of sedimentary deposition.

2.2.3. Replicates and blanks

One quadruplicate and three replicates were run (Table 3). The average external reproducibility was 12.4% for total uranium concentration, 2.6% for ^{230}Th concentration and 2.1% for ^{232}Th concentration. The poor average reproducibility for uranium was due to the uranium reproducibility of one sediment sample from core V21-29. This one sample had an average external reproducibility of 42.8%. We are uncertain as to why the uranium reproducibility of this one sample is so poor. Not including the uranium reproducibility results for core V21-29 leads to an average uranium reproducibility of about 2.2%, similar to the thorium reproducibility. For samples that have been replicated, the replicate averages are displayed in Table 3. Our thorium and uranium blanks consistently make up less than 1% of analyte, and therefore no blank corrections were necessary.

Table 2.2. Uranium, thorium results for Panama Basin cores (see Figure 2.1 for location)

Cores	Depth (cm)	Years (a)	^{238}U (dpm/g)	$xs^{230}Th_o$ (dpm/g)	^{232}Th (dpm/g)
V19-27	**Water depth = 1373m**		**Latitude = -0.46**		**Longitude= -82**
	35.5	4500	3.66	1.65	1.08
	45.5	5500	1.58	1.17	1.73
	64.5	10091	1.48	1.98	0.59
	84.5	15218	2.23	1.94	0.23
	94.5	17389	2.65	1.94	0.2
	114.5	22000	3.82	2.19	0.22
RC8-102	**Water depth = 2180m**		**Latitude = -1.4**		**Longitude= -86.8**
	2	5600	0.73	4.22	0.1
	15	9050	5.14	3.85	0.1
	45	15500	4.65	2.04	0.05
	60	17850	2.53	3.19	0.09
	75	19800	2.73	3.3	0.09
	105	23800	5.93	2.43	0.09
TR163-11	**Water depth = 1950m**		**Latitude = 6.4**		**Longitude= -85.8**
	11	4900	1.83	5.11	0.28
	16	9000	2.59	5.21	0.31
	22	13200	3.25	4.67	0.31
	28	16200	4.92	5.25	0.28
	33	18830	5	4.62	0.27
	39	25340	3.93	4.85	0.26
V21-29	**Water depth = 720m**		**Latitude = -1.0**		**Longitude= -89.3**
	19	3933	2.17	1.77	0.04
	57	9394	3.2	1.8	0.05
	76	12269	3.44	1.71	0.05
	95	14856	7.06	1.51	0.05
	114	16146	4.96	1.52	0.04
	133	16808	4.98	2.02	0.05
ME0005A-43JC	**Water depth = 1368m**		**Latitude = 7.8**		**Longitude= -83.6**
	3	857	4.52	1.92	0.4
	43	6808	5.01	1.82	0.38
	83	10710	4.53	1.48	0.32
	123	14726	5.57	1.62	0.37
	163	18600	4.35	1.8	0.37
	206	21920	3.91	1.37	0.32

Table 2.2. *Continued.*

Cores	Depth (cm)	Years (a)	^{238}U (dpm/g)	$xs^{230}Th_o$ (dpm/g)	^{232}Th (dpm/g)
TR163-22	**Water depth = 2830m**		**Latitude = 0.5**		**Longitude= -92.4**
	75	10600	3.69	5.29	0.09
	112	14500	3.72	5.1	0.11
	150	18200	5.01	5.55	0.15
	187	21800	4.58	5.29	0.2
	225	25300	3.77	5.27	0.17
Y69-106P	**Water depth = 2870m**		**Latitude = 2.9**		**Longitude= -86.5**
	2	4456	1.01	6.52	0.17
	11	7861	2.89	5.73	0.19
	20	11876	3.62	6.24	0.26
	35	20783	2.51	4.57	0.2
	44	26127	3.15	6.14	0.23
TR163-38	**Water depth = 2200m**		**Latitude = -1.3**		**Longitude= -81.5**
	19	4560	2.76	2.07	0.68
	38	8510	3.39	1.82	0.9
	57	10910	6.43	2.48	0.5
	76	13730	6.6	2.11	0.48
	95	16500	7.32	1.91	0.59
	114	19000	7.56	1.85	0.47
	133	22750	8.74	2.25	0.56
TR163-33	**Water depth = 2230m**		**Latitude = -1.9**		**Longitude= -82.5**
	30	5580	3.78	3.48	0.38
	45	8410	3.47	3.13	0.29
	60	10900	3.22	2.69	0.25
	75	19700	3.87	2.72	0.3
	90	21200	4.13	2.67	0.33

Table 2.3. Uranium, thorium isotopes reproducibility results (STDev represents one standard deviation from the mean, %rsd represents the relative standard deviation in %).

Core ID	Depth (cm)	[^{235}U] (dpm/g)	[^{238}U] (dpm/g)	[^{230}Th] (dpm/g)	[^{232}Th] (dpm/g)
V21-29	76	0.21	4.52	2.16	0.04
	76	0.29	6.28	2.22	0.05
	76	0.43	9.40	2.27	0.05
	76	0.17	3.62	2.00	0.05
	Average=	0.27	5.95	2.16	0.05
	STDev=	0.12	2.55	0.12	0.001
	%rsd=	42.84	42.84	5.51	2.80
TR163-33	30	0.17	3.78	3.77	0.38
	30	0.19	4.04	3.93	0.39
	30	0.18	3.86	3.83	0.40
	Average=	0.18	3.89	3.84	0.39
	STDev=	0.01	0.13	0.08	0.01
	%rsd=	3.41	3.43	2.20	2.63
ME0005A-43JC	3	0.19	4.16	No data	No data
	3	0.18	4.00	2.17	0.39
	3	0.19	4.09	2.12	0.38
	Average=	0.19	4.08	2.14	0.38
	STDev=	0.004	0.08	0.03	0.01
	%rsd=	1.91	1.91	1.41	1.72
ME0005A-43JC	123	0.25	5.53	2.37	0.37
	123	0.25	5.41	2.37	0.38
	123	0.26	5.55	2.42	0.37
	Average=	0.25	5.50	2.38	0.38
	STDev=	0.004	0.08	0.03	0.005
	%rsd=	1.42	1.42	1.31	1.27

2.2.4. Core chronologies

Focusing factors are the ratio of the inventory of sedimentary $^{230}Th_{xs}$ averaged over some depth interval to its production in the overlying water column. The greatest uncertainty in the focusing factor is caused by inaccuracies in the age model (Francois et al., 2004; Kienast et al., 2007). We tried to avoid age model problems in our calculations by choosing well-constrained, best available age models for our cores, and to average the data over longer time spans. Age models for cores V19-27, RC8-120 and V21-29 are based on oxygen isotope records of planktonic foraminfera (*G. sacculifer* and *G. ruber*) and 10 planktonic radiocarbon dates (*N. dutertrei*: Koutavas and Lynch-Steiglitz 2003). Age models for cores TR163-38 and TR163-33 are based on high-resolution (~0.5 to 1 ka) planktonic $\delta^{18}O$ records and 3 radiocarbon dates on *N. dutertrei*, while the age model for TR163-11 is based on high-resolution (~0.5 to 1 ka) planktonic $\delta^{18}O$ (Martinez et al., 2003). The age model for core ME0005A-43JC is based on combination of planktonic $\delta^{18}O$ stratigraphy as well as six radiocarbon dates on *N. dutertrei* (Benway et al., 2006). Core chronology of TR163-22 is based on $\delta^{18}O$ in *G. ruber* and nine radiocarbon dates (Lea et al., 2006) on *N. dutertrei*. The chronology of Y69-106 is based on planktonic $\delta^{18}O$ stratigraphy (Pisias and Mix, 1997). Hence, of the nine cores analyzed here, all have oxygen isotope stratigraphy, and seven have ages calibrated by radiocarbon dating. Errors introduced into our focusing factor calculations because of chronological uncertainty are less than 30%. A 30% misestimate of the Holocene MAR, for example, would require that we misplace the MIS 2/1 boundary by ~4 kyr.

2.3. Results

Our MAR and $xs^{230}Th$ results in addition to those studied previously (Kienast et al., 2007) are presented (Table 1) with respect to their temporal and spatial (latitudinal, bathymetric and distance from continental margin) variability. In order to investigate temporal variability of MARs and sediment focusing factors, and to be consistent with

the study of Kienast et al. (2007), we average such parameters for intervals of sediment deposited during the Holocene (0-13 ka; the Holocene) and the last glacial (13-25 ka; glacial). To describe the latitudinal spatial variability of xs^{230}Th-derived MARs and focusing factors, we have divided all cores (Table 2.1) into equatorial cores (nine out of fifteen cores that are located within ± 2° of equator) and non-equatorial cores (six out of fifteen cores that are located outside ± 2° of equator). Our subdivision of latitudinal spatial variability into equatorial and non-equatorial cores is based on the fact that most of the upwelling driven productivity, which may have an effect on the scavenging efficiency of ^{230}Th, is taking place close to the equator (Broecker, 2008; Thomas et al., 2000).

To describe the bathymetric spatial variability, which in effect is a way to test the downslope transport mechanism to explain higher inventory of xs^{230}Th in the deeper parts of the basin, we have chosen a bathymetric division of 2300 m. We use the terms "shallow" for cores collected at depths <2300 meters (Table 2.1) and "deep" for those collected at depths >2300 meters (Table 2.1). The shallowest sill depth in the Panama Basin is close to 2300 meters (Lonsdale and Malfait, 1974; Lonsdale, 1977), and is located at a saddle in the Carnegie Ridge. This location may serve as one entryway through which deep water enters the Panama Basin from the Peru Basin (Tsuchiya and Talley, 1998)—the other being the Peru trench, at a similar depth, in the eastern part of the basin. An additional spatial variability constraint is distance from the continental margin. We have used our ^{232}Th flux data (discussed in section 2.4.3) to divide the studied cores into "margin" (within 300 km of continental margin; Table 2.4) and "non-margin" cores (more than 300 km away from continental margin; Table 4). ^{232}Th flux is a proxy for continentally-derived detrital material (Marcantonio et al., 2001b; Pourmand et al., 2004; Anderson et al., 2006; McGee et al., 2007; Winckler et al., 2008). The division of cores into margin and non-margin cores is based on a dramatic decrease in the detrital flux with respect to distance from the continental margin (occurs at approximately 300 km; see section 4.3).

2.3.1. Spatio-temporal variability of mass accumulation rates (MARs)

For all nine cores analyzed here and the six cores from Kienast et al. (2007), xs^{230}Th-normalized and oxygen isotope age-model-derived MARs were calculated and averaged for sediments deposited during the Holocene and glacial (Table 2.1). For the equatorial cores, average xs^{230}Th-normalized MARs for sediment deposited during the Holocene and glacial are 1.7 and 1.8 $g \cdot cm^{-2} \cdot ka^{-1}$, respectively, suggesting no significant temporal change in xs^{230}Th-normalized MARs. In contrast, the average oxygen isotope age-model-derived MAR for the same cores was higher by ~50% during glacial compared to that measured during Holocene (5.4 $g \cdot cm^{-2} \cdot ka^{-1}$ vs 3.6 $g \cdot cm^{-2} \cdot ka^{-1}$). Similarly, xs^{230}Th-normalized average MARs for sediment in the non-equatorial cores are 1.5 and 1.6 ($g \cdot cm^{-2} \cdot ka^{-1}$) during the Holocene and glacial, respectively. Again, there is an insignificant temporal change in xs^{230}Th-normalized MARs measured in non-equatorial cores for sediment deposited during the Holocene and glacial. Average oxygen isotope age-model-derived MARs for sediment deposited in the non-equatorial cores are 2.4 and 3.5 ($g \cdot cm^{-2} \cdot ka^{-1}$) during the Holocene and glacial, respectively. There is no difference between the Holocene and glacial average xs^{230}Th-normalized MARs for sediments analyzed in the margin cores (each 2.1 $g \cdot cm^{-2} \cdot ka^{-1}$). In contrast, in the same margin cores, the average age-model-derived MARs are higher (35%) during the last glacial (4.2 $g \cdot cm^{-2} \cdot ka^{-1}$) than during the Holocene (3.1 $g \cdot cm^{-2} \cdot ka^{-1}$) (Table 2.1). Similarly, the average xs^{230}Th-normalized MAR of the non-margin cores is 1.3 $g \cdot cm^{-2} \cdot ka^{-1}$ during the Holocene compared to 1.4 $g \cdot cm^{-2} \cdot ka^{-1}$ during glacial. For the non margin cores, average age-model-derived MARs are always higher (3.1 and 4.9 $g \cdot cm^{-2} \cdot ka^{-1}$) for the Holocene and glacial, respectively; Table 2.1) than MARs determined using xs^{230}Th normalization.

The average xs^{230}Th-normalized MARs for shallow cores are 1.8 and 1.9 ($g \cdot cm^{-2} \cdot ka^{-1}$) for sediments deposited during the Holocene and glacial, respectively. For the same shallow cores, the average age-model-derived MARs are 3.0 and 4.5 $g \cdot cm^{-2} \cdot ka^{-1}$ for the Holocene and glacial, respectively (Table 2.1). For the deep cores, the average xs^{230}Th-derived

MARs are 1.3 and 1.5 ($g \cdot cm^{-2} \cdot ka^{-1}$) during the Holocene and glacial, respectively, versus age-model-derived MARs of 3.3 and 4.7 ($g/cm^2/ka$) during the same time periods. The $xs^{230}Th$-normalized method of calculating MARs reveals higher MARs for the shallower cores in comparison to those for the deeper cores, in contrast to the age-model method, which suggests similar MARs regardless of depth.

2.3.2. Spatio-temporal variability of $xs^{230}Th$-derived sediment focusing factors

Sediment focusing factors were calculated and averaged for sediments deposited during the Holocene and glacial. During the last glacial, average focusing factors of all cores are 50% more than those during the Holocene (3 versus 2; our data and data from Kienast et al., 2007; Table 2.1). Focusing factors in equatorial cores display greater variability than those in non-equatorial cores, and range from ~1 to 5 in the Holocene, and from ~1 to 11 in glacial. The percentage increase in Holocene to glacial change of focusing factors in the equatorial cores ranges from no change (TR163-38) to about 170% (V21-29). Average focusing factors for equatorial cores are 2.3 and 3.6 during the Holocene and last glacial, respectively. In the non-equator cores, the percentage increase in focusing factor from the Holocene to glacial ranges from 12% (TR163-11) to 118% (TR163-31). Only one non-equatorial core, Y69-106P, has a lower focusing factor (~36%) during the last glacial (Table 2.1). This core resides within the Panama Basin at the base of the Cocos Ridge at a water depth of 2870 m. Also, average focusing factors for non-equatorial cores are 1.6 and 2.1 for the Holocene and glacial, respectively (Table 1). Cores closest to the equator not only have the highest focusing factors in the Panama Basin over the past 25 ka, but also the greatest relative temporal change in focusing factors, i.e., higher focusing factors during glacial than in the Holocene. For margin cores, the average focusing factors during the Holocene and glacial are 1.6 and 2.1, respectively, so glacial focusing factors are on average 31% greater than the Holocene. For non-margin cores these factors are 2.3 for the Holocene and 3.5 for the glacial (Table 2.1). For non-margin cores, the increase in average focusing factor during glacial

compared to the Holocene is greater (52%). Cores studied here and by Kienast et al. (2007) have water depths that range from 712 to 3209 meters (Table 2.1). Nine of these fifteen cores were at or close to the tops of ridges that bound the Panama Basin (Carnegie and Cocos Ridges), and have depths of less than 2300 m. These shallower cores have average focusing factors during the Holocene and glacial of 1.8 and 2.9, respectively. Focusing factors for these shallower cores vary from 0.7 (TR163-11, depth 1950 meters) to 3.9 (V21-29, depth 712 meters) in the Holocene (Figure 2.4), and from 0.8 (TR163-11, depth 1950 meters) to 10.5 (V21-29, depth 712 meters) in glacial. The shallowest core, V21-29 has the highest focusing factors during both the Holocene (4.5) and glacial (12). Similarly, the average focusing factor of our deeper cores during the Holocene and glacial is 2.3 and 3.0, respectively. For cores Y69-106P and TR163-22, the deepest cores studied by us here within the basin proper, focusing factors were 1.1 and 2.3 during the Holocene, and 0.7 and 3.7 during glacial, respectively 2). No significant correlation exists between focusing factors and depth of cores (Figure 2.2).

2.3.3. Spatio-temporal variability of ^{232}Th fluxes

Average ^{232}Th fluxes, estimated using the xs^{230}Th-normalized MARs are calculated for the Holocene and last glacial (Table 2.4). During the Holocene and last glacial an apparently exponential decay of detrital fluxes away from the continent is observed. ^{232}Th fluxes were higher during glacial than those during the Holocene in all cores with the exceptions of Carnegie Ridge cores V19-27, ME0005-27JC and TR163-38, which are closest to the South American margin (Figure 2.3). ^{232}Th fluxes derived using oxygen isotope age models show similar glacial-interglacial trends in margin and non-margin cores. This is because changes in ^{232}Th fluxes are controlled almost entirely by changes in ^{232}Th concentration. In general, sites that are within about 300 km of a continental margin (see section 2.4.3) have ^{232}Th fluxes that are up to an order of magnitude higher throughout the past 25 ka compared to the same fluxes at sites that are further than 300 km from a continental margin.

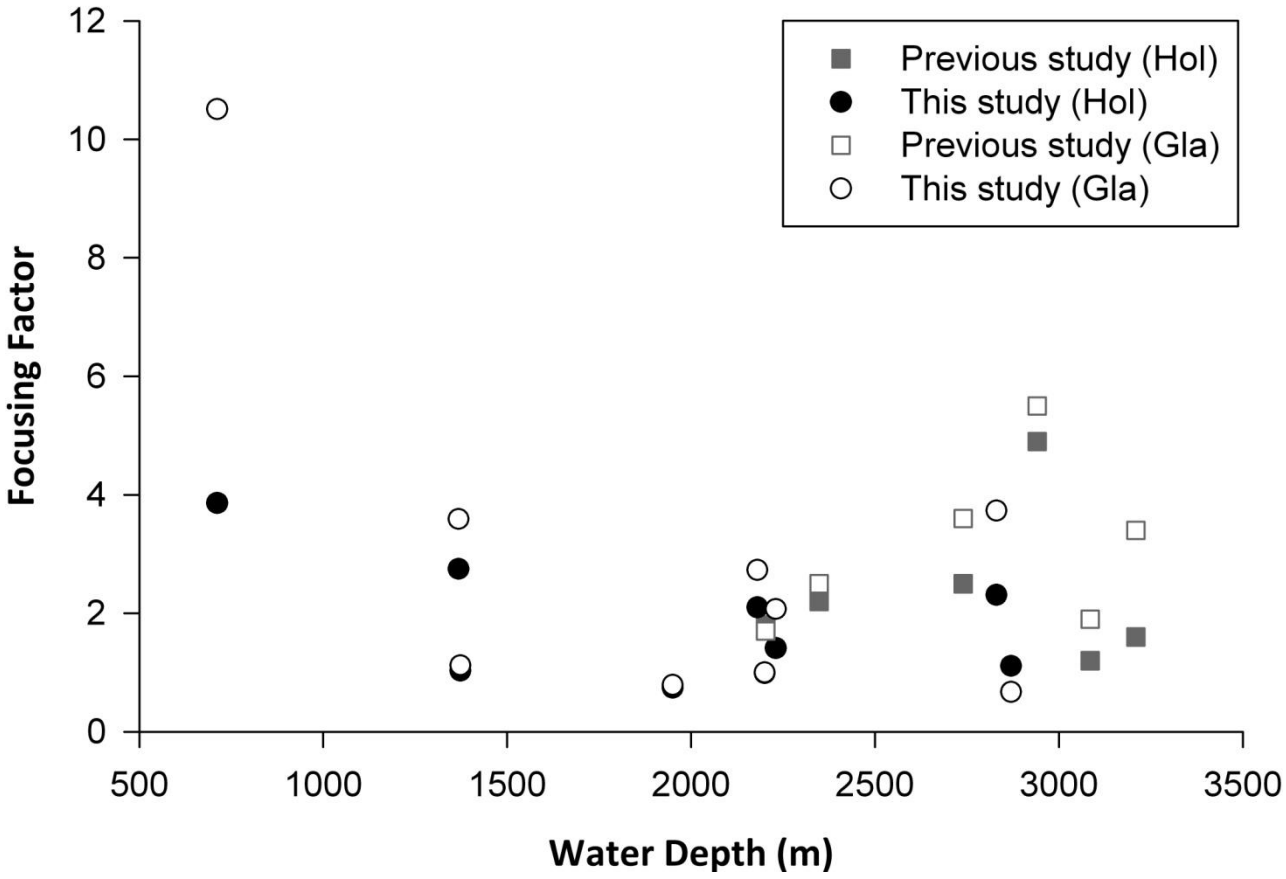

Figure 2.1. Bathymetric distribution of average focusing factors for Panama Basin sediment deposited during the Holocene (0-13 ka) and glacial (13-25 ka). Gray data points represent data from Kienast et al. (2007) and black data points represent data obtained in this study.

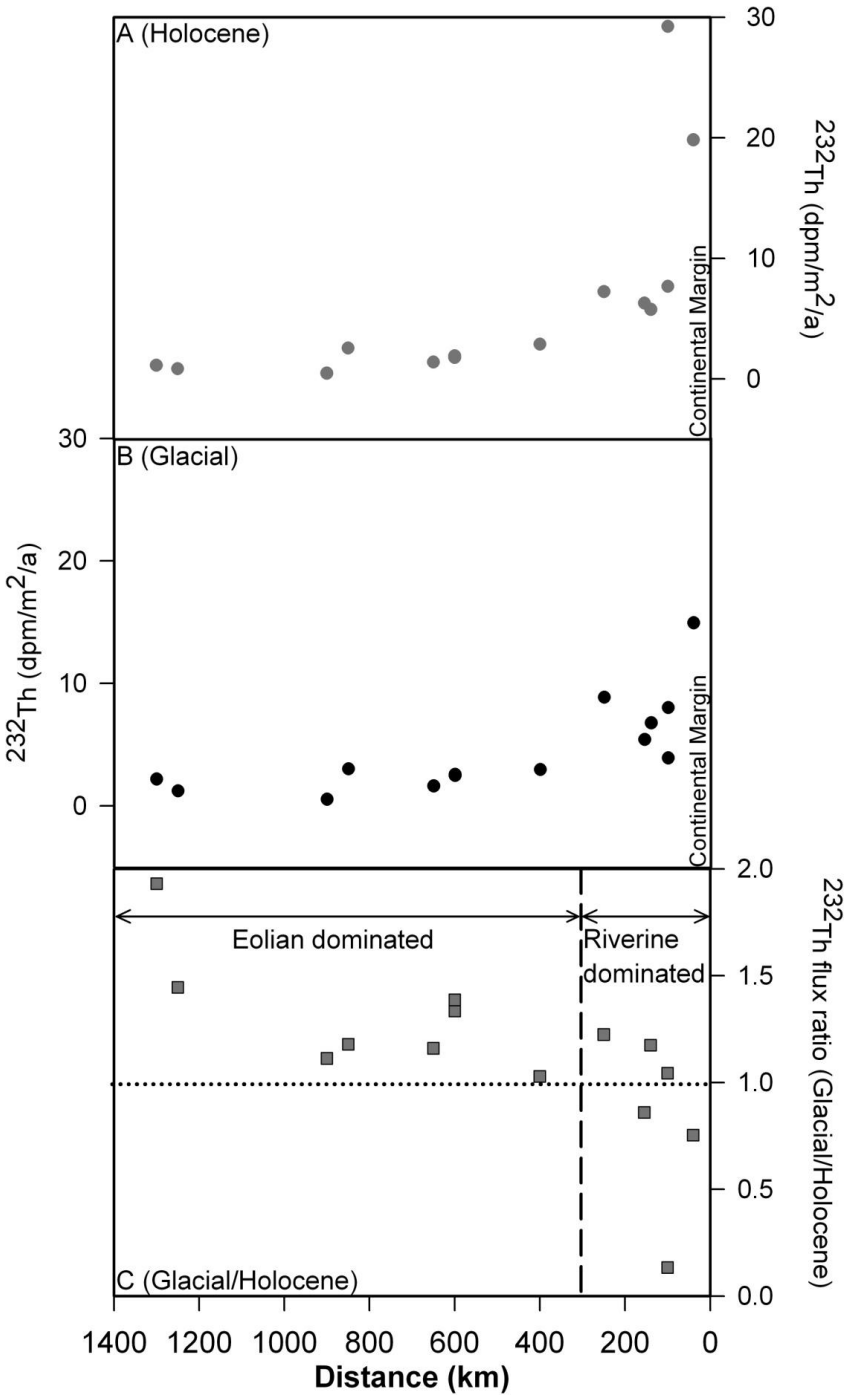

Figure 2.2. Variation of ^{232}Th flux as measured by distance between core location and continental margin for sediment deposited during a) the Holocene (0-13 ka) and b) the last glacial (13-25 ka). Panel c) displays the ratio of the glacial ^{232}Th flux to the Holocene ^{232}Th flux. ^{232}Th flux has been plotted at the same vertical scale for the Holocene and glacial for comparison. Long-dashed line in panel C separates cores which are proximal to the continent from cores which are more distant.

Table 2.4. Spatio-temporal variability of ^{232}Th flux in the Panama Basin. ^{232}Th flux data for the first five cores are from a previous study (Kienast et. al., 2007), while the remaining data are from this study. Bold letters represent cores that are close to continent (see results and discussion).

Core ID	Approximate distance from continent (km)	^{232}Th flux (dpm/m^2/a)		
		Holocene	glacial	glacial/ Holocene
ME0005-24JC	600	1.9	2.6	1.3
Y69-71	600	1.8	2.5	1.4
ME0005-27JC	**155**	**6.3**	**5.4**	**0.9**
TR163-19	1250	0.8	1.2	1.4
TR163-31	**250**	**7.2**	**8.9**	**1.2**
V19-27	**100**	**29.2**	**3.9**	**0.1**
RC8-102	650	1.4	1.6	1.2
TR163-11	400	2.9	3.0	1.0
V21-29	900	0.5	0.5	1.1
ME0005A-43JC	**100**	**7.7**	**8.0**	**1.0**
TR163-22	1300	1.1	2.2	1.9
Y69-106P	850	2.6	3.0	1.2
TR163-38	**40**	**19.8**	**14.9**	**0.8**
TR163-33	**140**	**5.8**	**6.8**	**1.2**

2.4. Discussion

2.4.1. $xs^{230}Th$ from ridge tops surrounding Panama basin

Previous ^{230}Th studies suggest significant amounts of lateral redistribution of sediments (i.e., focusing factor values > 1) in the deeper sections (2700-3200 m) of the Panama Basin (Kienast et al., 2007; Kusch et al., 2010; Loubere et al., 2004). Similar $xs^{230}Th$ inventories with focusing factor values > 1 have been found throughout the equatorial Pacific Ocean suggesting that sediment focusing is a widespread phenomenon throughout the equatorial sector of the western (Higgins et al., 2002), central (Marcantonio et al., 2001a; Marcantonio et al., 1996), and eastern (Broecker, 2008; Kienast et al., 2007; Loubere et al., 2004; McGee et al., 2007) Pacific Ocean. Focusing factor values are highest for the equatorial Pacific Ocean in the Panama Basin where much contention over their meaning has arisen (Broecker, 2008; Francois et al., 2007; Kienast et al., 2007; Loubere et al., 2004; Lyle et al., 2005; Lyle et al., 2007).

Kienast et al. (2007) hypothesized that this extra sedimentary $xs^{230}Th$ in the Panama Basin may have been derived from the top (shallower regions) of the Carnegie Ridge through downslope transport of sediments. Here, we further test this hypothesis by measuring $xs^{230}Th$ in seven cores located in the topographically highest regions (i.e., ridge tops; 712-2230m) of the Panama Basin to test downslope transport. While there clearly is erosion over parts of the Carnegie Ridge (Malfait and van Andel, 1980), other parts of the Carnegie Ridge, e.g., around V19-27 are clearly depositional, as we will discuss later.

For all but one of seven shallow cores (TR163-11), focusing factors are greater than 1 for both the Holocene and glacial (Figure 2.2). If the underlying assumption of the $xs^{230}Th$ normalization technique is correct (i.e., that the flux of ^{230}Th to the ocean floor is constant), the ubiquitous presence (hills and basins) of inventories of $xs^{230}Th$ that are

greater than what is expected from water column production alone means that sediment focusing is taking place everywhere in the Panama Basin, even near the tops of ridges (Figure 2.2). Moreover, the average focusing factors in the topographically highest regions of the basin (1.8 and 2.9 for Holocene and last glacial, respectively) are similar to those recorded in the deepest parts of the basin (2.3 and 3.0 for Holocene and last glacial, respectively).

Our finding that focusing factors are greater than 1 on or near the tops of ridges does not agree with the typical observation from high resolution seismic reflection studies that show basins catch more sediment than hills, with occasional erosion from highs (Mollenhauer et al., 2002; Tominaga et al., 2011, in press). Two hypotheses could explain the observation, either that (1) the sediments sampled on top of the ridges exhibit ponding (local focusing from surrounding ridge terrain), or (2) the cores receive their extra inventories of ^{230}Th in another way that is not reflective of horizontal sediment movement. Several seismic reflection profiles of the seafloor in the Panama Basin (available at www.geomapapp.org) clearly show some erosional and nondepositional surfaces in the topographically highest regions of the basin. For example, the seismic profile from the Vema cruise V2104 that passed across the V21-29 site (core with the highest focusing factor) shows that about 2/3 of the seafloor in the vicinity of the core is bare, and fits with the idea that some horizontal advection has taken place at the site of V21-29. Areas around the Carnegie Ridge gap (~85-86°W) are clearly erosional (Malfait and van Andel, 1980; Lonsdale and Malfait, 1974). These regions have not yet been studied for their ^{230}Th systematics but parts have been surveyed in 2010 and will be studied in the future.

It is clear that in deeper parts of the Panama basin that the xs^{230}Th technique suggests extensive sediment focusing, and that the flux of laterally advected sediments are 2-4 times greater than the flux of that which is rained vertically through the ocean (Kienast et al., 2007). Sedimentological evidence for significant horizontal transport around the

Panama basin is also extensive (Lonsdale and Malfait, 1974; Malfait and Van Andel, 1980). The earliest sedimentological mapping of the Panama Basin is based on grain size distribution (Dowding, 1977), visual observations of erosional surfaces (Heezen and Rawson, 1977), mineralogy (Heath et al., 1974), coarse component of surface sedimentary cover (Kowsmann, 1973), distribution of suspended particles (Plank et al., 1973), and textural and dispersal patterns (Van Andel, 1973). Much of this and seismic work on the ridges (Van Andel, 1973; Lonsdale and Malfait, 1974, Malfait and van Andel, 1980) suggest that the sedimentary cover in significant parts of the basin is heavily reworked by deep water currents, most notably at saddles in ridges and to the north of saddle. The studies by Lonsdale and Malfait (1974) and by Malfait and Van Andel (1980), in the Carnegie Gap area of Carnegie Ridge, found areas of erosion that have a complete absence of sediment cover, and where downslope transport probably occurred. One can surmise that such regions of erosion or non-deposition should contain deficits of ^{230}Th or, at the very least, show much smaller inventories of ^{230}Th than those in the deeper parts of the basin. With more detailed studies (in progress) near where the sediments should have been transported, these movements can be better quantified.

Other parts of the Carnegie Ridge, around V19-27 for example, are clearly depositional and probably have not supplied much additional sediment to the Panama Basin (Figure 2.4). On ridges especially, one must worry about sampling bias, i.e., that piston cores tend to be taken from basins where the sediments are thickest (Francois et al., 2007). The area around V19-27 was surveyed for drilling on ODP Leg 202 (Site 1239; Mix et al., 2003), so good information exists about the sediment cover (Figure 2.4). About 20% of the ridge top was surveyed while trying to locate Site 1239. Of the area surveyed about 75% was thickly covered with sediment. All the smooth topography in Figure 2.4 represents sediment-covered terrain, for example. Even the highest portion of the ridge just north of V19-27 has discontinuous sediment cover. Along line 6 it is possible to estimate how variable the average sedimentation rates have been based on the depth to the first major seismic horizon compared to its depth at Site 1239. Site 1239,

incidentally, has a sedimentation rate of 4.8 cm/kyr in the upper 50 m, only slightly lower than that of V19-27 (5.2 cm/kyr). Along line 6, 60% of the profile has a sedimentation rate between 0.5 and 1.5 x that of Site 1239, 15% of the profile has rates > 1.5 x that of Site 1239, and a little less than 20% of the profile has sedimentation rates ~0.5 x that of Site 1239. Based on this and inspection of the other seismic lines, the site at V19-27 actually has a sedimentation rate only slightly higher than average, and is, therefore not an anomalously "ponded" site in comparison to the rest of the ridge where sedimentation appears uniform. Lastly, the observation that focusing factors are not less than one at V19-27 suggests that this site and the entire ridge area surrounding it likely did not serve as a source of focused sediment in the deeper parts of the Panama Basin. Other site surveys were made along Cocos and Carnegie Ridge in order to locate other shallow drillsites for ODP Leg 202 (<2300 m) sites 1238, 1239, 1241 and 1242 (Mix et al., 2003; see UTIG marine seismic data portal, http://www.ig.utexas.edu/sdc/cruise.php?cruiseIn=nemo03mv). The seismic reflection profiles show erosional areas but also many areas of sediment accumulation. The flanks of the ridges, e.g. around Site 1238 on the S flank of Carnegie Ridge, are mostly depositional regions. Areas of nondeposition on the ridges are significantly smaller than the areas estimated in the simple box model used to articulate the problem of ridge sources of ^{230}Th and sediment (Lyle et al, 2007).

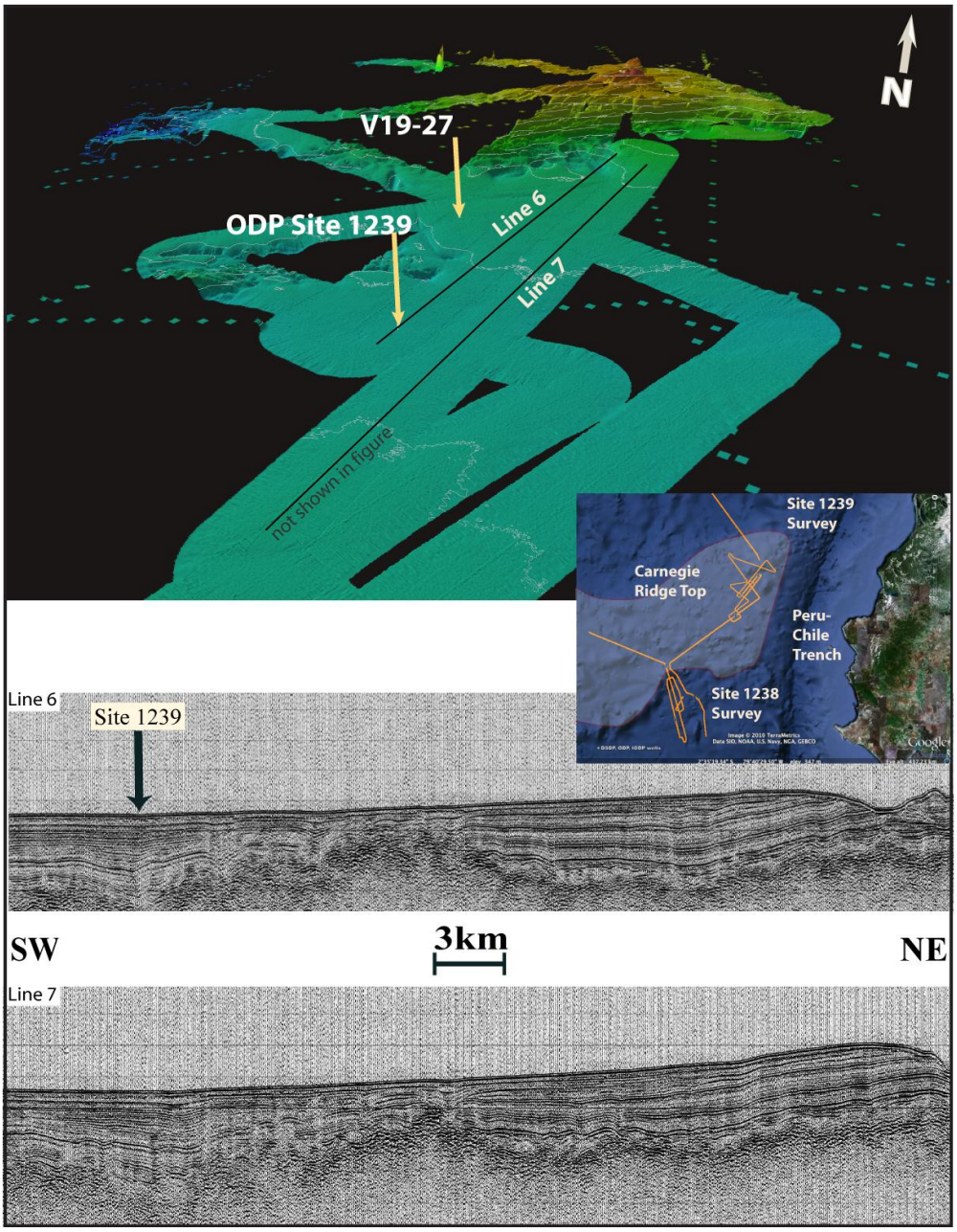

Figure 2.3. Bathymetric and seismic profiles from ODP Leg 202 Site survey (ODP Leg 202 Initial Reports volume, seismic data from NEMO-3, available at the University of Texas Marine Seismic Data Portal; http://www.ig.utexas.edu) from the top of Carnegie Ridge. It shows the position of core V19-27 studied here relative to the location of ODP Site 1239. Bathymetric map shows locations of bare zone near rugged topography towards the north as well as sediment accumulation zones just south of ridge tops.

If sampling bias is not an issue, and the source of additional sedimentary $xs^{230}Th$ inventory is not derived within the basin from the ridge tops, then it is possible that there is an extra-basinal source of $xs^{230}Th$ which derives from the Peru Basin located south of the Panama Basin. Sedimentary $xs^{230}Th$ from the Peru Basin might be laterally advected into the Panama Basin along with bottom water through the Ecuador Trench and/or across the central saddle of the Carnegie Ridge (Lonsdale, 1977). However, we do not have any evidence that Peru Basin sediment is a source of sedimentary $xs^{230}Th$. Based on the strong temporal correspondence of alkenone, total organic carbon and foraminifera fractions (from fine-grained to coarse-grained) in late-glacial to Holocene sediments of the Panama Basin, Kusch et al. (2010) argue that the source of any additional $xs^{230}Th$ has to be transported in a syn-depositional fashion from a local source of $xs^{230}Th$. If the source is extra-basinal, one would expect to see a temporal decoupling among sediment fractions with different grain sizes since the finest grain particles that might be transported long distances (Kusch et al., 2010) would be, presumably, older. There is the possibility that upwelled intermediate and surface currents might transport very fine particles from surrounding, less distal, shelf regions toward the Panama Basin bringing additional $xs^{230}Th$ which could explain higher focusing factors found throughout the region. Indeed, research has shown that finer particles have higher inventories of $xs^{230}Th$ (Kretschmer et al., 2010, McGee et al., 2010) and, in some cases, cause an overestimation of focusing factors. Although fine-grained sediment transport from-mid-depth waters is a possibility, there is no data to suggest that this occurs. We therefore consider alternative explanations.

2.4.2. Potential for boundary scavenging effects in the Panama basin

The main assumption of the ^{230}Th CFP technique is that the flux of ^{230}Th to the ocean floor is equal to the production of ^{230}Th by the decay of ^{234}U in the water column. For ^{230}Th to be a perfect CFP, the residence time of ^{230}Th should be zero, and it should be scavenged instantaneously as modeled in equation [1]. Most researchers agree that there is a limit to this assumption. The extent of lateral movement of ^{230}Th in the water column is defined by its residence time in the ocean (τ_{230Th}). In turn, its residence time is defined by the extent to which thorium is particle reactive (i.e., the degree to which Th is insoluble in seawater). It is obvious from measurements of dissolved ^{230}Th in the water column that the τ_{230Th} in the ocean is not zero. General circulation models which impart oceanic particle-flux fields (e.g., Henderson et al., 1999; Marchal et al., 2000; Siddall et al., 2005; Siddall et al., 2008) estimate a τ_{230Th} of about 20 years, suggesting that within 70% of the world's oceans the flux of ^{230}Th is within about 30% of its production rate.

The margins of the Pacific Ocean, for example (Anderson et al., 1983; Anderson et al., 1990; Lao et al., 1992; Lao et al., 1993), are regions with increased particle fluxes where the flux of ^{230}Th is higher than its known production rate. The increased scavenging efficiency of ^{230}Th in such regions leads to what is known as the boundary scavenging effect. In such cases, the ^{230}Th normalization technique would underestimate MARs, and overestimate the degree to which sediment focusing takes places.

Broecker (2008) suggests that enhanced particle flux due to enhanced upwelling and associated higher productivity along the equator delivers larger-than-expected inventories of xs^{230}Th to the underlying sediments. This extra xs^{230}Th is speculated to be supplied by "lateral mixing of equatorial waters with water adjacent to the equator" (Broecker, 2008), in essence, a boundary scavenging effect along the equator. In contrast, a recent model paper detailing the behavior of ^{230}Th in the open-ocean equatorial Pacific suggests that a particle flux effect cannot explain the higher than

expected inventories of ^{230}Th in equatorial Pacific sediments (Siddall et al., 2008). However, this result relies on the approximation of ocean mixing processes at the equator by isopycnal and vertical diffusion terms (Siddall et al 2008).

The flow of deep waters into the Panama Basin is relatively rapid, and potentially the large particulate fluxes and rapid exchange of water could interact to be an effective stripping mechanism of ^{230}Th. Residence time of water within the basin is short because of high geothermal heating (50-80 years; Detrick et al., 1974). Other estimates of the Panama Basin water residence time range from 42 years (Mix et al., 1995 [ODP138 Scientific Results]) to less than 50 years (Lonsdale, 1977). These estimates are on the order of the residence time of thorium in seawater, suggesting the potential for an underestimation of the flux of ^{230}Th to underlying sediments.

To investigate the possibility that there are enhanced removal rates of ^{230}Th in regions of high particle flux within the Panama Basin, and given the potential for overestimating the degree of sediment redistribution, we compared ^{230}Th-derived focusing factors (Figure 2.1; Table 2.1) between equatorial and non-equatorial regions (see section 2.3 for definition of regions) using our data and data from Kienast et al. (2007). We excluded continental margin cores that are influenced by high riverine inputs (section 2.4.3) because we wanted to restrict our analysis to the open ocean. There does seem to be a general relationship between proximity to the equator (a region of high particle flux) and higher apparent focusing factors (Figure 2.1). This holds true during both the Holocene and the last glacial, with the latter period having proportionally higher apparent focusing factors. Indeed, cores closest to the equator where primary production is the greatest today have focusing factors that are about twice as high during the last glacial than during the Holocene (average focusing factor of 3.6 versus 2.3, respectively; Table 2.1; Figure 2.1).

This finding is corroborated by a recent latitudinal transect study in the eastern equatorial Pacific, west of Panama Basin at 110°W, that show latitudinal distribution in focusing factor where the highest focusing factor was recorded near equator (McGee et al., 2007). For the non-equatorial cores, the average $xs^{230}Th$-derived focusing factors are smaller and more similar (~1.6 versus 2.1) during both the Holocene and last glacial, respectively (Table 1; Figure 1). If we are to take the model of Siddall et al. (2008) at face value, then ^{230}Th-derived fluxes can, at most, only overestimate focusing (or underestimate MARs) by a factor of 1.3. For the equatorial cores, therefore, average focusing factors can, at most be reduced to about 2.8 and 1.8 for the last glacial and Holocene, respectively.

Although our data point toward the possibility that enhanced focusing factors nearest the equator may be a consequence of increased productivity and enhanced scavenging efficiency of ^{230}Th (greater than that predicted by the model of Siddall et al., 2008), additional sediment data is required to further evaluate this possibility. There is the additional caveat that certain particle types, such as carbonates (Chase et al., 2002) and hydrothermal manganese (Frank et al., 1994), may also have an effect on the scavenging efficiency of $xs^{230}Th$. Hence, it may be possible that current models underestimate the ^{230}Th-particle flux (or scavenging efficiency) effect, which may be greater than 30%. The pertinent question is: is it possible to obtain better estimates of the scavenging effect so that we can quantitatively unravel it from calculated focusing factors based on ^{230}Th systematics? Additional water column ^{230}Th data is required to rigorously measure the particle-flux effect on ^{230}Th. Specifically the extent to which a latitudinal diffusion gradient in dissolved ^{230}Th concentration exists, with lowest dissolved concentrations at the equator where productivity is the greatest, needs to be investigated.

2.4.3. ^{232}Th fluxes in the Panama Basin

^{232}Th fluxes are used as a proxy for the flux of detrital continental material, and have been useful in deciphering past dust dynamics and changes in wind patterns/strength associated with climate change (Anderson et al., 2006; Marcantonio et al., 2001b; Pourmand et al., 2004; McGee et al., 2007; Winckler et al., 2008). Here, we use ^{230}Th-derived ^{232}Th fluxes in order to easily compare our detrital fluxes with other studies. More importantly (as we note in section 2.3.3), although absolute detrital fluxes calculated using age-model-derived MARs are not identical with those calculated using ^{230}Th-derived MARs, relative differences from core to core remain the same. Dust flux analyses based on ^{232}Th data suggest that there were two-fold increases in eolian fluxes during glacial in the central equatorial (Anderson et al., 2006) and eastern equatorial Pacific Ocean (McGee et al., 2007). In our study, the core furthest to the west at 92.4ºW (core TR 163-22), the glacial/the Holocene ^{232}Th flux ratio is about 2, identical to the Glacial/Holocene ratios at both 110ºW (McGee et al., 2007) and 140ºW (Anderson et al. 2006). It is clear that the major part of the detrital fractions at these last two locations is eolian. Hence, based on the similar Glacial/Holocene ^{232}Th flux ratios, we interpret our detrital signal at 92.4ºW to be predominantly eolian derived. Comparing average ^{232}Th flux over the past 25 ka, we find similar values at 140ºW and 110ºW (~0.6 dpm m^{-2} a^{-1}). At 92ºW, however, the average ^{232}Th flux is 1.8 dpm m^{-2} a^{-1} (Table 2.3), or 3 times higher than that at 140ºW and 110ºW. East of 92ºW, great increases in the detrital flux (average flux over 25 ka as high as 17 dpm m^{-2} a^{-1}) are due to the non-eolian detrital component, which is most likely made up of clays transported to the margin by riverine runoff and diffused out to sea.

Although most of the measured ^{232}Th fluxes in our non-margin cores are higher in glacial than in the Holocene (Figure 2.3; Table 2.3), three out of the six margin cores closest to the margin (Table 2.3), including those studied by Kienast et al. (2007), have higher ^{232}Th fluxes during the Holocene (Figure 2.3). As one moves away from the

continent the glacial/the Holocene detrital flux ratio (Figure 2.3c) increases. Margin cores which record higher terrigenous runoff during the Holocene have glacial/Holocene ^{232}Th flux ratios less than 1 (Figure 2.3c), while non-margin cores have glacial/the Holocene ^{232}Th flux ratios greater than 1. We suggest that the increase in this ratio, as distance to the margin increases, represents an increase in the detrital component being more influenced by eolian- relative to riverine-borne material. Furthermore, we believe the higher detrital fluxes for the cores closest to the margin are due to increased continental runoff during the Holocene in Central America and northern South America in agreement with a recent study by Rincon-Martinez et al. (2010). The significant spatial distribution of our cores (Figure 2.1), in addition those studied previously (Kienast et al., 2007), enables us to approximate the threshold distance where the detrital component transitions from being mainly composed of river-borne material versus being mainly composed of wind-blown material (Figure 2.3). Indeed, this threshold distance may be coincident with the location at which the glacial/Holocene detrital flux ratio is approximately equal to 1, i.e., at about 300 km (Figure 2.3).

2.5. Summary and conclusions

In the Panama Basin, xs^{230}Th-derived MARs are lower than age-model derived MARs, and leads to the prediction that significant sediment focusing (i.e., lateral redistribution of sediments by deep-sea currents) occurs. Downslope transport from surrounding ridge tops has been proposed as a source for excess inventory of xs^{230}Th found in the deepest parts of the basin. We have tested this hypothesis and find an ubiquitous presence of larger-than-expected inventories of xs^{230}Th on the tops and flanks of ridges that surround the Panama Basin. Focusing factors in these regions are as high as those in the deeper parts of the basins suggesting the ridges and flanks are not supplying the high inventories of xs^{230}Th to the deep basin.

The spatio-temporal distribution of focusing factors and MARs are such that the highest average values are those determined for sediment deposited during the last glacial in the equatorial cores. Lowest sediment focusing factors (still greater than 1, for the most part) are determined for the non-equatorial cores during the Holocene. Higher equatorial focusing factors during the glacial could be related to scavenging effects on ^{230}Th driven by higher productivity in the Panama Basin. To determine whether this is the case, more data is needed: specifically, a complementary latitudinal transect study of water column ^{230}Th between high- and low-particle flux regions, and better control on the erosional areas. Based on ^{232}Th flux measurements, we hypothesize that the location at which eolian (as opposed to riverine) fluxes dominate the detrital flux occurs at approximately 300 km from the margin.

CHAPTER III
WATER COLUMN ^{230}TH SYSTEMATICS IN THE EASTERN EQUATORIAL PACIFIC OCEAN AND IMPLICATIONS FOR SEDIMENT FOCUSING

3.1. Introduction

Thorium-230 (^{230}Th) is a particularly useful tracer for particles in the ocean because of its relative insolubility in seawater. ^{230}Th ($T_{1/2}$= 75380 years) is produced *in situ* by the decay of ^{234}U, uniformally distributed and dissolved in seawater. It is adsorbed onto sinking particles (a process called "scavenging") and is quickly removed from the water column to the underlying sediments. Because of the short residence time of ^{230}Th in the ocean, it is assumed that the flux of ^{230}Th (F_{Th}) to the sediments should equal its rate of production in the water column, P_{Th}, by the decay of ^{234}U (Bacon, 1984; Francois et al., 2004; Henderson et al., 1999; Krishnaswami, 1976). This assumption has been examined rigorously through model simulations (Henderson et al., 1999; Marchal et al., 2000) and sediment trap studies (Scholten et al., 2005; Yu et al., 2001), which suggest that the flux of scavenged ^{230}Th to sediment at the seafloor remains within about 30% of P_{Th} in ~70% of the world's oceans.

Reversible exchange between dissolved and particulate ^{230}Th in the water column predicts a linear increase in dissolved ^{230}Th concentration with depth in the water column (Bacon and Anderson, 1982; Moran et al., 1997; Moran et al., 2002; Moran et al., 2001; Nozaki et al., 1981; Nozaki et al., 1987; Scholten et al., 2005; Van der Loeff and Berger, 1993). However, such linear profiles are the exception rather than the rule and have only been found in sub-Antarctic (Chase et al., 2003; Rutgers van der Loeff and Berger, 1993), Central Pacific (RoyBarman et al., 1996) and western north Pacific waters (Nozaki et al., 1981). Non-linear profiles occur throughout the world's oceans, e.g., Sulu and South China Seas (Okubo et al., 2007); Labrador Sea (Moran et al., 1997); eastern North Atlantic (Vogler et al., 1998); Andaman Sea (Okubo et al., 2004); Indian

(Venchiarutti et al., 2008) and Atlantic sector of Southern Ocean (Venchiarutti et al., 2011), Norwegian Sea and Denmark Strait (Moran et al., 1995), Japan Sea (Nozaki and Yamada, 1987), Nansen basin (Cochran et al., 1995), Crozet Basin (Coppola et al., 2006), Arctic Ocean (Bacon et al., 1989; Edmonds et al., 1998), Canada Basin (Trimble et al., 2004), coastal southern California (Huh and Beasley, 1987), Mediterranean Sea (Roy-Barman et al., 2002) and the north Pacific (Okubo et al., 2012). The causes of the non-linear ^{230}Th profiles are manifold. They may be a consequence of renewal of basin waters with different dissolved Th concentrations and/or enhanced scavenging of Th in high particle flux productive zones near the equator or the continental margins (Anderson et al., 1983). Reversible scavenging models often neglect advection and diffusion of ^{230}Th in the water column, as these terms are thought to be trivial due to the radionuclide's short residence time in the ocean. Recently, however, Venchiarutti et al. (2008) reported, based on their particle dynamics study near the Kerguelen plateau in the southern Indian Ocean, that the advection of ^{230}Th off of the plateau is required to explain the vertical profiles of ^{230}Th.

Here, part of the impetus for studying water profiles within and outside of the Panama Basin is that the sediments there have ^{230}Th inventories that are much greater than what is expected from production of ^{234}U in the water column (Kienast et al., 2007; Loubere et al., 2004; Singh et al., 2011). Although higher-than-expected inventories of ^{230}Th occur within almost all equatorial Pacific sediments studied thus far, the greatest inventories are found within the Panama Basin (Kienast et al., 2007; Loubere et al., 2004; Singh et al., 2011). Indeed, over the last decade or so attempts to explain these high Panama Basin inventories of ^{230}Th have been controversial (Broecker, 2008; Francois et al., 2004; Francois et al., 2007; Kienast et al., 2007; Kusch et al., 2010; Loubere et al., 2004; Lyle et al., 2005; Lyle et al., 2007; Singh et al., 2011). Some believe the excess inventories of ^{230}Th are due to sediment focusing (i.e., lateral redistribution of sediments at the seafloor; Kienast et al., 2007; Loubere et al., 2004), while others believe that water-column or particle-dynamic processes are creating the excesses (e.g., Broecker,

2008; Lyle et al., 2005; Lyle et al., 2007). For example, Broecker (2008) discounted the sediment focusing idea and suggested that the higher ^{230}Th inventory in the Panama Basin is supplied through lateral mixing of particle-rich equatorial waters with the particle-poor waters adjacent to it. Singh et al. (2011) further proposed that the higher-than-expected ^{230}Th in the Panama Basin may result from advection of ^{230}Th from the low-particle-flux Peru Basin, located south of the Panama Basin. Waters from the Peru Basin enter the Panama Basin through Carnegie Ridge sills at the Carnegie saddle (between ~85°– 86°W at 2300m) and along the Ecuador trench (~81°– 82°W at 2900 m). Here, we explore the controversy concerning sedimentary ^{230}Th further, by measuring profiles of dissolved and particulate ^{230}Th in the water column within the Panama and Peru Basins. We investigate the potential mechanisms, both physical (advection) and chemical (scavenging), that control the distribution of ^{230}Th in the eastern tropical Pacific along a meridional transect (Figure 3.1) that encompasses a variety of particle-dynamic environments.

3.1.1. CTD data and hydrography of the eastern tropical Pacific

A detailed hydrography of the eastern tropical Pacific has been presented previously (Fiedler and Talley, 2006; Kessler, 2006; Tsuchiya and Talley, 1998). We have measured the hydrological properties of the water masses along our transect (Figure 3.1) that are relevant to the discussion of the dissolved Th data (Salinity (S)—potential temperature (T*pot*-0)—potential density (σ_0) diagrams; Figure 3.2).

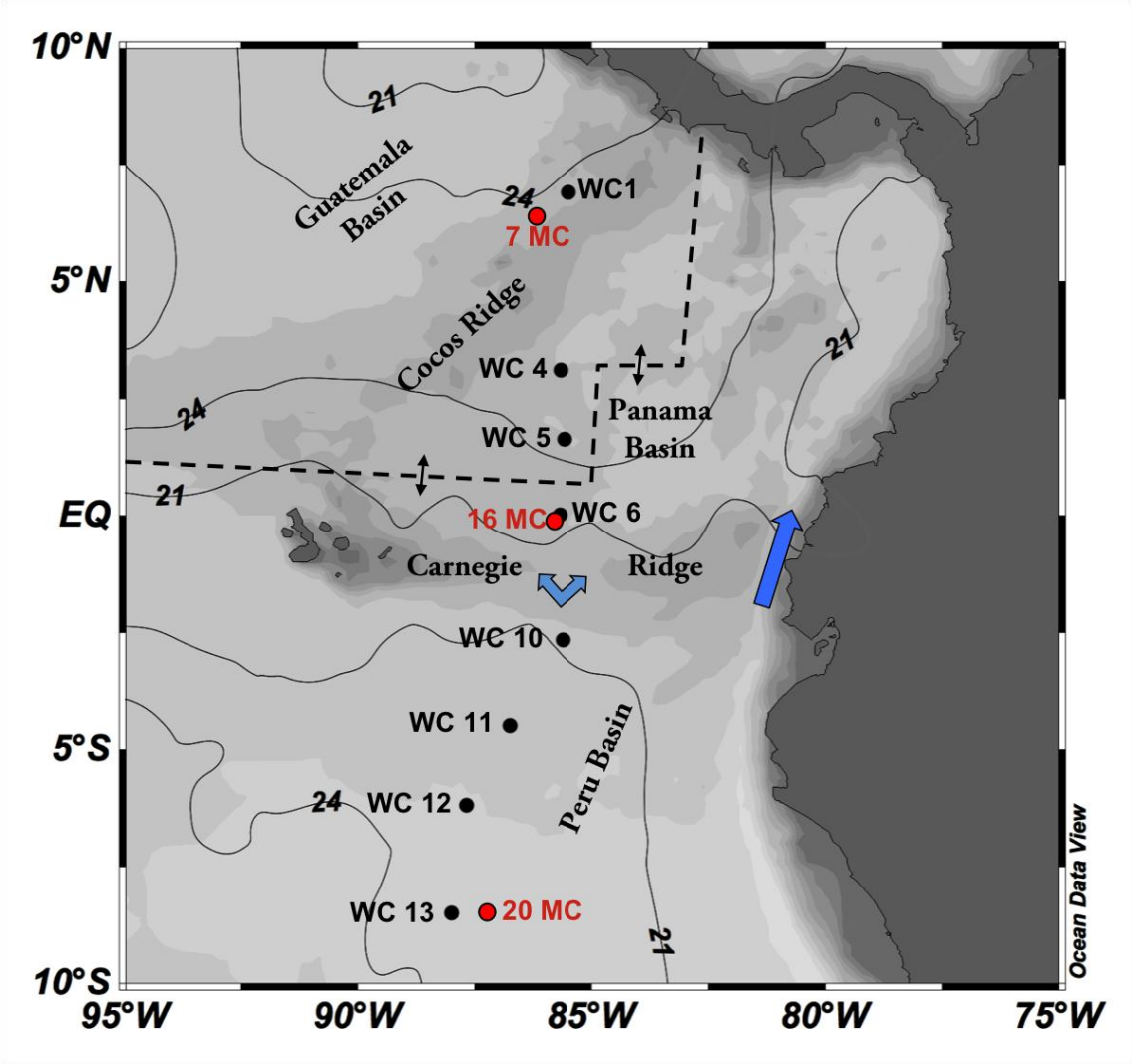

Figure 3.1. Location map for water casts and multicores collected during cruise MV1014. Solid contour lines represent annually averaged isotherms at 30 m depth. Data for annual temperature was obtained from the World Ocean Atlas 09 (Locarnini et al., 2010). WC 1 is located just north of the Cocos Ridge in the Guatemala Basin. WC 4, 5 and 6 are located in the Panama Basin, bounded by Carnegie Ridge and Cocos Ridge. WC 10, 11, 12 and 13 are situated south of the Carnegie Ridge in the Peru Basin. Dashed-dotted lines and arrows represent ocean-ridge spreading centers. Arrows show inflow of Peru Basin waters into the Panama Basin.

Antarctic Intermediate Water (AAIW) can be identified (Figure 3.2) based on its low-salinity (<34.5) and temperature (3-7ºC) properties (Fiedler and Talley, 2006). AAIW extends from north of the Subantarctic front into both the Peru and Panama Basins between 500-1000m (Figure 3.2). Below AAIW (~1000 m), the deep water in the eastern tropical Pacific is Pacific Deep Water (PDW). Water masses below 4000 m have been classified as the Lower Circumpolar Water (Fiedler and Talley, 2006) and such waters are present only at water cast station 13 (WC 13). PDW below 2000 m has similar properties in the Peru (σ_0=27.76-27.67) and Panama Basins (σ_0=27.71-27.69). PDW flows into the Panama Basin through sills of the Carnegie Ridge (Laird, 1971; Lonsdale, 1977). The slightly lower value and narrower range of σ_0 in the Panama Basin (compared with the same values in the Peru Basin) is due to geothermal heating (Detrick et al., 1974); Mix et al., 1995) and the semi-enclosed nature of the Panama Basin (Laird, 1971; Lonsdale, 1977). Our profiles are concentrated almost entirely within the PDW or AAIW masses (Figure 3.2) because our primary goal is to understand deep-water processes, where the bulk of seawater ^{230}Th resides. We categorize surface and subsurface water masses as tropical surface water (TSW). Surface waters at WC 1, 4, and 5 have the lowest salinities because of their location within the precipitation band of the intertropical convergence zone (ITCZ). The strong upwelling during the La Niña event (November 2010) is evident in the outcropping of the thermocline at station WC10 (~2°S). At WC13 a sharp increase in salinity exists in the surface water (subtropical surface water, STSW) because of its location in the South Pacific subtropical gyre, where a high-pressure zone intensifies the evaporation of surface water.

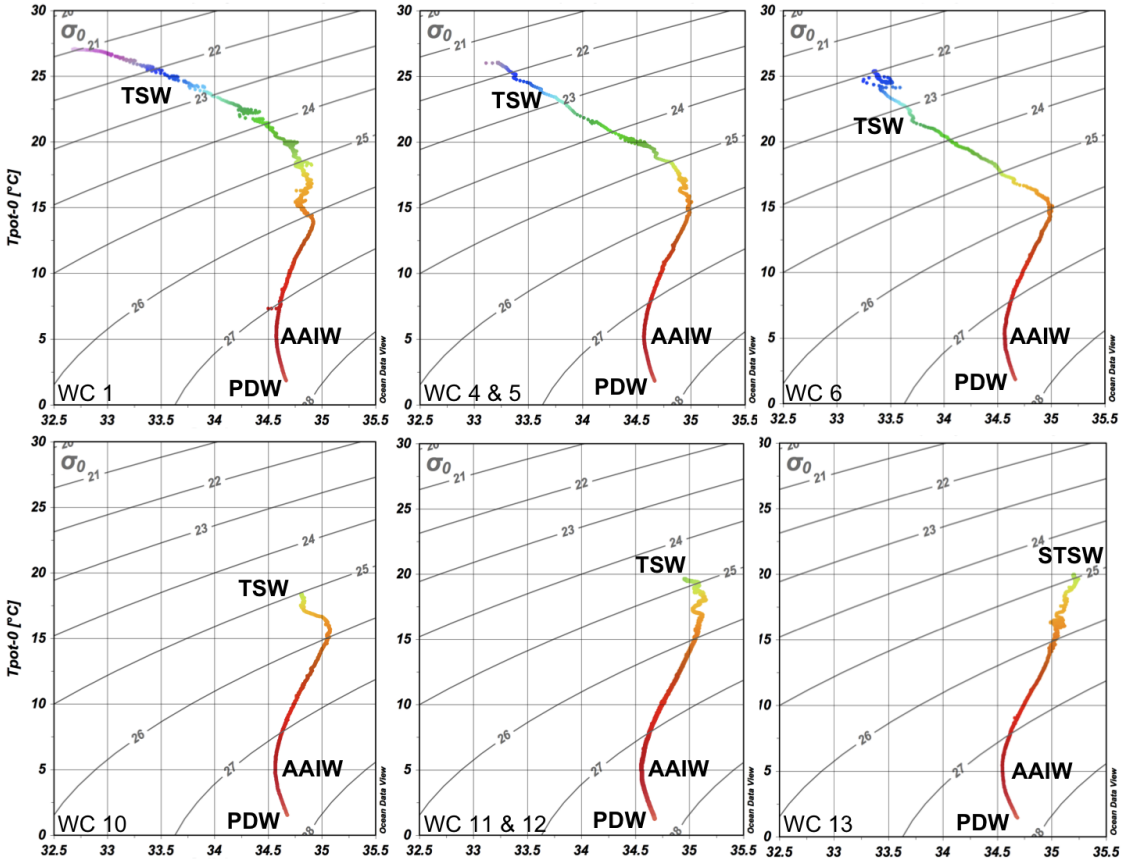

Figure 3.2. *θ–S* diagrams for all water casts collected during cruise MV1014. The main identified water masses are Pacific Deep Water (PDW), Antarctic Intermediate Water (AAIW), Tropical Surface Water (TSW) and Subtropical Surface Water (STSW). Each *θ–S* diagram has been plotted on the same scale to make for an easy comparison among sites and between basins. Potential density contours have units of kg m^{-3} and potential temperature is referenced to 0 db.

3.2. Methodology

3.2.1. Seawater sampling

Seawater samples were collected during an oceanographic expedition on the R/V Melville (MV1014) between October 17 and November 14, 2010. Ten-liter samples at several depths were collected at each water cast station using 24 PVC Niskin bottles mounted on a conductivity-temperature-depth (CTD) rosette system. The samples were gathered to test for advection of dissolved ^{230}Th from the low-particle-flux Peru Basin into the high-particle-flux Panama Basin (Singh et al., 2011), and the potential for lateral mixing of equatorial water with adjacent waters (Broecker, 2008). We profiled, for total and dissolved ^{230}Th (unfiltered and filtered, respectively), eight stations along a meridional transect (~between 85°W-88°W) from ~9°S – 7°N, a region that encompasses both high- and low-particle flux zones of the eastern tropical Pacific (Figure 3.1, Table 3.1). Samples from Water Casts (WC) 4, 5 and 6 were collected within the Panama Basin. Samples from WC 1 were collected on the NW slope of the Cocos Ridge in the Guatemala Basin. Samples from WC 10, 11, 12 and 13 were collected in the Peru Basin, with WC 10 being close to the southern slope of Carnegie Ridge and WC 13 being the farthest south in the Peru Basin within the South Pacific gyre.

Seawater samples were transferred from the Niskin bottles through acid-washed Teflon tubing to prewashed 10-L polyethylene-collapsible cubitainers within an hour of collection. Each cubitainer was washed with trace metal grade acid (~10% HCl), rinsed with Milli-Q water three times, air-dried in a laminar airflow hood and packed separately in new plastic bags inside the clean laboratory at Texas A&M University. For each depth, we sampled 20 L of seawater (2 Niskin bottles) in order to provide us with 10 L samples for duplicate analysis of dissolved ^{230}Th and ^{232}Th. We used 0.45-μm Acropak filters to separate the dissolved fraction from the particulate fraction during the transfer

of seawater into the cubitainers. Before sampling, each cubitainer was rinsed with small aliquots of seawater before the final transfer of the full seawater sample. For depths greater than 3000 m, we collected 10-L filtered and 10-L unfiltered seawater to study the dissolved and particulate fractions of ^{230}Th and ^{232}Th. We assume that the difference in concentrations of ^{230}Th and ^{232}Th between filtered (dissolved) and unfiltered (total) seawater represents the ^{230}Th and ^{232}Th concentrations in the particulate fraction of the seawater sample. All samples were acidified with concentrated (~9 N) ultrapure (Optima-grade) HCl to a pH of ~1.5 and shipped back to Texas A&M University where the radionuclide analyses were performed.

3.2.2. Radionuclide measurements

Radionuclides measurements for dissolved and particulate ^{230}Th and ^{232}Th were analyzed using the revised protocol of the GEOTRACES program (Anderson et al., 2012). Water samples were weighed (total weight minus cubitainer weight) and spiked with ^{229}Th for isotope dilution analysis of the Th isotopes. Purified Fe-carrier was added to the sample for $Fe(OH)_3$ precipitation. The Fe-carrier solution (as $FeCl_3$) was purified by back extraction into isopropyl ether. After addition of the ^{229}Th spike and Fe carrier to the seawater sample, it was left to equilibrate for 2-3 days before being brought to a pH of between 8 and 9 using trace metal-grade NH_4OH. At this pH, iron hydroxide [$Fe(OH)_3$] is precipitated and quantitatively scavenges virtually all of the Th within the sample. The precipitate was left undisturbed to settle at the bottom of the cubitainer for another 4-6 days, after which it was separated from the supernatant solution through siphoning and centrifugation before dissolution in ultrapure 8N HNO_3. The resulting solution was then processed through anionic ion-exchange columns (0.5-ml volume) to purify the Th for isotope ratio measurement. The purified Th was then dried to a small drop (~0.1 ml) and taken up in 2% HNO_3 (1 ml) for isotope ratios analysis on the Element XR magnetic sector ICP-MS housed in class 1000 R. Ken Williams Radiogenic Isotope Geoscience Laboratory at Texas A&M University.

Table 3.1. Summary of partition coefficients (K) for depths (in brackets) at which we have data. K values are based on $^{230}Th_p/^{230}Th_d$ ratios (data from Table 3.2).

Water Cast/Multicore	Latitude	Longitude	Bottom Depth (m)	Partition coefficient (K)
WC-01	6.5	-85.3	2525	No data
WC-04	3.6	-85.4	3140	0.21 (3130)
WC-05	1.4	-85.4	3325	0.48 (3250)
				0.75 (3315)
WC-06	0.0	-85.4	2997	No data
WC-10	-2.4	-85.4	3180	0.35 (3170)
WC-11	-4.3	-86.5	3506	0.52 (3250)
				0.37 (3496)
WC-12	-6.1	-87.4	3917	0.23 (3250)
				0.26 (3500)
				0.33 (3750)
				0.49 (3907)
WC-13	-8.3	-88.0	4178	0.38 (3250)
				0.33 (3500)
				0.06 (3750)
				0.14 (4000)
				0.67 (4168)
MV1014-07MC	6.1	-86.0	1995	NA
MV1014-16MC	-0.1	-85.5	2846	NA
MV1014-20MC	-8.3	-87.0	4407	NA

3.2.3. Trace metal analysis

Minor and trace metal analyses (Fe, Mn, Al, Ti) were performed on three multicores (MV1014 – 7MC, 16MC & 20MC) that were also collected during the MV1014 cruise (Figure 3.1). For trace metal analysis, sediments were dried and homogenized. Approximately 0.3 g of each sample from intervals of sediment within the top 20 cm of the sediment pile was completely digested in Teflon beakers using trace metal grade HNO_3, HF, HCl and $HClO_4$. After sediment digestion, samples were diluted with 2% HNO_3 and analyzed on the Element XR magnetic sector ICP-MS at Texas A&M University.

3.2.4. Blanks and reproducibility

Uncertainties in each thorium analysis were calculated at the 1-sigma level based on a standard propagation of errors associated with counting statistics, and uncertainties in the spike calibration and instrumental mass bias. Instrumental mass bias was determined by measuring $^{238}U/^{235}U$ isotope ratios in the National Institute of Standards and Technology Uranium Standard (NISTU500) several times between thorium runs (one standard run every five samples), and assuming a similar mass fractionation between uranium and thorium. Mass bias corrections did not vary significantly within daily runs, but during the course of this study ranged from about 0 to 0.3‰/amu. Average procedural blanks (n=15) were 4.9±0.4 fg for ^{230}Th and 7.9±0.6 pg for ^{232}Th, respectively. A procedural blank was processed with each batch of seawater analyses. Average blank contributions were 6.3% and 5.7% for ^{230}Th and ^{232}Th, respectively. However, given the reproducibility of our blank, we have a high degree of confidence in our blank corrections. The external reproducibility of the thorium analyses was measured by analyzing two 10-L samples collected separately from the same depth and water cast. Each duplicate sample was processed and analyzed in exactly the same way. We performed a total of 5 duplicate analyses from WC4 (1000 & 2500m), WC10

(1000m) and WC13 (2500 & 2749m) (Table 2). We have reported the average value for the duplicates that were reproduced within 5% of each other. Two duplicates had lower reproducibility, and we chose to report the value that had smaller error associated with it. The average external reproducibilities (1-sigma) of the ^{230}Th and ^{232}Th analyses are 4% and 12%, respectively. Our dissolved ^{232}Th concentrations are so low at each site that *it is clear* that the detrital fraction of the ^{230}Th is negligible.

3.3. Results

3.3.1. Guatemala basin

WC 1 (6.5°N, -85.3°W; 2522 m water depth) is our northernmost station (Figure 3.1) and lies on the northwestern flank of the Cocos Ridge within the Guatemala Basin. Dissolved ^{230}Th concentrations range from 2 fg/kg at 100 m to 11.4 fg/kg at 2000 m. The ^{230}Th profile (Figure 3.3) shows an approximately linear increase in concentration with depth in the top 2000 m, after which the concentration decreases toward the seafloor (Fig 3.3). The average concentrations of ^{230}Th and ^{232}Th are 7.9 fg/kg and 14.2 pg/kg respectively.

Since we did not sample unfiltered water in our only cast in the Guatemala Basin we do not have any particulate ^{230}Th data to report. However, given the similarity between our dissolved ^{230}Th from WC 1 and previously reported dissolved ^{230}Th values from nearby stations in the Guatemala Basin (Bacon and Anderson, 1982), we assume that the particulate ^{230}Th would be similar to these previously reported values. The average value of particulate ^{230}Th as derived from four stations in the Guatemala Basin study by Bacon and Anderson (1982) (i.e., stations 1114, 1117, 1120 and 1122) suggests that about 16% of the total ^{230}Th likely resides in the particulate fraction.

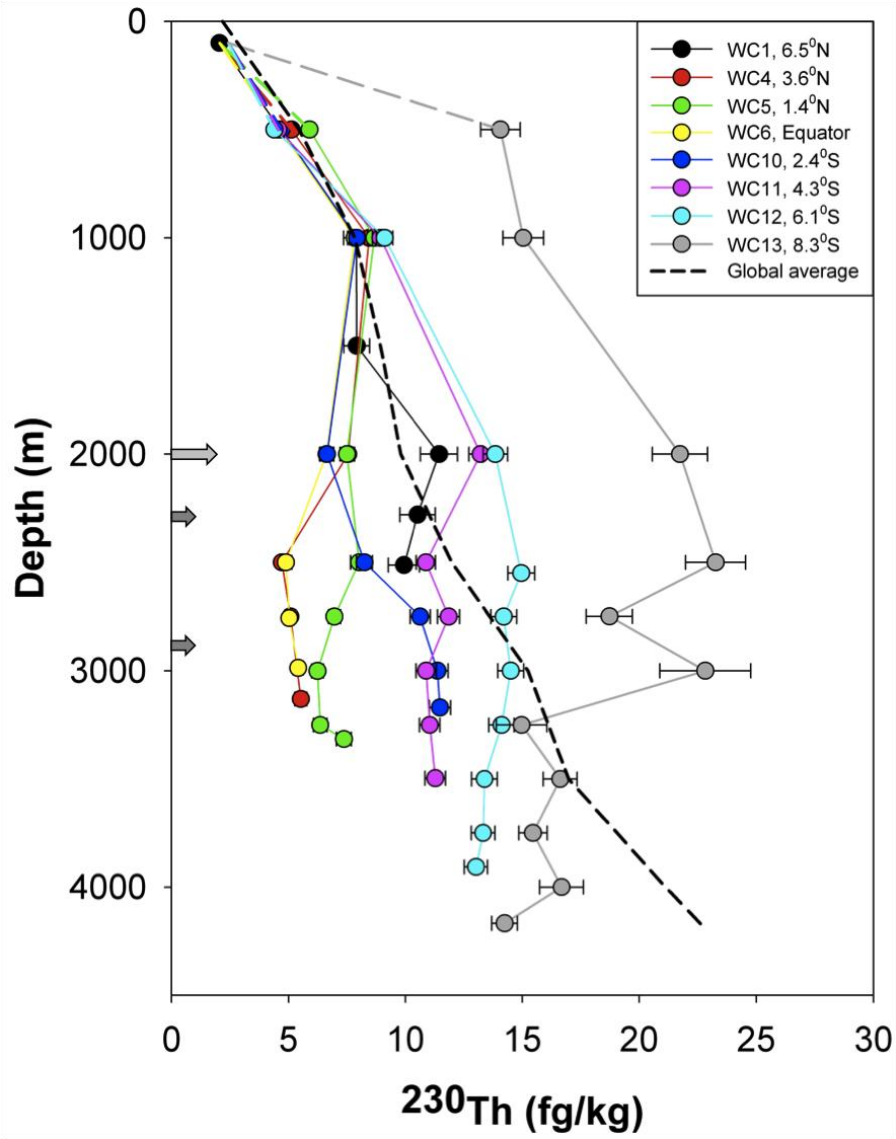

Figure 3.3. Depth profiles of dissolved ^{230}Th (fg/kg) along the MV1014 transect in the Eastern Tropical Pacific Ocean. Dashed black line represents the globally averaged dissolved ^{230}Th data from Henderson et al. (1999), and is generally consistent with a reversible scavenging model for ^{230}Th.Except for WC 13, profiles show a linear increase from 0 – 1000 m. Colored dashed lines represent extrapolations between 100 – 500 m in that dissolved ^{230}Th concentrations at 100 m are assumed to be similar to those measured at 100 m for WC 1 and WC 14 (close to WC 13). Gray arrows on the Y-axis represent sill depths (2300 m and 2900 m) at Carnegie Ridge and approximate average ridge height of Cocos Ridge (2000 m).

3.3.2. Panama basin

Three sites were profiled for seawater thorium concentrations in the Panama Basin: WC 4 (3.6°N, -85.4°W, 3140 m water depth), WC 5 (1.4°N, -85.4°W, 3325 m water depth) and WC 6 (0°N, -85.4°W, 2997 m water depth). At each site, we sampled the water column from 500 m to 10 m above the seafloor. Concentrations of ^{230}Th and ^{232}Th at 500 and 1000 m at all three Panama Basin sites and the Guatemala Basin site were identical within error (Table 3.2 and Figure 3.3). Although shallow water (100 m) was not sampled in the Panama Basin, we assume that that there is little variability in the ^{230}Th concentration at 100 m depth across the MV1014 transect (note that water profiles extend to 100 m using dashed lines in Figure 3.3). An identical maximum ^{230}Th concentration (8 fg/kg) is reached at 1000 m at all 3 Panama Basin sites. Below 1000 m, ^{230}Th concentrations show a gradual decrease of about 30-50% (compared to the value at 1000 m) until about 500 m above the seafloor at each site. Below 500 m, as the seafloor is approached, ^{230}Th concentrations either stabilize or show a slight increase (Figure 3.3). The average dissolved ^{230}Th seawater concentrations in samples from WC 4, WC 5, and WC 6 are 6, 7.1, and 5.7 fg/kg, respectively. WC 6, at the equator north of the Carnegie saddle, has the lowest average ^{230}Th concentration.

^{232}Th concentrations are extremely low and average about 11.8 pg/kg (Figure 3.4; Table 3.2). Indeed, the dissolved ^{232}Th concentrations are so low at each site that *it is clear* that the detrital fraction of the ^{230}Th is negligible. There is little variation in ^{232}Th with depth. ^{232}Th concentrations are slightly higher at the station situated furthest north in the Panama Basin (WC4), the site closest to the continental margin.

Particulate ^{230}Th in the Panama Basin (measured in one unfiltered deep water sample in WC 4 and two unfiltered deep water samples in WC 5) ranges from 18% (WC 4, 3130m) to 42% (WC 5, 3315m) of the total ^{230}Th (Table 3.1). The average particulate ^{230}Th in Panama Basin deep water measured here based on WC 4 and 5 is 27% of the total ^{230}Th,

which is about 70% higher than that of the average particulate ^{230}Th measured in the Guatemala Basin by Bacon and Anderson (1982).

3.3.3 Peru basin

In the Peru Basin, we determined thorium isotope profiles at four sites (WC 10, 2.4°S, -85.4°W, 3180 m water depth; WC 11, 4.3°S, -86.5°W, 3506 m water depth; WC 12, 6.1°S, -87.4°W, 3917 m water depth; WC 13, 8.3°S, -88°W, 4178 m water depth; Figure 3.1). At WC 14 (8.5°S, -87.3, 4355 m water depth), we sampled shallow water at a depth of 100 m. Peru Basin dissolved ^{230}Th concentrations range from 2.4 fg/kg (WC 14, 100 m) to 22.8 fg/kg (WC 13, 3000 m). The average dissolved ^{230}Th concentrations measured in samples from WC 10, 11, 12 and 13 are 7.9, 9.4, 11.6 and 16.5 fg/kg respectively (Figure 3.3). Average dissolved ^{230}Th concentrations increase to the south from WC 10, at 2.4°S, to WC 13, at 8.3°S. Moreover, at equivalent depths, the ^{230}Th concentrations always are higher toward the south, except for WC 11 below 3000 m. The average dissolved ^{230}Th in the Peru Basin is higher (11.5 fg/kg) than that in both the Panama (6.2 fg/kg) and Guatemala (7.9 fg/kg) Basins.

Particulate ^{230}Th fractions range from 5% (WC 13, 3750) to 40% (WC 13, 4168m) of the total ^{230}Th. For WC 13, 12, 11 and 10, the average fraction of the total ^{230}Th contained in the particulate fraction is 22%, 24%, 30% and 26%, respectively. Therefore, the average particulate ^{230}Th fraction in Peru Basin seawater is 25%, which is similar to that that for Panama Basin seawater (27%) and higher than that for Guatemala Basin seawater (16%).

Table 3.2. Thorium isotope data for seawater samples collected during cruise MV1014. Lightly shaded of depths represent data for total (unfiltered) Th concentrations, while unshaded depths represent data for the dissolved (filtered) Th concentrations. Data in bold represent replicate analyses. For those samples measured for both filtered and unfiltered thorium, the difference between these values represents the particulate Th concentration (see section 2.1). Errors represent 1 standard deviation.

Water Cast (ID)	Depth (m)	^{230}Th (fg/kg)	±	^{232}Th (pg/kg)	±
WC-1	100	2.05	0.15	11.57	0.4
	1000	7.9	0.55	14.93	0.21
	1500	7.92	0.55	17.6	0.31
	2000	11.44	0.79	14.61	0.3
	2280	10.51	0.76	12.33	0.33
	2512	9.93	0.67	116.55	1.67
WC-4	500	5.13	0.19	9.78	0.14
	1000	**8.45**	**0.33**	**11.8**	**0.24**
	1000	**7.79**	**0.3**	**19.08**	**0.46**
	2000	7.54	0.28	15.66	0.38
	2500	**4.71**	**0.18**	**13.9**	**0.26**
	2500	**4.45**	**0.16**	**13.79**	**0.26**
	2750	5.08	0.22	10.83	0.3
	3130	5.52	0.26	6.72	0.25
	3130	6.7	0.26	7.67	0.18
WC-5	500	5.9	0.22	18.1	0.41
	1000	8.67	0.3	11.3	0.09
	2000	7.5	0.31	10.17	0.16
	2500	8.02	0.37	7.7	0.24
	2750	6.96	0.26	9.13	0.2
	3001	6.24	0.25	15.76	0.43
	3250	6.35	0.29	12.16	0.35
	3250	9.27	0.38	16.7	0.45
	3315	7.37	0.32	11.66	0.35
	3315	12.69	0.61	28.24	1.23

Table 3.2. *Continued*.

Water Cast (ID)	Depth (m)	230Th (fg/kg)	±	232Th (pg/kg)	±
WC-6	500	4.64	0.21	9.4	0.27
	1000	7.83	0.3	10.95	0.09
	2000	6.63	0.3	8.58	0.18
	2500	4.89	0.26	7.24	0.26
	2757	5.03	0.2	8.58	0.13
	2987	5.41	0.22	9.24	0.16
WC-10	500	4.7	0.19	11.86	0.15
	1000	7.93	0.32	14.43	0.25
	1000	7.7	0.27	15.1	0.15
	2000	6.64	0.27	11.71	0.15
	2500	8.24	0.34	12.07	0.21
	2750	10.63	0.43	14.7	0.26
	3000	11.36	0.46	13.59	0.25
	3170	11.48	0.45	13.85	0.21
	3170	15.45	0.6	28.69	0.4
WC-11	500	4.57	0.2	16.05	0.4
	1000	8.92	0.34	15.7	0.16
	2000	13.22	0.5	26.68	0.17
	2500	10.88	0.42	19.34	0.15
	2750	11.85	0.47	11.91	0.16
	3000	10.89	0.44	11.7	0.17
	3250	11.04	0.43	11.87	0.13
	3250	16.61	0.7	18.88	0.36
	3496	11.27	0.44	9	0.11
	3496	15.39	0.6	17	0.23

Table 3.2. *Continued*.

Water Cast (ID)	Depth (m)	230Th (fg/kg)	±	232Th (pg/kg)	±
WC-12	500	4.4	0.18	10.98	0.15
	1000	9.1	0.35	13.18	0.11
	2000	13.85	0.53	15.69	0.14
	2550	14.96	0.57	12.72	0.09
	2750	14.21	0.55	11.88	0.14
	3000	14.51	0.55	12.84	0.1
	3250	14.12	0.54	11.97	0.14
	3250	17.25	0.67	14.52	0.18
	3500	13.38	0.56	11.41	0.2
	3500	16.73	0.64	17.72	0.16
	3750	13.32	0.51	21.06	0.22
	3750	17.6	0.67	28.74	0.19
	3907	13.02	0.5	15.38	0.18
	3907	19.25	0.75	36.75	0.4
WC-13	500	14.07	0.85	10.25	0.35
	1000	15.04	0.87	15.51	0.46
	2000	21.74	1.18	13.37	0.29
	2500	22.72	1.28	15.68	0.39
	2500	20.17	1.15	14.54	0.38
	2749	18.73	0.99	12.46	0.2
	2749	22.33	1.3	18.49	2.57
	3000	22.82	1.94	10.3	0.57
	3250	14.97	1.08	11.18	0.47
	3250	20.66	0.9	12.9	0.27
	3500	16.62	0.73	11.62	0.28
	3500	22.09	1.01	15.87	0.32
	3750	15.46	0.6	26.5	0.28
	3750	16.36	0.65	17.48	0.25
	4000	16.68	0.94	14.32	0.38
	4000	19.06	0.79	38.69	0.79
	4168	14.24	0.55	18.54	0.14
	4168	23.68	1	44.19	0.8

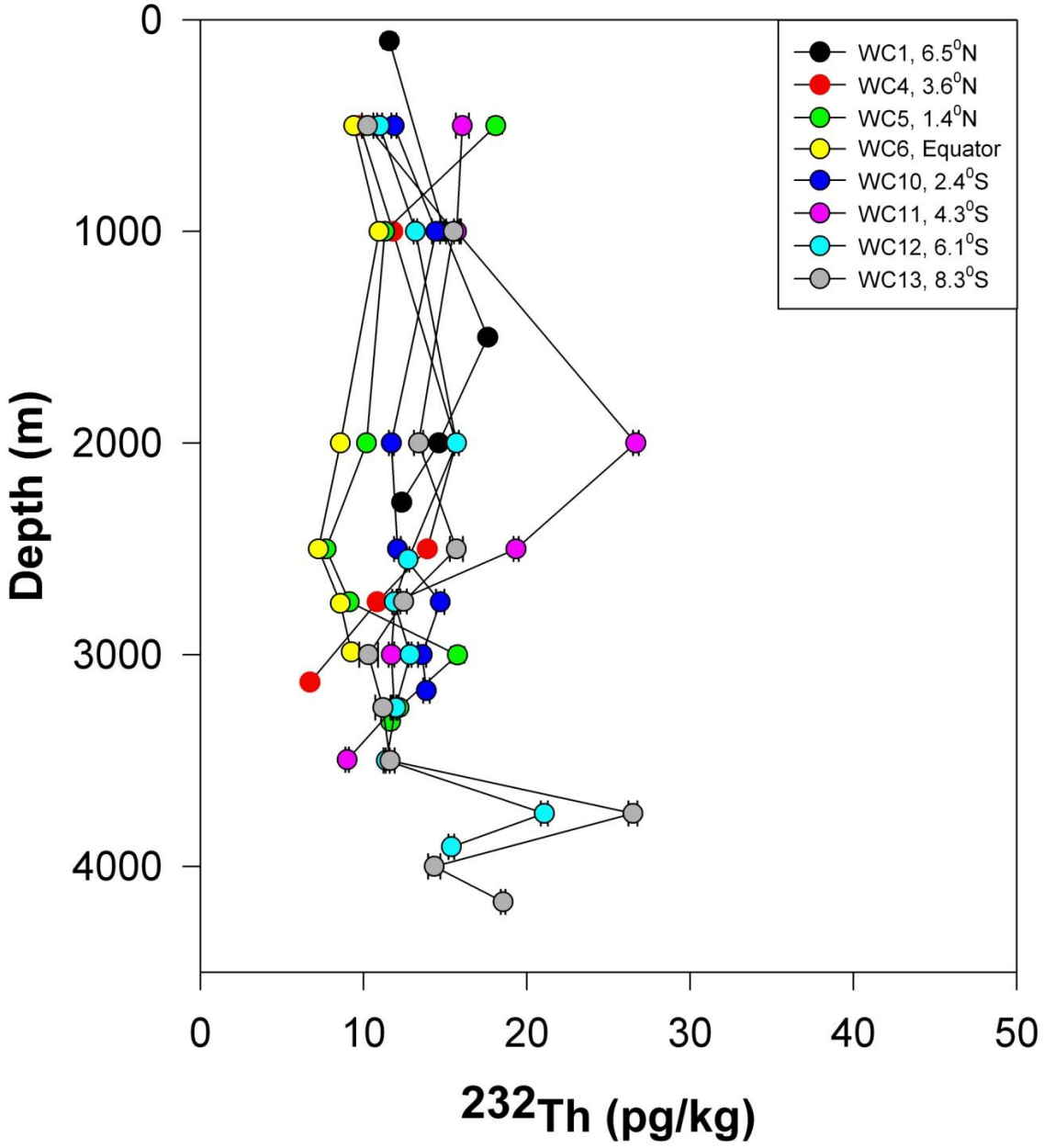

Figure 3.4. Depth profiles of dissolved ^{232}Th (pg/kg) along the MV1014 transect in the Eastern Tropical Pacific Ocean.

3.4. Discussion

3.4.1. ^{230}Th

Of the three basins we investigated here, the lowest dissolved ^{230}Th concentrations were measured in the Panama Basin, and the highest were measured in the Peru Basin. There is a gradual latitudinal decrease in average dissolved ^{230}Th concentrations in waters below 1000 m from the south in the Peru Basin towards the north in the Panama Basin (Figure 3.3). Indeed, this gradient is readily observed in a contour map along the meridional section for dissolved ^{230}Th concentration (Figure 3.5). Along the 2000-m isobath, for example, dissolved ^{230}Th concentrations range from greater than 21 fg/kg in the Peru Basin to less than 7 fg/kg in the Panama Basin. The distribution of dissolved ^{230}Th with depth does not match a simple production-reversible scavenging model, which assumes a constant settling rate and constant rates of adsorption and desorption as particles settle in the water column. In such a model there should be a linear increase of dissolved ^{230}Th with depth. Indeed, below 1000 m, none of the profiles fit a reversible scavenging model. If one were to assume a linear increase from the surface to the bottom (i.e., continuing the pattern shown from 0–1000 m), there appears to be a deficit of ^{230}Th (Figure 3.3) in all three basins. In addition, the depth at which a deficit is seen in the Panama and Guatemala Basins is shallower (1000 m) than that in the Peru Basin (2000 m). Furthermore, the depth at which ^{230}Th profiles start showing deficits increases from north to south in the Peru Basin. The greatest deficit (~50%) based on the global average dissolved ^{230}Th profile (Henderson et al., 1999) is found in the deep waters of the Panama Basin.

At each site along the transect from the Peru to the Panama Basins, the gradient in dissolved ^{230}Th concentrations in the bottom 2000 m, or so, likely drives lateral mixing of dissolved ^{230}Th from the South Pacific gyre toward the equator. The direction of the gradient (from S to N) is coincident with the flow of deep water into the Panama Basin

through openings in the Carnegie Ridge (Laird, 1971; Lonsdale, 1977; Tsuchiya and Talley, 1998, Fiedler and Talley, 2006; Figure 3.1). Moreover, given the higher-than-expected inventories of ^{230}Th found in Holocene and Glacial sediment (Kienast et al., 2007; Loubere et al., 2004; Singh et al., 2011), it is, perhaps, not surprising that excess ^{230}Th advected from outside the Panama Basin is being buried in the sediments there. Indeed, advection seems likely given that the average ^{230}Th concentration below 2000 m at WC 10 (first station located just south of Panama Basin) is about 10 fg/kg, while average ^{230}Th values for water below 2000 m within the Panama Basin just north of this station are about half of this (5 fg/kg for WC4, WC5, and WC6).

There are two questions that need to be explored further: 1) What is the cause of the enhanced scavenging of ^{230}Th in the Panama Basin? 2) What is the extent to which extra ^{230}Th is being supplied to the sediments over and above that provided in the vertical water column? The answer to the latter question should yield insight into how ^{230}Th traces sediment focusing within the Panama Basin.

3.4.2. Enhanced scavenging of dissolved ^{230}Th

The residence time, calculated as described in Francois et al. (2004), for dissolved ^{230}Th (τ_{230Th}) in the Guatemala Basin (WC1) of 14 years is similar to that measured by Bacon and Anderson (1982). Lower-than-expected concentrations of ^{230}Th in the deep waters of the Panama Basin represent anomalously low average water-column τ_{230Th} in each of the Panama Basin stations (9 yr at WC4; 11 yr at WC5; and 8 yr at WC6). The average, ~10 years, is comparable to that for the Japan Sea (8-10 years, Nozaki and Yamada, 1987), Sulu Sea (13 years, Okubo et al., 2007) and South China Sea (14 years, Okubo et al., 2007).

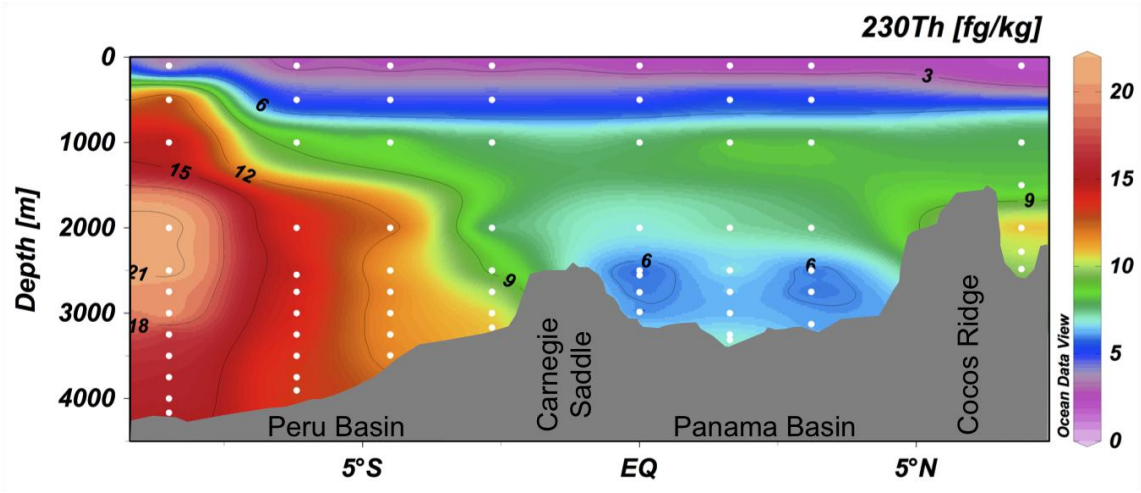

Figure 3.5. Latitudinal section of dissolved ^{230}Th concentrations in fg/kg. White dots on the plot represent ^{230}Th sample depths. We have assumed that the ^{230}Th concentrations at 100 m depth is the same for all stations (equal to the concentrations at WC 1 and WC 14). A gradient in ^{230}Th concentration from the Peru Basin toward the Panama Basin is apparent.

Such low average water column residence times of dissolved ^{230}Th are usually explained as being a function of enhanced scavenging due to increased particle fluxes (Anderson et al., 1983; Bacon and Anderson, 1982; Nozaki et al., 1987; Okubo et al., 2007; Okubo et al., 2004; Roy-Barman, 2009; Siddall et al., 2008). Average residence times of dissolved ^{230}Th at each of the stations in the Peru Basin increase from N to S (i.e., from ~13 yr at WC 10 to ~ 29 yr at WC 13), with the average residence time being approximately double that in the Panama Basin and slightly higher than that in the Guatemala Basin.

If surface productivity and associated water column scavenging of dissolved ^{230}Th were to control water column ^{230}Th concentrations, one would expect deficiencies in average water-column ^{230}Th concentrations to be spatially correlated with surface water productivity. Productivity has been estimated via satellite chlorophyll (Behrenfeld et al., 2005) and displays elevated productivity within 2° of the equator. Similarly, the average level of upwelling should be high where there is high surface productivity. Thermocline depth can be used as an indicator of upwelling, since high rates of upwelling shallows the thermocline. A thermocline map of the region (Figure 9a in Fiedler and Talley, 2006) shows a very shallow thermocline within ±2° of the equator east of the Galapagos that should mark a zone of high particle flux, and potentially high boundary scavenging (Figure 3.1). We also provide a meridional cross section of the isotherm at 30 m depth measured during the course of our study in Figure 3.1, and it agrees well the Fiedler and Talley (2006) synthesis of thermocline depths, which traces upwelling-derived-productivity as estimated by Behrenfeld et al. (2005) in the eastern tropical Pacific. Broadly the ^{230}Th data fit a pattern that is consistent with the geography of the upwelling area, i.e., lowest water column ^{230}Th concentrations lie within the region between ±2° of the equator. However, the high deficits of ^{230}Th north of 2°N (WC 1 and 4), where productivity is not as high, suggest additional scavenging might be occurring near the coast and within the northern Panama basin. The level of scavenging may reflect the larger net flux of particles through the waters of the Panama basin because of high productivity, but it might also be enhanced by the rebound of particles from the sea floor

(Walsh et al., 1988) with high chemical affinity for ^{230}Th. Walsh et al. (1988) showed that there is a fraction of particulate flux caught in sediment traps suspended within 500 m of the bottom that has a composition intermediate between surface sediments and falling particulate material in shallower traps. The 'rebound' particles are much higher in aluminosilicate and inorganic oxide content than particulate material falling through the water column.

As particles fall through the water column they adsorb (rate constant, k_1) and desorb (rate constant, k_2) dissolved ^{230}Th. The mean ratio of adsorption to desorption rate constants (i.e., k_1/k_2) is equal to the equilibrium ^{230}Th partition coefficient (K) between particles and water (Liter/Liter) (Bacon and Anderson 1982; Moran et al., 2002; Venchiarutti et al., 2008; Venchiarutti et al., 2011; Vogler et al., 1998). Adsorption is expected to vary with particle concentration, and generally increases with greater concentration of particulate matter. Since desorption is not related to particle concentration (Bacon and Anderson, 1982), higher K values are related to higher concentrations of suspended particles as depth increases in the water column (Krishnaswami, 1976). Average K values for ^{230}Th in the deep ocean are on the order of about 0.1 (Krishnaswami et al., 1976; Krishnaswami et al., 1981; Moore, 1981; Nozaki et al., 1981). In the Panama Basin, unusually high K values (see Table 1) suggest the presence of high suspended particulate matter loads. Indeed, Panama Basin K values are among the highest reported in the literature. High K values toward the bottom ~500m of the profiles are suggestive of resuspension of particulate matter.

Manganese (Mn) has been proposed as an efficient scavenger of ^{230}Th in the water column (Anderson et al., 1983; Bacon and Anderson, 1982; Roy-Barman et al., 2005; Roy-Barman et al., 2009). There is evidence of a strong correlation between ^{230}Th and Mn in different environmental settings, e.g., continental margins (Anderson et al., 1983; Shimmield et al., 1986; Shimmield and Price, 1988a), oxic-anoxic transition zones (Huh et al., 1994), and hydrothermal plumes (Dymond, 1981; Shimmield and Price, 1988b).

The MV1014 Mn/Al multicore data from N to S (from slightly south of the crest of the Cocos Ridge–Core 7MC, to slightly north of the Carnegie Ridge—Core 16MC, to the Peru Basin—Core 20MC) and surface sediment Mn/Al data from several cores located between 80-100ºW from Olivarez Lyle and Lyle (2005) all show Mn enrichments in the top few centimeters of the sediment pile (Figure 6). The enrichment at the top of the sediment pile is most likely a consequence of reduced and mobile Mn^{+2} migrating toward the oxic zone at the top of the sediment column (0-2 cm), a zone in which the Mn is oxidized to Mn^{4+} and precipitates to form Mn oxyhydroxides (e.g., Froelich et al., 1979). The depth of Mn burial is correlated to the flux of C_{org} to the sediments (Finney et al., 1988). Upon resuspension of the Mn oxyhydroxide fluff layer at the top of the sediment column, there is the likelihood that ^{230}Th is efficiently scavenged. The largest Mn enrichments, with Mn/Al ratios as high as 4.2 (absolute Mn concentrations reach 4.6%), were observed in surface sediments (~2 cm) at site 16MC (see Figure 3.1 for location) within the Panama Basin. The high Mn concentrations at the sediment surface at this site are likely due to a substantial supply of sedimentary Mn from hydrothermal vents (Dymond 1981) of the Galapagos Spreading Center (see Figure 3.1), and diagenetic mobilization of this Mn at depth caused by the high sedimentation rates (>5-10 cm/ka; Kienast et al., 2007; Koutavas and Lynch-Stieglitz, 2003) and high organic C contents (>1%; Pedersen and Price, 1980).

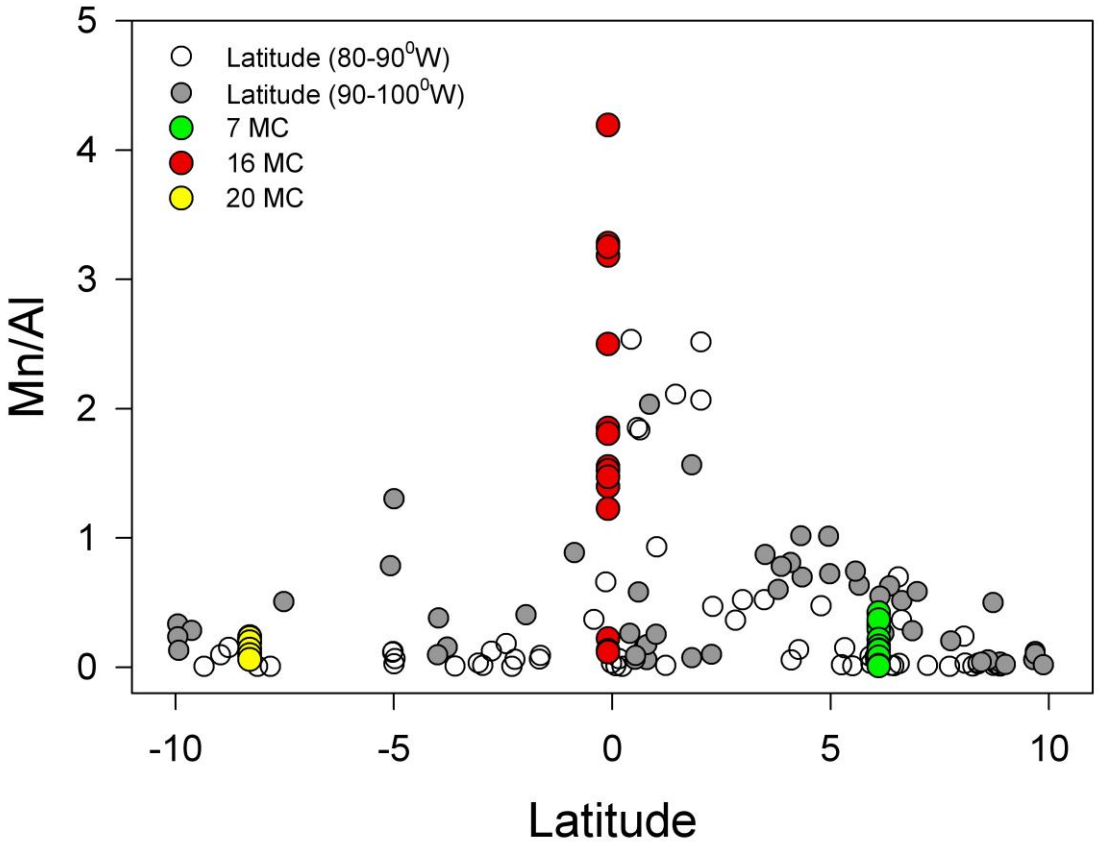

Figure 3.6. Mn/Al concentration ratios in surface sediments from three multicores (green, red, and yellow circles; 7, 16 & 20 MC) retrieved along our meridional transect, as well as literature Mn/Al data between 80-100ºW (open and gray-filled circles; Olivarez-Lyle and Lyle, 2005). Mn/Al ratios are highest in equatorial Panama Basin surface sediments.

As a result, Mn is reduced at relatively shallow depths in the sediment layer and is mobilized to the oxidized layer at the top of the sediment column akin to producing a core top zone-refined layer of Mn-rich particulates (Finney et al., 1988). Resuspension of this sediment fluff layer, which is enriched in Mn oxyhydroxides, may act as an enhanced sink for dissolved ^{230}Th in the Panama Basin and may partly cause the ~50% deficit (compared to the reversible exchange model and the global average) observed between 1000 m and the seafloor. Similar Mn enrichment near the sediment water interface should occur along the equator further to the west because the gradient of productivity produces enhanced Mn remobilization at the equator (Figure 3.6) (Lyle, 1992; data in Olivarez Lyle and Lyle, 2005). Hence, there is the potential for an enhanced scavenging behavior across the equatorial productivity bulge.

The difficulty with the Mn-scavenging hypothesis is the lack of shallow terrain to provide a flux of additional scavenging particles as shallow as 1000 m. Only at the Galapagos platform, around the Galapagos Islands is the water depth of the Carnegie Ridge consistently shallower than 1000 m. This area is more than 400 km west of the hydrographic transect. Along the Carnegie Saddle where water enters the basin from the south, water depths are consistently ≥2000 m. Sediment trap data suggest that resuspension of Mn-rich sediment might reach a maximum of ~500 m above the bottom (Walsh et al., 1988). This height of resuspension above the ridges might be adequate to achieve the added scavenging, since the ^{230}Th profiles are poorly constrained between 1000 and 2000 m.

3.4.3. Advection of ^{230}Th in the eastern tropical Pacific

Broecker (2008) suggested that the lateral mixing of equatorial waters with adjacent gyre water (from the northern and southern hemispheres) could be responsible for delivering an additional flux of ^{230}Th to the upwelling region of the equator, including the Panama Basin. To what extent does the deficiency of ^{230}Th in Panama Basin waters lead to lateral advection of ^{230}Th from the Peru Basin into the Panama basin? Given the short residence time of ^{230}Th in the water column (Francois et al., 2004; Henderson and Anderson, 2003), it is often assumed that advection and diffusion of ^{230}Th in water column can be neglected when modeling the water column ^{230}Th profile (Bacon and Anderson, 1982; Nozaki et al., 1981; Nozaki et al., 1987). Nevertheless, other studies have used ^{230}Th profiles to model deep water flow and have estimated up to a factor of 2 difference in ^{230}Th activity at a depth of 3 km across the North Atlantic (Marchal et al., 2007).

The ^{230}Th deficit, evidence for significant scavenging processes within the Panama Basin, and the gradient in ^{230}Th concentration from high values in the Peru Basin to low values in the Panama Basin is an indication for advection of dissolved ^{230}Th (Figure 3.5). Quantification of the dissolved ^{230}Th that is coming from deep waters of the Peru Basin is essential to understand the laterally-advected inventory of water column ^{230}Th into the Panama Basin. To estimate this inventory, we need to know the volume of water flowing into the Panama Basin along with its dissolved ^{230}Th concentration. Based on current-flow meter measurements and hydrographic similarities, there are two pathways along which deep water enters the Panama Basin: one through the Carnegie saddle at ~2300 m and the other along the Ecuador trench at ~2900 m (Laird, 1971; Lonsdale, 1977; Lonsdale and Malfait, 1974; Tsuchiya and Talley, 1988; Fiedler and Talley, 2006). Lonsdale (1977) suggested that the main entrance of water into the Panama Basin is through the trench at ~2900 m and that there are episodic influxes over the Carnegie saddle and into the Panama Basin. The first estimate of deep-water renewal in the

Panama Basin was 175-220 years (Laird, 1971), which was later revised down to a range of 50-80 years (Detrick et al., 1974) based on geothermal heat fluxes in the Basin. Lonsdale (1977) further revised the residence time of deep-waters (42 years) in the Panama Basin based on influxes of Peru Basin waters and flushing of Panama Basin waters. The most recent estimates of deep-water Panama Basin residence time are in rough agreement, and we will use the range of 40-80 years as the residence time of Panama basin water. We can calculate the net inflow of Peruvian waters by dividing the volume of water above the sills ($1.08\times10^{15}m^3$; Lyle et al., 2007) by the residence time (40-80 yr) of water in the Panama Basin. A shorter residence time for Panama Basin waters (40 yr) would mean that the volume of incoming water being transported into the basin would be about 0.86 Sv, while a longer residence time (80 yr) suggests a volume transport of about 0.43 Sv.

We now need to establish the dissolved ^{230}Th concentration of incoming Peru Basin waters in order to estimate the total dissolved ^{230}Th that is being transported into the Panama Basin. To do this, we assume that incoming Peru Basin water has the same ^{230}Th concentration as the average ^{230}Th concentration at WC10 located just south of Carnegie Ridge. The average dissolved ^{230}Th concentration at WC10 between 100-2920 m (depth of waters that make it into the Panama Basin) is 6.7 fg/kg (or 0.31 dpm m^{-3}). Multiplying this number by either the lower or the upper bound of inflowing Peru waters (0.43-0.86 Sv) and then dividing by the volume of water in the Panama Basin yields a range of 0.0038–0.0077 dpm m^{-3} yr^{-1} for the advected dissolved ^{230}Th flux (Figure 3.7). This advected extrabasinal dissolved ^{230}Th ranges, therefore, between 15 and 30% of the *in-situ* production rate of ^{230}Th (0.026 dpm m^{-3} yr^{-1}) in the Panama Basin water column. As the water leaves the Panama Basin and flows northward into the Guatemala Basin between the depths of 100 to 1500 m (average depth of the Cocos Ridge), the concentration of dissolved ^{230}Th does not change (i.e., the profile between 100-1500 m for WC 1 is approximately the same as that for WC 4, WC5, and WC 6). There does not seem to be further loss of ^{230}Th as water leaves the Panama Basin. For those depths

below 2000 m in the Guatemala Basin dissolved ^{230}Th concentrations are higher than those in the Panama Basin and more similar to those concentrations in the Peru Basin.

Models have predicted that the flux of ^{230}Th to sediments in most of the world's oceans is within 30% of that produced within the water column directly above the seafloor (e.g., Henderson et al., 1999, Siddall et al., 2008). Our estimate of advected ^{230}Th that is being delivered to the Panama Basin in dissolved form from the south falls within these model estimates. Not included in this estimate though is a small but significant fraction of particulate ^{230}Th from the Peru Basin (~25% of the total ^{230}Th in deepest (<3000 m) Peru Basin waters is in particulate form) which is also presumably advected and scavenged in the Panama Basin.

The additional dissolved ^{230}Th advected into the Panama Basin suggests that ^{230}Th-normalized mass accumulation rates (MARs) might be underestimated by 15-30%. As a consequence, sediment focusing factors would be overestimated by this same amount. If we assume that the oceanic conditions in the eastern tropical Pacific Ocean during the Holocene were similar to modern-day conditions, our new findings would mean that excess scavenging of ^{230}Th in the Panama Basin can only explain Holocene focusing factors less than about 1.15 – 1.30. Implementing corrections in this range to focusing factors reported in previous studies (Kienast et al., 2007; Singh et al., 2011) cannot explain significantly higher focusing factors for sediments in some regions of the Panama Basin. Such correction factors can, however, explain why focusing factors can be high as 1.3, even when winnowing might be expected, e.g., at the top of the Carnegie Ridge (Singh et al., 2011). Our findings suggest that it is unlikely that water column boundary scavenging of ^{230}Th can account for the high ^{230}Th-derived sediment focusing factors (>1.3) in the Panama Basin. Focusing factors estimated for the last glacial were even higher than those estimated for the Holocene (Loubere et al., 2004; Kienast et al., 2007; Singh et al., 2011). Although both advection of dissolved ^{230}Th from the Peru

Basin and scavenging within the Panama Basin might have been higher during the last glacial, we cannot address this possibility with the data we present here.

3.4.4. ^{232}Th in the eastern tropical Pacific

In remote regions of the ocean, far from continental riverine sources, detrital material from the continents is supplied to the sediments through eolian processes. ^{232}Th concentrations can act as a proxy for dust in the water and sediment. An understanding of dust supply to high nutrient, low chlorophyll regions of the ocean, such as the eastern tropical Pacific, is important because dissolution of dust provides Fe, a limiting micronutrient, to the water column (Jickells et al., 2005; Mahowald et al., 2005; Mahowald et al., 2009). Dissolved ^{232}Th concentration profiles from our water casts are relatively invariable over the depth of the entire water column implying that a) there is only one source of lithogenic input and that it is being delivered to the sea surface, and b) that this input is constant along our transect. Although dissolved ^{232}Th concentrations range from 6–26 pg/kg, in general, the concentrations mostly fall within a narrower range of about 10-15 pg/kg. Furthermore, the ^{232}Th concentrations reported in our study are lower than almost all the previously reported open ocean ^{232}Th values from the Pacific Ocean, i.e., the North Pacific Ocean (56-207 pg/kg, Huh and Beasley, 1987; ~80 pg/kg, Krishnaswami et al., 1976; ~80 pg/kg, Moore, 1981; 325-600 pg/kg, Somayajulu and Goldberg, 1966), the West Pacific Ocean (90-450 pg/kg, Nozaki et al., 1987), the Southern Indian Ocean (16-450 pg/kg, Venchiarutti et al., 2008), the Eastern Pacific Ocean (<40-80 pg/kg, (Knauss et al., 1978), and the Central Pacific Ocean (10-150 pg/kg; Roy-Barman et al., 1996). Concentrations of ^{232}Th, similar (although with a broader range) to those found here, have recently been reported for the Southern Ocean (19-75 pg/kg, Venchiarutti et al., 2011).

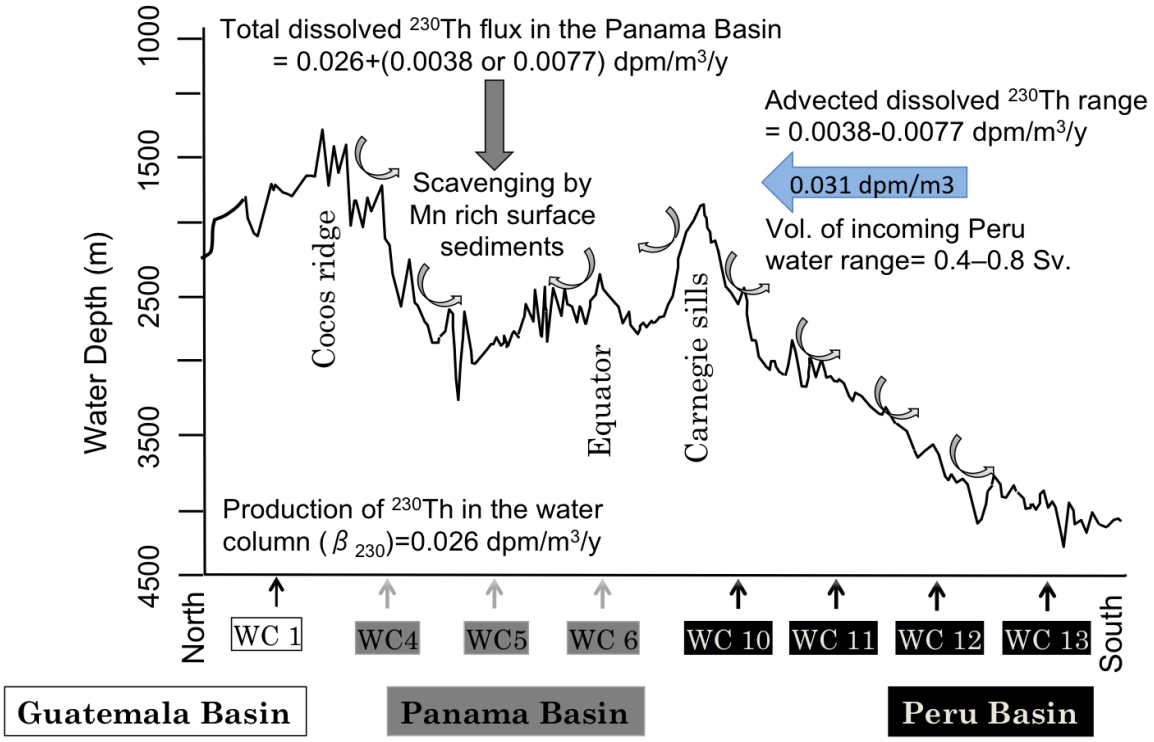

Figure 3.7. Schematic model showing scavenging and advection of dissolved ^{230}Th in the eastern tropical Pacific Ocean. The estimated advected dissolved ^{230}Th making it into the Panama Basin from the Peru Basin ranges from 0.0038 to 0.0077 dpm/m^3/y, based on an estimated water volume transport into the Panama Basin of between about 0.4 to 0.8 Sv. Curved arrows schematically indicate resuspension of surface sediments that are likely enriched in Mn in the eastern tropical Pacific.

Since our sites are far from continental margin rivers, the low ^{232}Th concentrations suggest low eolian fluxes being supplied to this region. These findings are in agreement with the extremely low dust fluxes estimated for the eastern tropical Pacific in a general circulation model study (Gao et al., 2003). Moreover, a present-day compilation of global dust fluxes measured using satellite optical depth, *in situ* concentration, and depositional observations identify the eastern tropical Pacific Ocean as having one of the world's lowest dust flux (Jickells et al., 2005; Maher et al., 2010). Indeed dust fluxes range between 0.01-0.1 g m^{-2} a^{-1} and average around 0.05 g m^{-2} a^{-1} (Jickells et al., 2005).

3.5. Summary

Dissolved ^{230}Th concentrations are lowest in Panama Basin waters, and highest in Peru Basin waters. Reversible scavenging cannot explain ^{230}Th profiles below 1000 m in the Panama Basin and below 2000 m in the Peru Basin, and intensified scavenging below these depths needs to be invoked. It is likely that both increased particle fluxes near the equator and resuspension of Mn-rich particulates play an important role in causing the ^{230}Th deficits encountered in deep waters of the Panama and Peru Basins.

Since we know that deep waters in the Panama Basin are being flushed with waters from the Peru Basin, we can estimate the advection of dissolved ^{230}Th to the Panama Basin using a simplified one-dimensional model. Based on the best estimate for Panama Basin deep-water residence time, we have estimated the advected flow of ^{230}Th from the Peru Basin to be between about ~0.0038 and 0.0077 dpm m^{-3} yr^{-1}. These values suggest an additional 15-30% of ^{230}Th is being delivered to the Panama Basin over that which is produced *in situ* there. General Circulation Models (Henderson et al., 1999; Siddall et al., 2008) suggest a similar sensitivity for the ^{230}Th constant-flux technique. Finally, our dissolved ^{232}Th concentrations are among the lowest measured in the world's oceans, and are consistent with the low eastern tropical Pacific Ocean dust fluxes modeled in recent studies (Jickells et al., 2005; Maher et al., 2010; Mahowald et al., 2005).

CHAPTER IV
PALEOPRODUCTIVITY AND PALEOREDOX CONDITIONS IN THE PANAMA BASIN FOR THE LAST 25KA

4.1. Introduction

The Eastern Equatorial Pacific (EEP) is a dynamic and significant part of the global carbon biogeochemical cycle (e.g., Chavez et al., 1999; Murray et al., 1994), where upwelling of "cold tongue" waters releases CO_2 into the atmosphere accounting for two-thirds of the net CO_2 efflux into the atmosphere today (Takahashi et al., 2002; Toggweiler et al., 1991). The release of CO_2 in the EEP is the net output which partially compensates for the CO_2 sequestration that occurs during primary production in the nutrient-rich-upwelled waters off the Peruvian coast and in the equatorial divergence regions (Fiedler et. al., 1991; Pennington et al., 2006). The presence of a shallower thermocline (nutricline) in the EEP allows efficient vertical mixing to bring cold-nutrient rich waters to the surface. However, surface productivity in the EEP has been found to be limited by silicic acid (Dugdale and Wilkerson, 1998) and iron availability (Coale et al., 1996; Moore et al., 2004), making the EEP one of the high-nutrient and low-chlorophyll (HNLC) regions of the world ocean. These limitations impede accessible nutrient utilization (i.e., uptake/supply, Sigman and Boyle, 2000), which, in turn, affect the amount of CO_2 sequestration by phytoplankton in the photic surface water and the eventual export of CO_2 to the deeper parts of the ocean.

The EEP has shown a strong linkage with climate changes at higher latitudes (Kienast et al., 2006; Leduc et al., 2007) through its association with the equatorial undercurrent (EUC) and Subantarctic Mode Water (SAMW) (Cravatte et al., 2007; Leduc et al., 2009; Lucas, 1986; Martinez and Robinson, 2010; Toggweiler et al., 1991; Sarmiento et al., 2004). Atmospheric carbon dioxide (pCO_2) records from Antarctica clearly show that the atmospheric concentration of CO_2 has varied over several glacial-interglacial cycles and was ~80–100 parts per million by volume (p.p.m.v) lower during glacial times compared

to CO_2 concentration during interglacial times (Barnola et al., 1987; Luthi et al., 2008; Petit et al., 1999). Furthermore, it is likely that oceanic conditions were responsible for such changes in CO_2 on glacial-interglacial timescales since the deep ocean overturning rate is ~1500 years and its carbon reservoir is approximately 25 times larger than the combined carbon reservoir of the atmosphere and surface ocean (Broecker, 1982; Sigman and Boyd, 2000).

Several attempts have been made to explain the oscillation of glacial-interglacial CO_2 and, yet, a consensus on a single mechanism has not been reached (e.g., Archer et al., 2000; Sigman and Boyle, 2000). Several studies have focused to explain the cyclic variations in CO_2 at lower latitudes by concentrating on oceanic phenomena that take place on glacial-interglacial timescales. Studies explain this by following one or more of the following approaches. 1. Productivity was not limited by micro- or macro- nutrients (Coale et al., 1996; Dugdale et al., 1995; Dugdale and Wilkerson, 1998; Martin 1990; Wilkerson and Dugdale, 1996) in the glacial EEP and carbon fixation by phytoplankton was greater in surface waters than the release of carbon (i.e., CO_2) through upwelling [The Silicic Acid Leakage Hypothesis, SALH, (Brzezinski et al., 2002; Matsumoto et al., 2002) and the Iron Hypothesis (Martin 1990)]. Increased productivity in the surface waters may have lead to greater export production in the upwelling regions during glacial times (Pedersen, 1983; Lyle et al., 1988; Paytan et al., 1996) and, hence, a more efficient biological carbon pump (Broecker, 1982a/b) 2. A transfer of nutrients from an intermediate to deeper oceanic reservoirs led to a stratification of the glacial ocean [Nutrient Deepening Hypothesis (Boyle 1988) or the modified and newer version of nutrient deepening hypothesis "respired-carbon deepening hypothesis" (Jaccard et al., 2009)].

It is possible that more than one of the abovementioned processes were operating simultaneously during glacial times. A recent study (Bradtmiller et al., 2010) evaluated the respired-carbon hypothesis of Jaccard et al. (2009) by measuring biogenic opal,

authigenic Uranium (U_{auth}) in 3 cores and brassicastrol in 1 core in the EEP. Their study supports the idea that glacial carbon storage was greater potentially due to the transfer of carbon into deeper parts of the Pacific Ocean. However, sediment cores used in their study represented upwelling regions only. Here we have measured two paleoproductivity proxies, i.e., biogenic barium (BioBa) and opal, in nine cores to constrain changing patterns of organic carbon export and paleoproductivity over the past 25 kyr. In the same nine cores we also analyzed for the redox sensitive authigenic uranium (U_{auth}) to constrain potential changing patterns of the sedimentary redox state of during the past 25kyr. Our core sites span different hydrographic regimes which include continental marginal regions, equatorial divergence regions and those that underlie intertropical convergence zone (ITCZ), and the upwelling cold tongue region that has been studied previously (i.e., Bradtmiller et al., 2010. Kienast et al., 2006). We further test the ideas of Jaccard et al. (2009) and Bradtmiller et al. (2010) with respect to glacial carbon storage in deeper parts of the EEP.

4.2. Study area, sediment sampling and age-model

4.2.1. Oceanographic setting of study area

Our study area represents the eastern most part of the equatorial Pacific Ocean that is bounded by the South American continent. The main climatic feature of the EEP is the interplay of intertropical convergence zone (ITCZ) with the cold-tongue system (Koutavas and Jean-Stiglitz, 2003). The cold-tongue represents the upwelling of cold and nutrient rich water, mainly the equatorial undercurrent (EUC) fed by the Peru Current (PC) and upwelled waters at the equatorial divergence. Upwelling of the cold (T~22°C), salty (S>34psu) and nutrient-rich water creates a zonal and meridional temperature gradient in the EEP (Figure 4.1).

The higher chlorophyll concentrations clearly show a tight relationship with the

upwelling pattern in the EEP (Figure 4.1). Sediments underlying this highly productive region should record higher biogenic sediment accumulation during times of higher biological productivity. Sea-surface temperatures increases from south of equator to the north and the front that separates cold waters just south of equator from warm waters to the north is known as the equatorial front which is generally located close to 2°N. Waters north of the equatorial front are less saline and more stratified because of dilution by rainfall associated with the ITCZ precipitation band. Intensification of trade winds results in intensified upwelling resulting in greater zonal gradient in temperature. The South Equatorial and Peru currents transport nutrient-rich cold waters near the Galapagos Islands (Figure 4.1). The North Equatorial Current carries warm and less saline water from the northeast and flows westward (Figure 4.1).

4.2.2. Sediment sampling and chronologies

In order to synthesize productivity and redox changes in the EEP for the last 25 kyr at a regional scale, our goal was to sample sediments that represent different environmental regimes. To achieve this we collected sediment samples (Table 1) in upwelling regions south of equatorial front (i.e. sites TR 163-31, TR163-33, RC8-102 and V21-29) within the equatorial divergence and cold tongue region (TR163-22), continental marginal regions (within 300 km) where terrigenous sediments are abundant (TR163-33, 163-38, V19-27 and ME0005-43JC), and less-productiv regions located north of the equatorial front in the warmer waters (Y69-106, TR163-11 and ME0005-43JC). In addition to representing different environmental regimes, our sample collection spans a water depth from 712 to 2870 m). Age models for Holocene (0-13000 years) and glacial (13000-25000 years) sediments used in this study are well constrained with radiocarbon ages in conjunction with oxygen isotope records of planktonic foraminifera from previous studies (Table 4.1). A brief description of the age models and their accuracy is given in Singh et al. (2011).

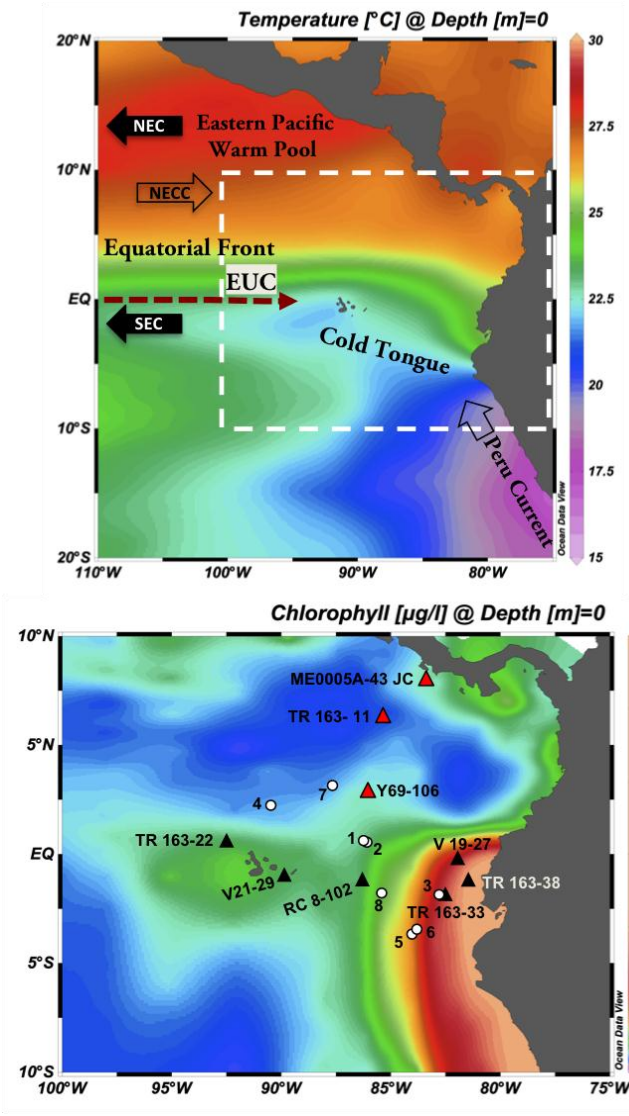

Figure 4.1. Oceanographic setting of our study area. A. The zonal gradient in sea surface temperature and its relation to surface and subsurface ocean currents is shown for the Eastern Tropical Pacific Ocean. Dotted rectangle in this figure is enlarged (Figure 1B) to show ours and previously studied sediment-sampling location. B. Spatial distribution of Chlorophyll concentration shows clear relation between productivity pattern being higher in the upwelling systems of cold-tongue and equatorial divergence regions in the EEP. Temperature and chlorophyll data is from World Ocean Atlas 09. Cores analyzed in our study are shown as triangles and the cores analyzed in previous studies, data source of authigenic U and biogenic silica, are numbered and shown as circles. Cores numbered from 1 – 5 are from Kienast et al. (2007) and 6 – 8 are from Bradtmiller et al. (2010). The numbered cores are mentioned in table 4.1.

Table 4.1. List of cores analyzed in this and included from previous study. Cores name from previous studies are italicized and their data sources are referenced. Negative sign in latitude denotes cores that are located south of equator while the positive sign denotes cores that are located north of equator. Numbers next to core names represent that core in figure 4.1.

Core	Latitude	Longitude	Depth (m)	Age-model references and data sources
V19-27	-0.47	-82.07	1373	$\delta^{18}O$ and ^{14}C, Koutavas and Lynch-Stieglitz 2003
RC8-102	-1.42	-86.85	2180	$\delta^{18}O$ and ^{14}C, Koutavas and Lynch-Stieglitz 2004
TR163-11	6.45	-85.82	1950	$\delta^{18}O$, Martinez et al., 2003
V21-29	-1.05	-89.35	712	$\delta^{18}O$ and ^{14}C, Koutavas and Lynch-Stieglitz 2003
ME0005A-43JC	7.86	-83.61	1368	$\delta^{18}O$ and ^{14}C, Benway 2006
TR163-22	0.52	-92.40	2830	$\delta^{18}O$ and ^{14}C, Lea et al., 2006
Y69-106P	2.98	-86.55	2870	$\delta^{18}O$, Pisias and Mix 1997
TR163-38	-1.34	-81.58	2200	$\delta^{18}O$, Martinez et al., 2003
TR163-33	-1.91	-82.57	2230	$\delta^{18}O$, Martinez et al., 2004
1. *Y69-71*	0.1	-86.48	2740	Auth U data, Kienast et al., 2007
2. *ME0005-24JC*	0.02	-86.46	2941	Auth U data, Kienast et al., 2007
3. *ME0005-27JC*	-1.85	-82.79	2203	Auth U data, Kienast et al., 2007
4. *TR163-19*	2.26	-90.95	2348	Auth U data, Kienast et al., 2007
5. *TR163-31*	-3.6	-83.95	3209	Auth U data, Kienast et al., 2007
6. *V19-30*	-3.38	-85.52	3091	Auth U & Opal data, Bradtmiller et al., 2010
7. *RC13-140*	2.87	-87.75	2246	Auth U & Opal data, Bradtmiller et al., 2010
8. *RC11-238*	-1.52	-85.82	2573	Auth U & Opal data, Bradtmiller et al., 2010

4.3. Analytical methods

4.3.1. Uranium and thorium

All uranium and thorium data are from a previous study by Singh et al. (2011). The methodology for the radionuclide measurements, error analyses, blank contributions and reproducibilities is given in Singh et al. (2011).

4.3.2. Barium

Total barium (Ba) concentrations were measured using the Element XR high resolution inductively-coupled plasma mass spectrometer (HR-ICP-MS) at Texas A&M University (TAMU) using isotope dilution. Homogenized sediment samples (~50 mg) were spiked with ^{135}Ba and completely digested using a cocktail of HNO_3, HF, and $HClO_4$. Our external reproducibility for Ba concentration using this methodology is about 5% (see Piela et al., 2011). Our Ba blanks are minimal and constitute about 0.02% of the analyte, so that no blank corrections were necessary. Biogenic Barium (bioBa) concentrations, defined as the fraction of total Ba not associated with terrigenous material, were estimated by subtracting the concentration of detrital barium from the total measured barium. The detrital fraction of Ba was estimated assuming that the Ba/Th ratio of the sediments is same as the Ba/Th ratio of average upper crust (i.e., 550 ppm for Ba and 10.7 ppm for Th, Taylor and McLennan, 1985). Therefore, [BioBa] =$[Ba_{total}]_{measured}$ [Ba/Th]terrigenous*^{232}Th.

4.3.3. Silica

Biogenic silica measurements were performed in the Department of Oceanography at TAMU using the method described in detail in Olivarez Lyle and Lyle (2002). In brief, ~ 30 mg of dried and homogenized samples were pretreated with hydrogen peroxide and

hydrochloric acid to remove organic matter and carbonates, respectively. Then samples were rinsed, decanted and dried in an oven. After drying, the biogenic silica in samples was extracted in 1M KOH overnight (9.5 hours) at 85ºC. Finally, the extracts were measured for dissolved biogenic silica concentrations using the molybdate blue method with a Hach DR/4000 spectrophotometer. A detailed description of the reproducibility and blanks of our opal measurements is presented in Piela et al. (2012).

4.4. Proxies

4.4.1. ^{230}Th normalization

We used the ^{230}Th profiling technique (Bacon 1984; Francois et al., 2004; Henderson and Anderson, 1999; Siddall et al., 2008) to evaluate the mass accumulation rates (MARs) of biogenic sedimentary components such as biogenic barium and opal. The vertical flux of such sedimentary components can be calculated as $F_v = (conc)_i * ß * z/[^{230}Th_{xs}]$, where $(conc)_i$ is the concentration of component "i"; ß is the production rate of ^{230}Th (0.026 dpm/m^3/y); z is the water depth (m) and $^{230}Th_{xs}$ is the excess, water-column scavenged ^{230}Th (corrected for the detrital and authigenic component of ^{230}Th, and decay-corrected for time since deposition). This method is based on the assertion that the flux of $^{230}Th_{xs}$ to the sediments on the seafloor is known and is equal to its production rate through decay of well-mixed ^{234}U in the overlying water (Bacon, 1984; Krishnaswami, 1976).

This assumption has been assessed in ocean general circulation models (Henderson and Anderson, 1999; Marchal et al., 2000; Siddall et al., 2008) and sediment trap studies (Yu et al., 2001). Such studies suggest that the flux of ^{230}Th to the seafloor is within about 30% of the produced in the water column within 70% of the world's oceans. A recent study based on dissolved^{230}Th measurements along a meridional transect (86ºW) in the eastern tropical Pacific Ocean (a region within which our samples for this study are derived) further corroborates the validity of the ^{230}Th technique (Singh et al., 2012,

submitted). The ^{230}Th methodology is particularly useful in the Panama basin because the technique is able to correct for syndepositional sediment redistribution, which is known to occur there (e.g., Francois et al., 2007; Kowsmann, 1973; Lonsdale and Malfait, 1974; Lyle et al., 2005; Lyle et al., 2007; Malfait and van Andel, 1980; Kienast et al., 2007; Singh et al., 2011; Van Andel, 1973).

4.4.2. Biogenic barium (BioBa)

Nutrient-like profiles of dissolved Ba and formation of barite crystals in undersaturated seawater suggests direct involvement of Ba in the marine biological cycle (Goldberg and Arrhenius, 1958; Monnin et al., 1999). Culture experiments show that barite ($BaSO_4$) forms upon decomposition of plankton, and barite abundance increases with further decomposition (Ganeshram et al., 2003). It is further noticed that there is a linear relationship between an increase in Ba concentration and increased fluxes of organic carbon (Dymond et al., 1992; Francois et al., 1995). For this reason, studies have focused on understanding the fluxes of barite in marine environments and implications such fluxes have on a better understanding of changes in paleoproductivity (Bishop, 1988; Dymond et al., 1992; Francois et al., 1995; Schmitz et al., 1987; Paytan et al., 1996; Paytan and Griffith, 2007).

One major limitation of bioBa as a paleoproductity proxy is that it dissolves under sulfate reducing conditions (Brumsack and Gieskes, 1983; Dymond et al., 1992; Francois et al., 1995; Paytan and Griffith, 2007). Nevertheless, being highly refractive in nature, its preservation in oxic pelagic sediments is much higher (~30%) compared to other paleoproductivity proxies such as organic carbon and biogenic silica that have preservation efficiencies of less than 1% and 3%, respectively in marine sediments (Dymond et al., 1992; Treguer et al., 1995). To compensate for the dissolution limitations of bioBa fluxes, we also measured biogenic silica, which is not affected by sulfate reduction in marine sediments. Hence, bioBa measurements in conjunction with biogenic

silica measurements should together yield better estimates of paleoproductivity (Jaccard et al., 2009).

4.4.3. Biogenic silica

Biogenic opal flux and organic carbon export in the ocean is predominantly a consequence of diatom productivity in surface waters (Lyle et al., 1988; Nelson et al., 1995; Pedersen, 1988). The uptake of Si by diatoms is not limited by light but by the presence of silicic acid (e.g., Ragueneau et al., 2000) and micronutrients (mainly iron). Biogenic silica fluxes can have an impact on the drawdown of CO_2 from the atmosphere (Coale et al., 1996; Dugdale and Wilkerson, 1998; Dugdale et al., 2004; Francois et al., 1997). Since the ocean is undersaturated with respect to silica everywhere, 10-100% of the silica is dissolved in the upper 100 m (Ragueneau et al., 2000), and the resulting preservation efficiency in sediments is low (<3%, Treguer et al., 1995, <5%, Ragueneau et al., 2000).

4.4.4. Authigenic uranium (U_{auth})

In seawater, uranium is present dominantly in the dissolved form as hexavalent uranium (uranyl-carbonate complexes ($UO_2(CO_3)_3^{4-}$; Langmuir, 1978), which behaves conservatively in oxygenated waters (Ku et al., 1977; McManus et al., 2005). With a transition from oxic to suboxic/anoxic conditions in bottom waters, U gets reduced to tetravalent uranium as (UO_2), which is insoluble and precipitates (e.g., Klinkhammer and Palmer, 1991; Morford and Emerson, 1999). Formation of this authigenically-produced uranium (U_{auth}) in reducing sediments creates a concentration-gradient in which there are higher concentrations of dissolved U above the sediment-seawater interface and lower (absent) dissolved U within the pores of surface sediments (Barnes and Cochran, 1990). Reducing conditions in surface sediments can prevail either because of persistent low bottom water oxygen concentration or the consumption of bottom water oxygen due to

remineralization of organic matter (Kumar et al., 1995; MacManus et al., 1995).

If oceanic conditions did not change drastically, a sediment interval with increased U_{auth} would indicate either an increased particulate organic matter flux or reducing conditions at the time that sediment was deposited (Kumar et al., 1994). One can estimate the authigenic portion of the uranium in the sediment by subtracting away that component of uranium in the sediment derived from terrigenous sources. We have estimated our U_{auth} using the following equation: $(U_{auth}) = (^{238}U)_{measured} - (^{238}U/^{232}Th)_{crust} * (^{232}Th)_{total}$, where brackets represent activities in units of disintegrations per minute per gram (dpm/g). We have used 0.7 as the $(^{238}U/^{232}Th)$ activity ratio for the terrigenous fraction of the sediment (Henderson and Anderson, 2003).

4.5. Results and discussion

We present new records of ^{230}Th normalized fluxes of biogenic silica and Ba along with activities of redox sensitive U_{auth} in sediments deposited over the past 25 ka from 9 cores (Figure 4.1, Table 4.2) that vary spatially within a wide range of water column depths in the Panama Basin. We compare our opal and U_{auth} results (Figure 4.3) to those presented by others in the same region (Kienast et al., 2007 and Bradtmiller et al., 2010) as ratios (Figure 4.4) for the Holocene (0-13000 years) and glacial (13000-25000 years). We further compare ^{230}Th normalized fluxes of bioBa and silica to age-model derived fluxes (Figure 4.4).

Table 4.2. Thorium, barium and opal data from Panama Basin cores shown in figure 4.1.

Core ID	Depth cm	Ba (Total) (ug/g)	BioBa ug/g	xsTho dpm/g	SiO2 wt%	Authi U ppm
V19-27	35.5	1290	1064	1.65	14.7	3.9
Water Depth	45.5	1201	838	1.17	13.9	0.5
1373	64.5	975	851	1.98	9.9	1.4
	84.5	617	568	1.94	5.4	2.8
	94.5	452	409	1.94	3.4	3.4
	114.5	582	536	2.19	nd	4.9
RC8-102	2	1630	1609	4.22	5.4	0.9
Water Depth	15	1840	1819	3.85	6.5	6.8
2180	45	693	682	2.04	3.0	6.2
	60	1064	1045	3.19	3.5	3.3
	75	1015	996	3.30	1.6	3.6
	105	997	979	2.43	3.0	7.9
TR163-11	11	2135	2077	5.11	13.9	2.2
Water Depth	16	2195	2130	5.21	15.7	3.2
1950	22	1814	1749	4.67	15.2	4.1
	28	2007	1947	5.25	12.8	6.3
	33	1797	1741	4.62	11.6	6.5
	39	1781	1726	4.85	11.1	5.0
V21-29	19	305	296	1.77	4.3	2.9
Water Depth	57	233	224	1.80	3.1	4.2
712	76	183	174	1.71	3.1	4.6
	95	158	147	1.51	2.4	9.4
	114	114	104	1.52	1.9	6.6
	133	122	113	2.02	2.4	6.6
Y69-106P	2	2784	2749	6.52	7.6	1.2
Water Depth	11	2384	2343	5.73	4.1	3.7
2870	20	2408	2353	6.24	3.8	4.6
	35	2226	2184	4.57	4.2	3.2
	44	2521	2473	6.14	5.5	4.0

Table 4.2. *Continued*.

Core ID	Depth cm	Ba (Total) (ug/g)	BioBa ug/g	xsTho dpm/g	SiO2 wt%	Authi U ppm
TR163-38	19	1251	1108	2.07	11.1	3.1
Water Depth	38	1065	875	1.82	12.5	3.7
2200	57	1134	1028	2.48	10.5	8.1
	76	842	742	2.11	9.6	8.4
	95	617	494	1.91	9.2	9.3
	114	684	586	1.85	5.5	9.7
	133	919	802	2.25	9.5	11.2
TR163-33	45	1277	1216	3.13	7.3	4.4
Water Depth	60	1114	1061	2.69	11.0	4.1
2230	75	1026	964	2.72	3.6	4.9
	90	1112	1044	2.67	3.3	5.2
TR163-22	37	2469	2449	6.65	13.6	2.9
Water Depth	75	2047	2029	5.29	10.4	4.9
2830	112	1797	1775	5.10	20.3	4.9
	150	1714	1684	5.55	17.4	6.6
	187	1656	1614	5.29	21.0	5.9
	225	1671	1635	5.27	18.5	4.9
ME0005A-43JC	3	784	699	1.92	nd	5.7
Water Depth	43	744	663	1.82	11.0	6.4
1368	83	527	459	1.48	9.3	5.8
	123	528	450	1.62	nd	7.1
	163			1.80	22.6	5.5
	206	461	394	1.37	20.5	4.9

4.5.1. BioBa MARs and implications for paleoproductivity

^{230}Th-normalized bioBa MARs in the Panama Basin range between 104 – 3605 μg cm^{-2}ka^{-1} (Figure 4.2). The lowest bioBa MARwas observed in the shallowest core (V21-29, depth 712 m) and the highest bioBa MARin the deepest core Y69-106P (Figure 4.2) in our study. ^{230}Th-normalized bioBa MARs in our cores show a linear relationship with increasing depth in the water column (Figure 4.3). The correlation coefficient, r^2, for the linear regression of Holocene bioBa averages versus depth is 0.83, while that for glacial bioBa averages versus depth is 0.93 (Figure 4.3). Furthermore, the slopes of the correlation lines (Holocene and glacial) are identical, within error, and for any depth the ^{230}Th normalized MAR is higher during the Holocene than during the last glacial (Figure 3) suggesting that productivity was higher during the Holocene than during the last glacial. Our finding that fluxes of bioBa are generally lower in the glacial than in the Holocene is consistent with that of other bioBa MAR studies of the Southern Ocean (Jaccard et al., 2005), subarctic Pacific NW Pacific (Brunelle et al., 2007; Brunelle et al., 2010; Jaccard et al., 2009) and NE Pacific (Jaccard et al., 2009).

An increase in Ba concentration with depth is typical of dissolved Ba profiles in the Pacific Ocean (Chan et al., 1977; Monnin et al., 1999). Our bioBa MARs fit the perfect pelagic sedimentation pattern showing values that are lower at ridge tops (surrounding ridges of the Panama Basin include the Cocos and Carnegie Ridges) than those in deeper parts of the basin.

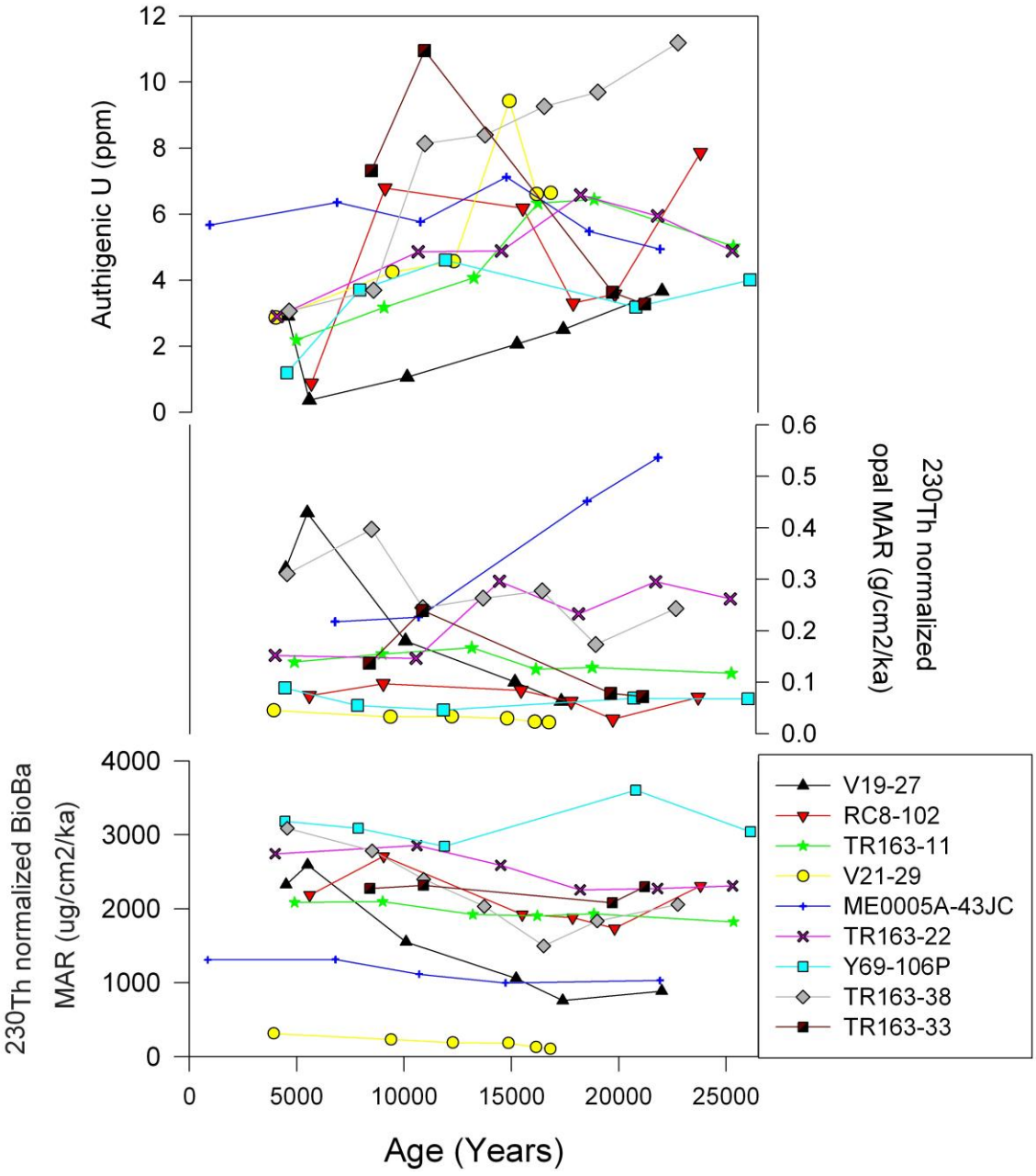

Figure 4.2. ^{230}Th normalized fluxes of biogenic Barium and Opal, and authigenic U at our study sites (Figure 4.1).

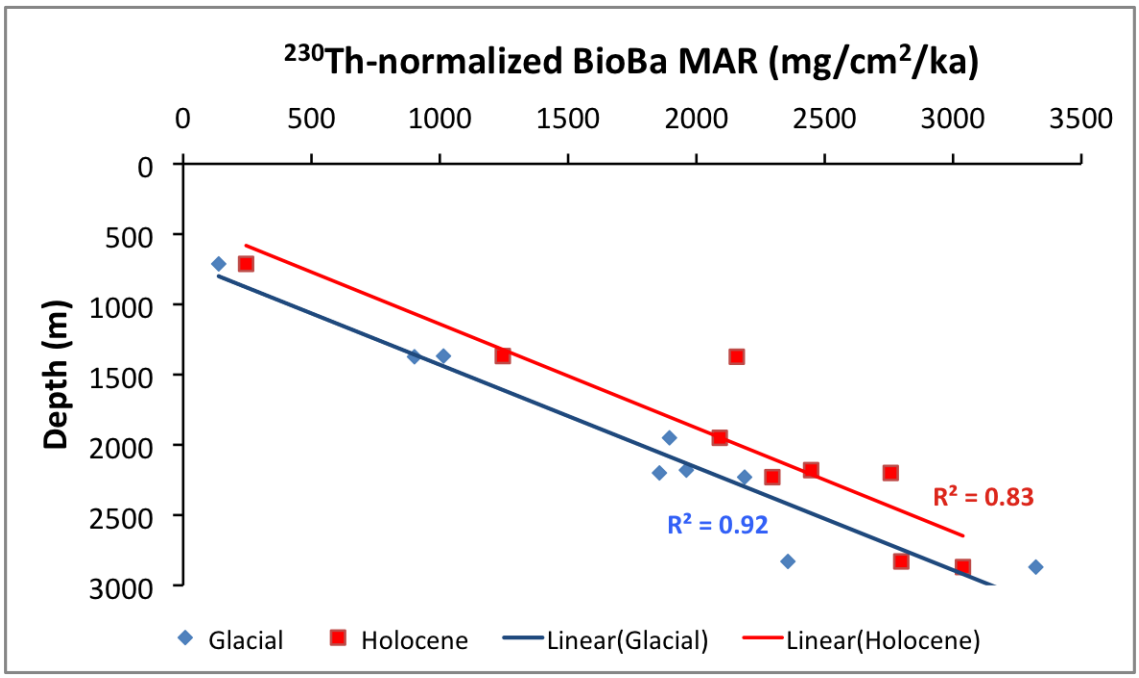

Figure 4.3. A linear relationship between ^{230}Th normalized bioBa and water depth for the Holocene and the last glacial is shown. Note that for any depth the Holocene bioBa MAR is always higher.

These observations provide support for the ideas put forward by Bishop (1988) according to which barite formation takes place in microenvironments of decaying remains of siliceous organisms. The similarity in bioBa and opal (next section) MARs (i.e. higher during Holocene than those during glacial) in the Panama Basin suggests that it is likely the barite formation takes place by decay of organic matter (Dymond et al., 1992), and probably regeneration at the ocean floor (Chan et al., 1977). Our bioBa concentrations either stayed stable or increased toward the surface, i.e., showing no signs of loss towards the surface, suggesting no loss of bioBa due to diagenetic mobilization as seen in some continental margin areas (McManus et al., 1998).

A linear relationship between bioBa concentration and water depth was also noted in marginal surface sediments of the western Indian subcontinent (Babu et al., 2002) and Peruvian slope and shelf (von Breymann et al., 1990). In addition, in both of these studies the pattern of bioBa concentration was coherent with surface productivity (von Breymann et al., 1990). Here, in both the Holocene and last glacial, our bioBa MARs follow neither surface productivity (surface chlorophyll, Figure 4.1) nor sedimentation rate patterns, despite the linear correlation with water depth.

4.5.2. Biogenic silica burial and implications for paleoproductivity

^{230}Th normalized fluxes of opal in our study area range between 0.02 (V21-29) – 0.54 (ME0005A-43JC) g cm^{-2} ka^{-1}. Our range of opal fluxes is slightly higher than the ranges in Bradtmiller et al. (~0.02–0.36 μg cm^{-2}ka^{-1}; 2006; 2010) and in Dubois et al. (~ 0.2–0.4 μg cm^{-2}ka^{-1}; 2010). ^{230}Th normalized opal MARs for 7 of our 9 cores are higher during the Holocene (1-13 ka). Only in cores ME0005A-43JC and TR163-22 are opal MARs higher during the last glacial (Figure 4.2). Our findings of lower glacial and higher Holocene ^{230}Th normalized opal fluxes are consistent with a three-box model estimate of ^{230}Th-normalized opal fluxes for the Holocene (0-10ka) and glacial (18-28ka) in the eastern, central and western equatorial Pacific Ocean (Bradtmiller et al., 2006). Further

corroborating evidence for lower opal burial in the Pacific during the last glacial (13-25 ka) comes from the NW and NE Pacific (Brunelle et al., 2007; Crusius et al., 2004; Jaccard et al., 2005; Jaccard et al., 2009; Galbraith et al., 2007), and SE Pacific (Muratli et al., 2010). Hence, there is a substantial body of evidence which suggests lower (or unchanged, western Pacific, Bradtmiller et al., 2010) opal burial during the last glacial throughout Pacific Ocean.

4.5.3. Authigenic uranium and implications for paleoredox conditions

Concentrations of U_{auth} range from 0.4 (ppm) in core V19-27 to 11.1 (ppm) in core TR163-38 (Figure 2). Our range is similar to that observed by Kienast et al. (2007) and Bradtmiller et al. (2010). U_{auth} in this study, in Bradtmiller et al. (2010) and in Kienast, et al. (2007) represent different hydrographic regimes and water depths from the EEP and yet they yield similar results, namely, that glacial U_{auth} concentrations were higher, up to 4 times, than those during the Holocene (except for core ME0005A-43JC on the Cocos Ridge). U_{auth} concentrations in Holocene sediments is low and approaches zero in some instances (Figure 2). The glacial-interglacial pattern of U_{auth} concentration is the opposite of that observed for both bioBa and opal fluxes. If bioBa and opal fluxes are controlled by the rate of organic matter supply, then the rate of organic matter supply was greater during the Holocene (Figure 2&3). Such findings suggest that the rate of organic matter supply is not driving the accumulation of U_{auth} in the sediments of EEP for the last 25 ka. This decoupling of sedimentary proxies for export production versus redox sensitivity is identical to that noted throughout the Pacific Ocean (Bradtmiller, et al., 2006; Bradtmiller et al., 2009; Crusius et al., 2004; Galbraith et al., 2007; Kienast et al., 2006, Jaccard et al., 2005, Jaccard et al., 2009).

4.5.4. Regional synthesis of paleoproductivity and paleoredox conditions and implications to atmospheric CO_2 variation

An understanding of changing export production on glacial-interglacial timescales in the EEP is important because this region is responsible for 18-56% of the global oceanic new productivity (Chavez and Barber, 1987), and export of CO_2 from the surface to the deep ocean (Broecker 1982a/b). Previous estimates of barite and calcite MARs have been based on calculating linear sedimentation rates that suggest that primary productivity and export production in the EEP was higher during the last glacial (Lyle et al., 1988; Lyle et al., 2002; Pedersen, 1983; Paytan et al., 1996). This view has been contradicted by estimates, based on ^{230}Th normalization, of biogenic silica and calcite fluxes, and bulk MARs during the last glacial (Bradtmiller et al., 2006; Bradtmiller et al., 2010; Loubere et al., 2004; Kienast et al., 2006; Kienast et al., 2007, Singh et al., 2011) that suggest that the productivity was not higher in the EEP and in the central Pacific Ocean (Marcantonio et al., 1996; Marcantonio et al., 2001). Our bioBa and opal MAR estimates based on ^{230}Th normalization technique in most cores also show lower glacial biogenic fluxes in the EEP compared to the same fluxes during the Holocene. If these fluxes are proxies for paleoproductivity then the implication is that a reduction in atmospheric CO_2 during the last glacial is not supported by the pattern of changing productivity in the EEP. In Figure 4, we have also summarized all of the available authigenic U data for the EEP. Almost always glacial/Holocene U_{auth} ratios are greater than 1 (Figure 4). Increased U_{auth} concentrations during glacial times when surface productivity was lower, as suggested by the bioBa and opal MARs, indicate that changes in redox conditions were not a byproduct of respiration of organic matter exported through the water column. Rather, it is likely that lower oxygen content in deep waters was causing an enrichment of U_{auth} in glacial sediments. Our findings are in agreement with those of Jaccard et al. (2009) in the north Pacific and Bradtmiller et al. (2010) in the EEP.

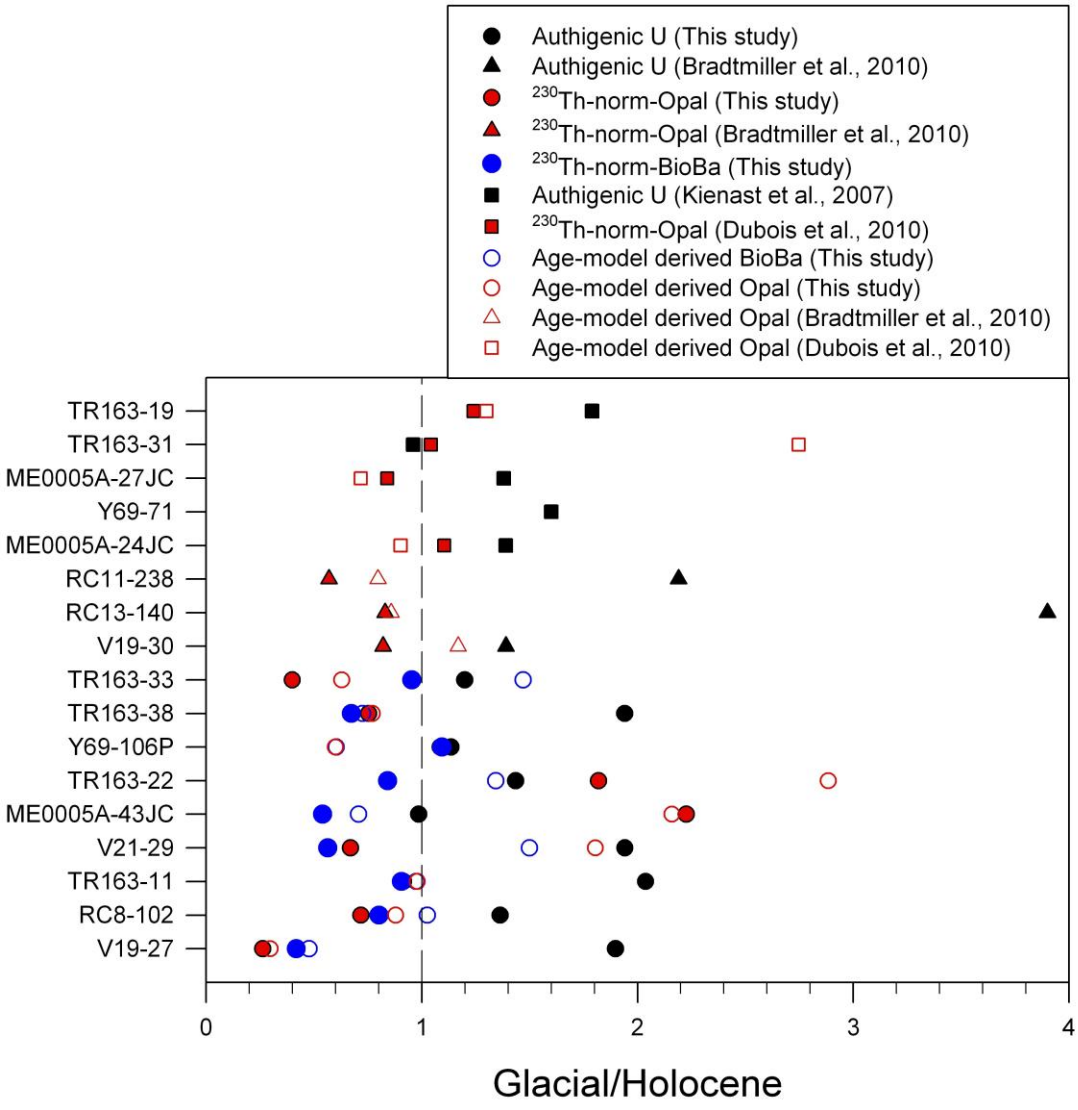

Figure 4.4 Glacial to Holocene ratios of authigenic Uranium in the EEP. It is obvious that U_{auth} is higher during the last glacial.

It has been suggested that during the last glacial silicic acid from the Southern Ocean leaked into EEP through the EUC and SAMW resulting in higher opal burial at lower latitudes (Brzezinski et al., 2002; Matsumoto et al., 2002). Silicate availability in the EEP would favor growth of diatoms over cocolithophores (Dugdale and Wilkerson, 2001), eventually leading to a lowering of CO_2 in the atmosphere by up to 50 ppmv (Archer et al., 2000). However, our opal fluxes in the EEP, in addition to those previously published (Bradtmiller et al., 2006; Bradtmiller et al., 2010; Kienast et al., 2006), are lower during the last glacial, suggesting that conditions in the EEP were still limited by silicic acid. Upon comparison to other opal flux estimates in the Pacific Ocean, it is evident that lower opal burial during the last glacial compared to that during the Holocene is a reality for most of the Pacific Basin (Brunelle et al., 2007; Bradtmiller et al., 2006; Bradtmiller et al., 2010; Crusius et al., 2004; Jaccard et al., 2005; Jaccard et al., 2009; Galbraith et al., 2007; Kienast et al., 2006; Muratli et al., 2010).

Bradtmiller et al. (2010) provide crucial biomarker evidence for a lower glacial opal flux in the EEP by showing that the brassicasterol flux (proxy for diatom production) is a function of opal flux and the oxygen content of bottom waters. In general, higher fluxes of brassicasterol during the last glacial was a function increased preservation efficiency because of low-oxygen bottom waters. Koutavas and Sachs (2008) have also shown that alkenone fluxes during glacial times were higher than those during the Holocene, probably due to higher preservation in low oxygen and high dissolved-nutrient waters, which is consistent with the deep water characteristics of the North Pacific during the glacial (Jaccard et al., 2009).

Fe, contained in dust is also a limiting micronutrient for phytoplankton growth (Martin 1990; Coale et al., 1996). In the EEP 25 ka dust fluxes were about a factor of 2 higher during the last glacial (Singh et al., 2011) compared to those during the Holocene. Similar patterns of glacial-interglacial dust flux variability were reported at sites throughout the equatorial Pacific (Anderson et al., 2006; McGee et al., 2007; Winckler et

al., 2008). Further support of increased glacial dust fluxes to the Panama Basin comes from a terrestrial derived C_{26}-alcohol proxy (Calvo et al., 2011). Given higher dust fluxes during the glacial, it is unlikely that export production was limited by Fe at this time.

Ocean stratification may be a mechanism that can explain the observed phenomena of lower biogenic fluxes along with higher authigenic U fluxes during the last glacial. It is likely that such a stratified ocean caused reduced upwelling/ventilation which, in turn, would cut off supply of CO_2 from the ocean to the atmosphere (Galbraith and Jaccard, 2008), prohibiting escape of respired carbon into the atmosphere (Sigman and Boyle, 2000; Toggweiler, 1999). Although sedimentary fluxes of bioBa and opal during the last glacial were lower, U_{auth} concentrations were higher suggesting glacial bottom waters were depleted in oxygen. This oxygen depletion may imply that the respired carbon in deep waters of the EEP were higher during glacial. Since the source of ^{14}C is atmospheric, once CO_2 is sequestered in the deep ocean carbon pool, ^{14}C will decay unless it is replenished by ventilation. Therefore the radiocarbon content of poorly ventilated waters should be very low. Reduced ventilation can be traced by analyzing radiocarbon age differences ($\Delta^{14}C$) in planktic-benthic formaminifera from the same sediment interval. The $\Delta^{14}C$ off the coast of Baja California has been found to be the highest during the last glacial maximum, and lowest between 15700-14600 and between 13500-12900 yr. B.P. (Marchitto et al., 2007). The $\Delta^{14}C$ results from the eastern Pacific is similar to studies suggesting that the North Pacific was also poorly ventilated during last glacial maximum, but that $\Delta^{14}C$ values increased during the deglacial (Galbraith et al., 2007). Such reduced interaction between surface and deep waters during the last glacial supports the idea that there was a greater transfer of respired carbon to the deeper parts of the ocean causing *p*CO2 to drop (Boyle 1988). Our finding of lower glacial biogenic fluxes in addition to higher glacial U_{auth} concentrations in the EEP support the arguments of Jaccard et al. (2009) and Bradtmiller et al. (2010) concerning a respired nutrient deepening as a cause for lowered CO_2 during the last glacial.

4.6. Conclusions

We have evaluated paleoproductivity and paleoredox conditions for the last 25ka of the EEP at a regional scale using bioBa, opal and U_{auth}. Our main findings are as follows:

1. BioBa MARs suggest that productivity was greater during the Holocene than that during the last glacial (Figure 3). Furthermore, bioBa MARs are positively correlated with water depth during the Holocene and the last glacial. At any depth in the water column the Holocene MAR is always higher than the glacial MAR, again suggesting higher productivity during the Holocene.
2. Opal MARs in the EEP are higher during the Holocene than those during the last glacial (Figure 2). Changing patterns of opal fluxes in the EEP during the last 25 kyr are similar to patterns observed throughout the equatorial Pacific Ocean and north Pacific.
3. U_{auth} is higher in sediments deposited during the last glacial than in those deposited during the Holocene. Since biogenic fluxes are lower during the glacial, enrichment of U_{auth} in glacial sediments suggest that low bottom water oxygen contents rather than respiration of organic matter driving U_{auth} enrichment.
4. The oxygen depletion in bottom waters during the last glacial suggests that bottom waters were enriched in respired carbon. Reduced glacial ventilation seems to further drive the intermediate nutrient gradient towards the seafloor. Such conditions during the glacial might have been responsible for lower pCO_2 of the atmosphere.

CHAPTER V
SUMMARY AND CONCLUSIONS

In the Panama Basin, xs^{230}Th-derived MARs are lower than age-model derived MARs, and leads to the prediction that significant sediment focusing (i.e., lateral redistribution of sediments by deep-sea currents) occurs. Downslope transport from surrounding ridge tops has been proposed as a source for excess inventory of xs^{230}Th found in the deepest parts of the basin. We have tested this hypothesis and find an ubiquitous presence of larger-than-expected inventories of xs^{230}Th on the tops and flanks of ridges that surround the Panama Basin. Focusing factors in these regions are as high as those in the deeper parts of the basins suggesting the ridges and flanks are not supplying the high inventories of xs^{230}Th to the deep basin.

The spatio-temporal distribution of focusing factors and MARs are such that the highest average values are those determined for sediment deposited during the last glacial in the equatorial cores. Lowest sediment focusing factors (still greater than 1, for the most part) are determined for the non-equatorial cores during the Holocene. Higher equatorial focusing factors during the glacial could be related to scavenging effects on ^{230}Th driven by higher productivity in the Panama Basin. To determine whether this is the case, more data is needed: specifically, a complementary latitudinal transect study of water column ^{230}Th between high- and low-particle flux regions, and better control on the erosional areas. Based on ^{232}Th flux measurements, we hypothesize that the location at which eolian (as opposed to riverine) fluxes dominate the detrital flux occurs at approximately 300 km from the margin.

Dissolved ^{230}Th concentrations are lowest in Panama Basin waters, and highest in Peru Basin waters. Reversible scavenging cannot explain ^{230}Th profiles below 1000 m in the Panama Basin and below 2000 m in the Peru Basin, and intensified scavenging below these depths needs to be invoked. It is likely that both increased particle fluxes near the

equator and resuspension of Mn-rich particulates play an important role in causing the ^{230}Th deficits encountered in deep waters of the Panama and Peru Basins.

Since we know that deep waters in the Panama Basin are being flushed with waters from the Peru Basin, we can estimate the advection of dissolved ^{230}Th to the Panama Basin using a simplified one-dimensional model. Based on the best estimate for Panama Basin deep-water residence time, we have estimated the advected flow of ^{230}Th from the Peru Basin to be between about ~0.0038 and 0.0077 dpm m^{-3} yr^{-1}. These values suggest an additional 15-30% of ^{230}Th is being delivered to the Panama Basin over that which is produced *in situ* there. General Circulation Models (Henderson et al., 1999; Siddall et al., 2008) suggest a similar sensitivity for the ^{230}Th constant-flux technique. Finally, our dissolved ^{232}Th concentrations are among the lowest measured in the world's oceans, and are consistent with the low eastern tropical Pacific Ocean dust fluxes modeled in recent studies (Jickells et al., 2005; Maher et al., 2010; Mahowald et al., 2005).

We have evaluated paleoproductivity and paleoredox conditions for the last 25ka of the EEP at a regional scale using bioBa, opal and U_{auth}. Our main findings are as follows. BioBa MARs suggest that productivity was greater during the Holocene than that during the last glacial (Figure 3). Furthermore, bioBa MARs are positively correlated with water depth during the Holocene and the last glacial. At any depth in the water column the Holocene MAR is always higher than the glacial MAR, again suggesting higher productivity during the Holocene. Opal MARs in the EEP are higher during the Holocene than those during the last glacial (Figure 2). Changing patterns of opal fluxes in the EEP during the last 25 kyr are similar to patterns observed throughout the equatorial Pacific Ocean and north Pacific. U_{auth} is higher in sediments deposited during the last glacial than in those deposited during the Holocene. Since biogenic fluxes are lower during the glacial, enrichment of U_{auth} in glacial sediments suggest that low bottom water oxygen contents rather than respiration of organic matter driving U_{auth} enrichment. The oxygen depletion in bottom waters during the last glacial suggests that bottom waters were

enriched in respired carbon. Reduced glacial ventilation seems to further drive the intermediate nutrient gradient towards the seafloor. Such conditions during the glacial might have been responsible for lower pCO_2 of the atmosphere.

REFERENCES

Anderson, R.F., Bacon, M.P., Brewer, P.G., 1983. Removal of Th-230 and Pa-231 at Ocean Margins. Earth and Planetary Science Letters, 66(1-3): 73-90.

Anderson, R.F., Fleisher, M.Q., Lao, Y., 2006. Glacial-interglacial variability in the delivery of dust to the central equatorial Pacific Ocean. Earth and Planetary Science Letters, 242 (3-4): 406-414.

Anderson, R.F., Lao, Y., Broecker, W.S., Trumbore, S.E., Hofmann, H.J., Wolfi, W., 1990. Boundary Scavenging in the Pacific-Ocean - a Comparison of Be-10 and Pa-231. Earth and Planetary Science Letters, 96(3-4): 287-304.

Archer, D., Winguth, A., Lea, D., Mahowald, N., 2000. What caused the glacial/interglacial atmospheric pCO(2) cycles? Reviews of Geophysics, 38(2): 159-189.

Babu, C.P., Brumsack, H.J., Schnetger, B., Bottcher, M.E., 2002. Barium as a productivity proxy in continental margin sediments: a study from the eastern Arabian Sea. Marine Geology, 184(3-4): 189-206.

Bacon, M.P., 1984. Glacial to Interglacial Changes in Carbonate and Clay Sedimentation in the Atlantic-Ocean Estimated from Th-230 Measurements. Isotope Geoscience, 2(2): 97-111.

Bacon, M.P., Anderson, R.F., 1982. Distribution of Thorium Isotopes between Dissolved and Particulate Forms in the Deep-Sea. Journal of Geophysical Research-Oceans and Atmospheres, 87(Nc3): 2045-2056.

Bacon, M.P., Huh, C.A., Moore, R.M., 1989. Vertical Profiles of Some Natural Radionuclides over the Alpha-Ridge, Arctic Ocean. Earth and Planetary Science Letters, 95(1-2): 15-22.

Barnes, C.E., Cochran, J.K., 1990. Uranium Removal in Oceanic Sediments and the Oceanic-U Balance. Earth and Planetary Science Letters, 97(1-2): 94-101.

Barnola, J.M., Raynaud, D., Korotkevich, Y.S., Lorius, C., 1987. Vostok Ice Core Provides 160,000-Year Record of Atmospheric Co2. Nature, 329(6138): 408-414.

Behrenfeld, M.J., Boss, E., Siegel, D.A., Shea, D.M., 2005. Carbon-based ocean productivity and phytoplankton physiology from space. Global Biogeochemical Cycles, 19, GB1006, doi:10.1029/2004GB002299.

Benway, H. M., A. C. Mix, B. A. Haley, and G. P. Klinkhammer 2006. Eastern Pacific warm pool paleosalinity and climate variability: 0–30 kyr, Paleoceanography, 21, PA3008, doi:10.1029/2005PA001208

Bishop, J.K.B., 1988. The Barite-Opal-Organic Carbon Association in Oceanic Particulate Matter. Nature, 332(6162): 341-343.

Boyle, E.A., 1988. Vertical Oceanic Nutrient Fractionation and Glacial Interglacial CO_2 Cycles. Nature, 331(6151): 55-56.

Bradtmiller, L.I., Anderson, R.F., Fleisher, M.Q., Burckle, L.H., 2006. Diatom productivity in the equatorial Pacific Ocean from the last glacial period to the present: A test of the silicic acid leakage hypothesis. Paleoceanography, 21(4). PA4201, doi:10.1029/2006PA001282

Bradtmiller, L. I., R. F. Anderson, J. P. Sachs, and M. Q. Fleisher., 2010. A deeper respired carbon pool in the glacial equatorial Pacific Ocean, Earth and Planetary Science Letters, 299(3-4), 417-425

Broecker, W., 2008. Excess sediment ^{230}Th: Transport along the sea floor or enhanced water column scavenging? Global Biogeochemical Cycles, 22, GB1006, doi:10.1029/2007GB003057.

Broecker, W.S., 1982a. Glacial to Interglacial Changes in Ocean Chemistry. Progress in Oceanography, 11(2): 151-197.

Broecker, W.S., 1982b. Ocean Chemistry during Glacial Time. Geochimica Et Cosmochimica Acta, 46(10): 1689-1705.

Brumsack, H.J., Gieskes, J.M., 1983. Interstitial Water Trace-Metal Chemistry of Laminated Sediments from the Gulf of California, Mexico. Marine Chemistry, 14(1): 89-106.

Brunelle, B.G. et al., 2007. Evidence from diatom-bound nitrogen isotopes for subarctic Pacific stratification during the last ice age and a link to North Pacific denitrification changes. Paleoceanography, 22(1).

Brunelle, B.G. et al., 2010. Glacial/interglacial changes in nutrient supply and stratification in the western subarctic North Pacific since the penultimate glacial maximum. Quaternary Science Reviews, 29(19-20): 2579-2590.

Brzezinski, M.A. et al., 2002. A switch from Si(OH)(4) to NO3- depletion in the glacial Southern Ocean. Geophysical Research Letters, 29(12).

Chan, L.H., Drummond, D., Edmond, J.M., Grant, B., 1977. Barium Data from Atlantic Geosecs Expedition. Deep-Sea Research, 24(7): 613-649.

Chase, Z., Anderson, R.F., Fleisher, M.Q., and Kubik, P.W., 2002. The influence of particle composition and particle flux on scavenging of Th, Pa and Be in the ocean. Earth and Planetary Science Letters 204, 215-229.

Chavez, F.P. et al., 1999. Biological and chemical response of the equatorial Pacific Ocean to the 1997-98 El Nino. Science, 286(5447): 2126-2131.

Chavez, F.P., Barber, R.T., 1987. An Estimate of New Production in the Equatorial Pacific. Deep-Sea Research Part a-Oceanographic Research Papers, 34(7): 1229-1243.

Coale, K.H. et al., 1996. A massive phytoplankton bloom induced by an ecosystem-scale iron fertilization experiment in the equatorial Pacific Ocean. Nature, 383(6600): 495-501.

Cochran, J.K., Hirschberg, D.J., Livingston, H.D., Buesseler, K.O., Key, R.M., 1995. Natural and anthropogenic radionuclide distributions in the Nansen Basin, Arctic Ocean: Scavenging rates and circulation timescales. Deep-Sea Research Part Ii-Topical Studies in Oceanography, 42(6): 1495-1517.

Coppola, L., Roy-Barman, M., Mulsow, S., Povinec, P., Jeandel, C., 2006. Thorium isotopes as tracers of particles dynamics and deep water circulation in the Indian sector of the Southern Ocean (ANTARES IV). Marine Chemistry, 100(3-4): 299-313.

Cravatte, S., Madec, G., Izumo, T., Menkes, C., Bozec, A., 2007. Progress in the 3-D circulation of the eastern equatorial Pacific in a climate ocean model. Ocean Modelling, 17(1): 28-48.

Crusius, J., Pedersen, T.F., Kienast, S., Keigwin, L., Labeyrie, L., 2004. Influence of northwest Pacific productivity on North Pacific Intermediate Water oxygen concentrations during the Boiling-Allerod interval (14.7-12.9 ka). Geology, 32(7): 633-636.

Dehairs, F., Chesselet, R., Jedwab, J., 1980. Discrete Suspended Particles of Barite and the Barium Cycle in the Open Ocean. Earth and Planetary Science Letters, 49(2): 528-550.

Detrick, R.S., Williams, D.L., Mudie, J.D., Sclater, J.G., 1974. Galapagos Spreading Center - Bottom-Water Temperatures and Significance of Geothermal Heating. Geophysical Journal of the Royal Astronomical Society, 38(3): 627-637.

Dowding, L.G., 1977. Sediment Dispersal within Cocos Gap, Panama Basin. Journal of Sedimentary Petrology, 47(3): 1132-1156.

Dubois, N. et al., 2010. Sedimentary opal records in the eastern equatorial Pacific: It is not all about leakage. Global Biogeochemical Cycles, 24: -.

Dugdale, R.C., Wilkerson, F.P., 1998. Silicate regulation of new production in the equatorial Pacific upwelling. Nature, 391(6664): 270-273.

Dugdale, R.C., Wilkerson, F.P., Minas, H.J., 1995. The Role of a Silicate Pump in Driving New Production. Deep-Sea Research Part I-Oceanographic Research Papers, 42(5): 697-719.

Dymond, J., 1981. Geochemistry of Nazca plate surface sediments: An evaluation of hydrothermal, biogenic, detrital and hydrogenous sources. Geol. Soc. Am. Mem. 154, 133–173

Dymond, J., Suess, E., Lyle, M., 1992. Barium in Deep-Sea Sediment: A Geochemical Proxy for Paleoproductivity. Paleoceanography, 7(2): 163-181.

Edmonds, H.N., Moran, S.B., Hoff, J.A., Smith, J.N., Edwards, R.L., 1998. Protactinium-231 and thorium-230 abundances and high scavenging rates in the western Arctic Ocean. Science, 280(5362): 405-407.

Fiedler, P.C., Philbrick, V., Chavez, F.P., 1991. Oceanic Upwelling and Productivity in the Eastern Tropical Pacific. Limnology and Oceanography, 36(8): 1834-1850.

Fiedler, P.C., Talley, L.D., 2006. Hydrography of the eastern tropical Pacific: A review. Progress in Oceanography, 69(2-4): 143-180.

Francois, R. et al., 2007. Comment on "Do geochemical estimates of sediment focusing pass the sediment test in the equatorial Pacific?" by M. Lyle et al. Paleoceanography, 22, PA1216, doi:10.1029/2005PA001235.

Francois, R., Frank, M., van der Loeff, M.M.R., Bacon, M.P., 2004. Th-230 normalization: An essential tool for interpreting sedimentary fluxes during the late Quaternary. Paleoceanography, 19, PA1018, doi:10.1029/2003PA000939.

Francois, R., Honjo, S., Manganini, S.J., Ravizza, G.E., 1995. Biogenic Barium Fluxes to the Deep-Sea - Implications for Paleoproductivity Reconstruction. Global Biogeochemical Cycles, 9(2): 289-303.

Frank, M., Eckhardt, J.-D., Eisenhauer, A., Kubik, P.W., Dittrich-Hannen, B., Segl, M., and Mangini, A., 1994. Beryllium 10, thorium 230, and protactinium 231 in Galapagos

Microplate sediments: implications of hydrothermal activity and paleoproductivity changes during the last 100,000 years. Paleoceanography 9, 559-578.

Froelich, P.N. et al., 1979. Early Oxidation of Organic-Matter in Pelagic Sediments of the Eastern Equatorial Atlantic - Suboxic Diagenesis. Geochimica Et Cosmochimica Acta, 43(7): 1075-1090.

Galbraith, E.D. et al., 2007. Carbon dioxide release from the North Pacific abyss during the last deglaciation. Nature, 449(7164): 890-U9.

Galbraith, E.D. et al., 2008. Consistent relationship between global climate and surface nitrate utilization in the western subarctic Pacific throughout the last 500 ka. Paleoceanography, 23(2).

Ganeshram, R.S., Francois, R., Commeau, J., Brown-Leger, S.L., 2003. An experimental investigation of Barite formation in seawater. Geochimica Et Cosmochimica Acta, 67(14): 2599-2605.

Gao, Y., Fan, S.M., Sarmiento, J.L., 2003. Aeolian iron input to the ocean through precipitation scavenging: A modeling perspective and its implication for natural iron fertilization in the ocean. Journal of Geophysical Research-Atmospheres, 108, 4221, doi:10.1029/2002JD002420

Goldberg, E.D., Arrhenius, G.O.S., 1958. Chemistry of Pacific Pelagic Sediments. Geochimica Et Cosmochimica Acta, 13(2-3): 153-212.

Heath, G.R., Moore, T.C., Roberts, G.L., 1974. Mineralogy of Surface Sediments from Panama-Basin, Eastern-Equatorial Pacific. Journal of Geology, 82(2): 145-160.

Heezen, B.C., Rawson, M., 1977. Visual Observations of Contemporary Current Erosion and Tectonic Deformation on Cocos Ridge Crest. Marine Geology, 23(1-2): 173-196.

Henderson, G.M., Anderson, R.F., 2003. The U-series toolbox for paleoceanography, Reviews in Mineralogy and Geochemistry "Uranium Series Geochemistry" 53 493 – 531.

Henderson, G.M., Heinze, C., Anderson, R.F., Winguth, A.M.E., 1999. Global distribution of the Th-230 flux to ocean sediments constrained by GCM modelling. Deep-Sea Research Part I-Oceanographic Research Papers, 46(11): 1861-1893.

Higgins, S.M., Anderson, R.F., Marcantonio, F., Schlosser, P., Stute, M., 2002. Sediment focusing creates 100-ka cycles in interplanetary dust accumulation on the Ontong Java Plateau. Earth and Planetary Science Letters, 203(1): 383-397.

Higgins, S.M., Broecker, W., Anderson, R., McCorkle, D.C., Timothy, D., 1999. Enhanced Sedimentation along the equator in the western Pacific. Geophysical Research Letters, 26(23): 3489-3492.

Hsieh, Y.T., Henderson, G.M., Thomas, A.L., 2011. Combining seawater Th-232 and Th-230 concentrations to determine dust fluxes to the surface ocean. Earth and Planetary Science Letters, 312(3-4): 280-290.

Huh, C.A., Beasley, T.M., 1987. Profiles of Dissolved and Particulate Thorium Isotopes in the Water Column of Coastal Southern-California. Earth and Planetary Science Letters, 85(1-3): 1-10.

Huh, C.A., Kelley, J.M., Murray, J.W., Wei, C.L., 1994. Water Column Distribution of Th-230 and Th-232 in the Black-Sea. Deep-Sea Research Part I-Oceanographic Research Papers, 41(1): 101-112.

Jaccard, S.L. et al., 2005. Glacial/interglacial changes in subarctic North Pacific stratification. Science, 308(5724): 1003-1006.

Jaccard, S.L. et al., 2009. Subarctic Pacific evidence for a glacial deepening of the oceanic respired carbon pool. Earth and Planetary Science Letters, 277(1-2): 156-165.

Jickells, T.D. et al., 2005. Global iron connections between desert dust, ocean biogeochemistry, and climate. Science, 308(5718): 67-71.

Kessler, W.S., 2006. The circulation of the eastern tropical Pacific: A review. Progress in Oceanography, 69(2-4): 181-217.

Kienast, S.S., Kienast, M., Jaccard, S., Calvert, S.E., Francois, R., 2006. Testing the silica leakage hypothesis with sedimentary opal records from the eastern equatorial Pacific over the last 150 kyrs. Geophysical Research Letters, 33(15): -.

Kienast, S.S., Kienast, M., Mix, A.C., Calvert, S.E., Francois, R., 2007. Thorium-230 normalized particle flux and sediment focusing in the Panama Basin region during the last 30,000 years. Paleoceanography, 22, , PA2213, doi:10.1029/2006PA001357.

Klinkhammer, G.P., Palmer, M.R., 1991. Uranium in the Oceans - Where It Goes and Why. Geochimica Et Cosmochimica Acta, 55(7): 1799-1806.

Knauss, K.G., Ku, T.L., Moore, W.S., 1978. Radium and Thorium Isotopes in Surface Waters of East Pacific and Coastal Southern-California. Earth and Planetary Science Letters, 39(2): 235-249.

Koutavas, A., and J. P. Sachs., 2008. Northern timing of deglaciation in the eastern equatorial Pacific from alkenone paleothermometry, Paleoceanography, 23, PA4205, doi:10.1029/2008PA001593.

Koutavas, A., Lynch-Stieglitz, J., 2003. Glacial-interglacial dynamics of the eastern equatorial Pacific cold tongue Intertropical Convergence Zone system reconstructed from oxygen isotope records. Paleoceanography, 18(4), 1089, doi:10.1029/2003PA000894.

Koutavas, A., Lynch-Stieglitz, J., Marchitto, T.M., Sachs, J.P., 2002. El Nino-like pattern in ice age tropical Pacific sea surface temperature. Science, 297(5579): 226-230.

Kowsmann, R.O., 1973. Coarse Components in Surface Sediments of Panama-Basin, Eastern Equatorial Pacific. Journal of Geology, 81(4): 473-494.

Kretschmer, S., Geibert, W., Rutgers van der Loeff, M.M., and Mollenhauer, G., 2010. Grain size effects on 230Thxs inventories in opal-rich and carbonate-rich marine sediments. Earth and Planetary Science Letters 294, 131-142.

Krishnaswami, S., 1976. Authigenic Transition-Elements in Pacific Pelagic Clays. Geochimica Et Cosmochimica Acta, 40(4): 425-434.

Krishnaswami, S., Lal, D., Somayajulu, B.L.K., Weiss, R.F., Craig, H., 1976. Large-Volume Insitu Filtration of Deep Pacific Waters - Mineralogical and Radioisotope Studies. Earth and Planetary Science Letters, 32(2): 420-429.

Krishnaswami, S., Sarin, M.M., Somayajulu, B.L.K., 1981. Chemical and Radiochemical Investigations of Surface and Deep Particles of the Indian-Ocean. Earth and Planetary Science Letters, 54(1): 81-96.

Kumar, N. et al., 1995. Increased Biological Productivity and Export Production in the Glacial Southern-Ocean. Nature, 378(6558): 675-680.

Kusch, S., Eglinton, T.I., Mix, A.C., Mollenhauer, G., 2010. Timescales of lateral sediment transport in the Panama Basin as revealed by radiocarbon ages of alkenones, total organic carbon and foraminifera, Earth and Planetary Science Letters, 290(3-4), 340-350. doi:10.1016/j.epsl.2009.12.030

Laird, N.P., 1971. Panama Basin Deep-Water - Properties and Circulation. Journal of Marine Research, 29(3): 226.

Langmuir, D., 1978. Uranium Solution-Mineral Equilibria at Low-Temperatures with Applications to Sedimentary Ore-Deposits. Geochimica Et Cosmochimica Acta, 42(6): 547-569.

Lao, Y. Anderson, W.S. Broecker, S.E. Trumbore, H.J. Hofmann, W. Wolfli., 1992. Transport and Burial Rates of Be-10 and Pa-231 in the Pacific-Ocean during the Holocene Period. Earth and Planetary Science Letters, 113(1-2): 173-189.

Lao, Y., Anderson, R.F., Broecker, W.S., Hofmann, H.J., Wolfli, W., 1993. Particulate Fluxes of Th-230, Pa-231, and Be-10 in the Northeastern Pacific-Ocean. Geochimica Et Cosmochimica Acta, 57(1): 205-217.

Lea, D.W. D.K. Pak, C.L. Belanger, H.J. Spero, M.A. Hall, N.J. Shackleton., 2006. Paleoclimate history of Galapagos surface waters over the last 135,000 yr. Quaternary Science Reviews, 25(11-12): 1152-1167.

Leduc, G. et al., 2007. Moisture transport across Central America as a positive feedback on abrupt climatic changes. Nature, 445(7130): 908-911.

Leduc, G., Vidal, L., Cartapanis, O., Bard, E., 2009. Modes of eastern equatorial Pacific thermocline variability: Implications for ENSO dynamics over the last glacial period. Paleoceanography, 24: -.

Locarnini, R. A., A. V. Mishonov, J. I. Antonov, T. P. Boyer, H. E. Garcia, O. K. Baranova, M. M. Zweng, and D. R. Johnson, 2010. World Ocean Atlas 2009, Volume 1: Temperature. S. Levitus, Ed. NOAA Atlas NESDIS 68, U.S. Government Printing Office, Washington, D.C., 184 pp.

Lonsdale, P., 1977. Inflow of Bottom Water to Panama Basin. Deep-Sea Research, 24(12): 1065-1101

Lonsdale, P., Malfait, B., 1974. Abyssal Dunes of Foraminiferal Sand on Carnegie Ridge. Geological Society of America Bulletin, 85(11): 1697-1712.

Loubere, P., Mekik, F., Francois, R., Pichat, S., 2004. Export fluxes of calcite in the eastern equatorial Pacific from the Last Glacial Maximum to present. Paleoceanography, 19, PA2018. doi:10.1029/2003PA000986

Lukas, R., 1986. The termination of the Equatorial Undercurrent in the eastern Pacific. Progress in Oceanography 16, 63–90

Luthi, D. et al., 2008. High-resolution carbon dioxide concentration record 650,000-800,000 years before present. Nature, 453(7193): 379-382.

Lyle, M., 1988. Climatically Forced Organic-Carbon Burial in Equatorial Atlantic and Pacific Oceans. Nature, 335(6190): 529-532.

Lyle, M., 1992. Composition maps of surface sediments of the eastern tropical Pacific Ocean. In Mayer, L., Pisias, N., Janecek, T., et al., Proc. ODP, Init. Repts., 138 (Pt. 1):College Station, TX (Ocean Drilling Program), 101–115

Lyle, M., A. Mix, N. Pisias., 2002. Patterns of CaCO3 deposition in the eastern tropical Pacific Ocean for the last 150 kyr: Evidence for a southeast Pacific depositional spike during marine isotope stage (MIS) 2, Paleoceanography, 17(2) , 1013, doi : 10 .1029/2000PA000538.

Lyle, M., N. Mitchell, N. Pisias, A. Mix, J. I. Martinez, A. Paytan., 2005. Do geochemical estimates of sediment focusing pass the sediment test in the equatorial Pacific?, Paleoceanography, 20, PA1005, doi:10.1029/2004PA001019.

Lyle, M., Pisias, N., Paytan, A., Martinez, J.I., Mix, A., 2007. Reply to comment by R. Francois et al. on "Do geochemical estimates of sediment focusing pass the sediment test in the equatorial Pacific?": Further explorations of Th-230 normalization. Paleoceanography, 22, PA1217. doi:10.1029/2006PA001373.

Maher, B.A. et al., 2010. Global connections between aeolian dust, climate and ocean biogeochemistry at the present day and at the last glacial maximum. Earth-Science Reviews, 99(1-2): 61-97.

Mahowald, N.M. et al., 2005. Atmospheric global dust cycle and iron inputs to the ocean. Global Biogeochemical Cycles, 19, GB4025, doi:10.1029/2004GB002402.

Mahowald, N.M. et al., 2009. Atmospheric Iron Deposition: Global Distribution, Variability, and Human Perturbations. Annual Review of Marine Science, 1: 245-278.

Malfait, B.T., Van Andel, T.H. 1980. A modern oceanic hardground on the Carnegie Ridge in the eastern Equatorial Pacific, Sedimentology 27 467–496.

Marcantonio, F. et al., 1996. Extraterrestrial He-3 as a tracer of marine sediment transport and accumulation. Nature, 383(6602): 705-707.

Marcantonio, F., R. F. Anderson, S. Higgins, M. Stute, P. Schlosser, P. W. Kubik., 2001a. Sediment focusing in the central equatorial Pacific ocean, Paleoceanography,16, 260– 267.

Marcantonio, F., R. F. Anderson, S. Higgins, M. Q. Fleisher, M. Stute, P. Schlosser., 2001b. Abrupt intensi¢cation of the SW Indian Ocean monsoon during the last deglaciation: constraints from Th, Pa, and He isotopes, Earth and Planetary Science Letters, 184, 505-514.

Marcantonio, F., Woodard, S., Thomas, D., Mcgee, D., Winckler, G., 2008. Extraterrestrial He-3 and constraints on eolian fluxes and provenance in sediments from the Shatsky Rise. Geochimica Et Cosmochimica Acta, 72(12): A591-A591.

Marchal, O., Francois, R., Scholten, J., 2007. Contribution of Th-230 measurements to the estimation of the abyssal circulation (vol 54, pg 557, 2007). Deep-Sea Research Part I-Oceanographic Research Papers, 54(8): 1448-1450.

Marchal, O., Francois, R., Stocker, T.F., Joos, F., 2000. Ocean thermohaline circulation and sedimentary Pa-231/Th-230 ratio. Paleoceanography, 15(6): 625-641.

Marchitto, T.M., Lehman, S.J., Ortiz, J.D., Fluckiger, J., van Geen, A., 2007. Marine radiocarbon evidence for the mechanism of deglacial atmospheric CO_2 rise. Science, 316(5830): 1456-1459.

Martin, J.H., 1990. Glacial-Interglacial Co2 Change: The Iron Hypothesis. Paleoceanography, 5(1): 1-13.

Martinez, I., Keigwin, L., Barrows, T.T., Yokoyama, Y., Southon, J., 2003. La Nina-like conditions in the eastern equatorial Pacific and a stronger Choco jet in the northern Andes during the last glaciation. Paleoceanography, 18(2), 1033.

Martinez, P., Robinson, R.S., 2010. Increase in water column denitrification during the last deglaciation: the influence of oxygen demand in the eastern equatorial Pacific. Biogeosciences, 7(1): 1-9.

Matsumoto, K., Sarmiento, J.L., Brzezinski, M.A., 2002. Silicic acid leakage from the Southern Ocean: A possible explanation for glacial atmospheric pCO(2). Global Biogeochemical Cycles, 16(3).

McGee, D., Marcantonio, F., Lynch-Stieglitz, J., 2007. Deglacial changes in dust flux in the eastern equatorial Pacific. Earth and Planetary Science Letters, 257(1-2): 215-230.

McManus, J. et al., 1998. Geochemistry of barium in marine sediments: Implications for its use as a paleoproxy. Geochimica Et Cosmochimica Acta, 62(21-22): 3453-3473.

McManus, J., Berelson, W.M., Klinkhammer, G.P., Hammond, D.E., Holm, C., 2005. Authigenic uranium: relationship to oxygen penetration depth and organic carbon rain. Geochimica Et Cosmochimica Acta, 69(1): 95-108.

Mix, A.C., N.G. Pisias, W. Rugh, J. Wilson, A. Morey, T. Hagelberg., 1995. Benthic foraminiferal stable isotope record from Site 849, 0-5 Ma: Local and global climate changes. In: Pisias, N.G., L. Mayer, T. Janecek, A. Palmer-Julson, T.H. van Andel (eds.), Proc. ODP, /Scientific Results/ 138, College Station, TX (Ocean Drilling Program), 371-412

Mix, A.C., Tiedemann, R., Blum, P., et al., 2003. Proc. ODP, Init. Repts., 202: College Station, TX (Ocean Drilling Program).doi:10.2973/odp.proc.ir.202.2003

Mollenhauer, G., R. R. Schneider, P. J. Muller,V. Spiess, G. Wefer., 2002. glacial/ interglacial variability in the Benguela upwelling system: Spatial distribution and budgets of organic carbon accumulation, Global Biogeochem. Cycles, 16(4), 1134, doi:10.1029/2001GB001488.

Monnin, C., Jeandel, C., Cattaldo, T., Dehairs, F., 1999. The marine barite saturation state of the world's oceans. Marine Chemistry, 65(3-4): 253-261.

Moore, J.K., Doney, S.C., Lindsay, K., 2004. Upper ocean ecosystem dynamics and iron cycling in a global three-dimensional model. Global Biogeochemical Cycles, 18(4).

Moore, W.S., 1981. The Thorium Isotope Content of Ocean Water. Earth and Planetary Science Letters, 53(3): 419-426.

Moran, S.B. et al., 2001. Constraints on deep water age and particle flux in the Equatorial and South Atlantic Ocean based on seawater Pa-231 and Th-230 data. Geophysical Research Letters, 28(18): 3437-3440.

Moran, S.B. et al., 2002. Dissolved and particulate Pa-231 and Th-230 in the Atlantic Ocean: constraints on intermediate/deep water age, boundary scavenging, and Pa-231/Th-230 fractionation. Earth and Planetary Science Letters, 203(3-4): 999-1014.

Moran, S.B., Charette, M.A., Hoff, J.A., Edwards, R.L., Landing, W.M., 1997. Distribution of Th-230 in the Labrador Sea and its relation to ventilation. Earth and Planetary Science Letters, 150(1-2): 151-160.

Moran, S.B., Hoff, J.A., Buesseler, K.O., Edwards, R.L., 1995. High-Precision Th-230 and Th-232 in the Norwegian Sea and Denmark by Thermal Ionization Mass-Spectrometry. Geophysical Research Letters, 22(19): 2589-2592.

Morford, J.L., Emerson, S., 1999. The geochemistry of redox sensitive trace metals in sediments. Geochimica Et Cosmochimica Acta, 63(11-12): 1735-1750.

Muratli, J.M., Chase, Z., Mix, A.C., McManus, J., 2010. Increased glacial-age ventilation of the Chilean margin by Antarctic Intermediate Water. Nature Geoscience, 3(1): 23-26.

Murray, J.W., Barber, R.T., Roman, M.R., Bacon, M.P., Feely, R.A., 1994. Physical and Biological-Controls on Carbon Cycling in the Equatorial Pacific. Science, 266(5182): 58-65.

Nelson, D.M., Treguer, P., Brzezinski, M.A., Leynaert, A., Queguiner, B., 1995. Production and Dissolution of Biogenic Silica in the Ocean - Revised Global Estimates, Comparison with Regional Data and Relationship to Biogenic Sedimentation. Global Biogeochemical Cycles, 9(3): 359-372.

Nozaki, Y., Horibe, Y., Tsubota, H., 1981. The Water Column Distributions of Thorium Isotopes in the Western North Pacific. Earth and Planetary Science Letters, 54(2): 203-216.

Nozaki, Y., Yamada, M., 1987. Thorium and Protactinum Isotope Distributions in Waters of the Japan Sea. Deep-Sea Research Part a-Oceanographic Research Papers, 34(8): 1417-1430.

Nozaki, Y., Yang, H.S., Yamada, M., 1987. Scavenging of Thorium in the Ocean. Journal of Geophysical Research-Oceans, 92(C1): 772-778.

Okubo, A., Obata, H., Gamo, T., Minami, H., Yamada, M., 2007. Scavenging of Th-230 in the Sulu Sea. Deep-Sea Research Part Ii-Topical Studies in Oceanography, 54(1-2): 50-59.

Okubo, A., Obata, H., Gamo, T., Yamada, M., 2012. 230Th and 232Th distributions in mid-latitudes of the North Pacific Ocean: Effect of bottom scavenging. Earth and Planetary Science Letters, Volumes 339–340, 15 July 2012, Pages 139–150

Okubo, A., Obata, H., Nozaki, Y., Yamamoto, Y., Minami, H., 2004. Th-230 in the Andaman Sea: Rapid deep-sea renewal. Geophysical Research Letters, 31, L22306, doi:10.1029/2004GL020226.

Olivarez Lyle, A., and Lyle, M., 2005. Organic carbon and barium in Eocene sediments: possible controls on nutrient recycling in the Eocene equatorial Pacific Ocean. In Wilson, P.A., Lyle, M., and Firth, J.V. (Eds.), Proc. ODP, Sci. Results,199: College Station, TX (Ocean Drilling Program), 1–33. doi:10.2973/odp.proc.sr.199.222.2005

Olivarez Lyle, A., and M. W. Lyle., 2002. Determination of biogenic opal in pelagic marine sediment: A simple method revisited, Proc. Ocean Drill. Program Sci. Results, 199, 1–21, doi:10.2973/odp.proc.ir.199.106.2002.

Paytan, A., Averyt, K., Faul, K., Gray, E., Thomas, E., 2007. Barite accumulation, ocean productivity, and Sr/Ba in barite across the Paleocene-Eocene Thermal Maximum. Geology, 35(12): 1139-1142.

Paytan, A., Griffith, E.M., 2007. Marine barite: Recorder of variations in ocean export productivity. Deep-Sea Research Part Ii-Topical Studies in Oceanography, 54(5-7): 687-705.

Paytan, A., Kastner, M., Chavez, F.P., 1996. Glacial to interglacial fluctuations in productivity in the equatorial Pacific as indicated by marine barite. Science, 274(5291): 1355-1357.

Pedersen, T.F., 1983. Increased Productivity in the Eastern Equatorial Pacific during the Last Glacial Maximum (19,000 to 14,000 Yr Bp). Geology, 11(1): 16-19.

Pedersen, T.F., Price, N.B., 1980. The Geochemistry of Iodine and Bromine in Sediments of the Panama Basin. Journal of Marine Research, 38(3): 397-411.

Pennington, J.T. et al., 2006. Primary production in the eastern tropical Pacific: A review. Progress in Oceanography, 69(2-4): 285-317.

Petit, J.R. et al., 1999. Climate and atmospheric history of the past 420,000 years from the Vostok ice core, Antarctica. Nature, 399(6735): 429-436.

Piela, C., Lyle, M., Marcantonio, F., Baldauf, J., Lyle, A.O., 2012. Biogenic sedimentation in the equatorial Pacific: Carbon cycling and paleoproduction, 12-24 Ma. Paleoceanography, 27.

Pisias, N.G., Mix, A.C., 1997. Spatial and temporal oceanographic variability of the eastern equatorial Pacific during the late Pleistocene: Evidence from Radiolaria microfossils. Paleoceanography, 12(3): 381-393.

Plank, W.S., Ronald, J., Pak, H., Zaneveld, V., 1973. Distribution of Suspended Matter in Panama Basin. Journal of Geophysical Research, 78(30): 7113-7121.

Pourmand, A., Marcantonio, Schilz, H., 2004. Variation in productivity and eolian fluxes in the northeastern Arabian Sea during the past 110 ka, Earth Planet. Sci. Lett., 221, 39-54.

Ragueneau, O. et al., 2000. A review of the Si cycle in the modem ocean: recent progress and missing gaps in the application of biogenic opal as a paleoproductivity proxy. Global and Planetary Change, 26(4): 317-365.

Reiner Schlitzer, Interactive analysis and visualization of geoscience data with Ocean Data View, Computers & Geosciences, Volume 28, Issue 10, December 2002, Pages 1211-1218.

Rincón-Martínez, D., F. Lamy, S. Contreras, G. Leduc, E. Bard, C. Saukel, T. Blanz, A. Mackensen, R. Tiedemann., 2010. More humid interglacials in Ecuador during the past 500 kyr linked to latitudinal shifts of the equatorial front and the Intertropical Convergence Zone in the eastern tropical Pacific, Paleoceanography, 25, PA2210, doi:10.1029/2009PA001868.

Robinson, L.F., Noble, T.L., McManus, J.F., 2008. Measurement of adsorbed and total (232)Th/(230)Th ratios from marine sediments. Chemical Geology, 252(3-4): 169-179.

Roy-Barman, M. et al., 2005. The influence of particle composition on thorium scavenging in the NE Atlantic ocean (POMME experiment). Earth and Planetary Science Letters, 240(3-4): 681-693.

Roy-Barman, M. et al., 2009. The influence of particle composition on Thorium scavenging in the Mediterranean Sea. Earth and Planetary Science Letters, 286(3-4): 526-534.

Roy-Barman, M., 2009. Modelling the effect of boundary scavenging on Thorium and Protactinium profiles in the ocean. Biogeosciences, 6(12): 3091-3107.

Roy-Barman, M., Coppola, L., Souhaut, M., 2002. Thorium isotopes in the western Mediterranean Sea: an insight into the marine particle dynamics. Earth and Planetary Science Letters, 196(3-4): 161-174.

RoyBarman, M., Chen, J.H., Wasserburg, G.J., 1996. Th-230-Th-232 systematics in the central Pacific Ocean: The sources and the fates of thorium. Earth and Planetary Science Letters, 139(3-4): 351-363.

Ruddiman, W. 1992. Calcium carbonate database. IGBP PAGES/World Data Center for Paleoclimatology Data Contribution Series #92-001. NOAA/NGDC Paleoclimatology Program, Boulder, Colorado, USA.

Ryan, W.B.F., S.M. Carbotte, J.O. Coplan, S. O'Hara, A. Melkonian, R. Arko, R.A. Weissel, V. Ferrini, A. Goodwillie, F. Nitsche, J. Bonczkowski, and R. Zemsky., 2009. Global Multi-Resolution Topography synthesis, Geochem. Geophys. Geosyst., 10, Q03014, doi:10.1029/2008GC002332.

Sarmiento, J.L., Gruber, N., Brzezinski, M.A., Dunne, J.P., 2004. High-latitude controls of thermocline nutrients and low latitude biological productivity. Nature, 427(6969): 56-60.

Schmitz, B., 1987. Barium, Equatorial High Productivity, and the Northward Wandering of the Indian Continent. Paleoceanography, 2(1): 63-77.

Scholten, J.C. et al., 2005. Radionuclide fluxes in the Arabian Sea: the role of particle composition. Earth and Planetary Science Letters, 230(3-4): 319-337.

Shimmield, G.B. et al., 1986. The Distribution and Behavior of Th-230 and Pa-231 at an Ocean Margin, Baja-California, Mexico. Geochimica Et Cosmochimica Acta, 50(11): 2499-2507.

Shimmield, G.B., Price, N.B., 1988a. Marine Scavenging of Th and Pa - Evidence from Mid Ocean Ridge, Continental-Margin and Open Ocean Sediments. Radionuclides : A Tool for Oceanography: 101-110.

Shimmield, G.B., Price, N.B., 1988b. The Scavenging of U, Th-230 and Pa-231 during Pulsed Hydrothermal Activity at 20-Degrees-S, East Pacific Rise. Geochimica Et Cosmochimica Acta, 52(3): 669-677.

Siddall, M., G. M. Henderson, N. R. Edwards, S. A. Muller, T. F. Stocker, F. Joos, and M. Frank., 2005. 231Pa/230Th fractionation by ocean transport, biogenic particle flux and particle type, Earth Planet. Sci. Lett., 237, 135– 155, doi:10.1016/j.epsl.2005.05.031.

Siddall, M., R. F. Anderson, G. Winckler, G. M. Henderson, L. I. Bradtmiller, D. McGee, A. Franzese, T. F. Stocker, and S. A. Muller., 2008. Modeling the particle flux effect on distribution of 230Th in the equatorial Pacific, Paleoceanography, 23, PA2208, doi:10.1029/2007PA001556.

Sigman, D.M., Hain, M.P., Haug, G.H., 2010. The polar ocean and glacial cycles in atmospheric CO_2 concentration. Nature, 466 (7302): 47-55.

Singh, A.K., Marcantonio, F., Lyle, M., 2011. Sediment focusing in the Panama Basin, Eastern Equatorial Pacific Ocean. Earth and Planetary Science Letters, 309(1-2): 33-44.

Snoeckx, H., D. K. Rea., 1994. Dry bulk density and CaCO3 relationships in upper Quaternary sediments of the eastern equatorial Pacific, Mar. Geol., 120, 327– 333.

Suman, D.O., Bacon, M.P., 1989. Variations in Holocene Sedimentation in the North-American Basin Determined from Th-230 Measurements. Deep-Sea Research Part a-Oceanographic Research Papers, 36(6): 869-878.

Takahashi, T. et al., 2002. Global sea-air CO2 flux based on climatological surface ocean pCO(2), and seasonal biological and temperature effects. Deep-Sea Research Part Ii-Topical Studies in Oceanography, 49(9-10): 1601-1622.

Taylor, S. R., and S. M. McClennan., 1985. The Continental Crust: Its Composition and Evolution, 312 pp., Blackwell Sci., Malden, Mass.

Thomas, E., Turekian, K.K., Wei, K.Y., 2000. Productivity control of fine particle transport to equatorial Pacific sediment. Global Biogeochemical Cycles, 14(3): 945-955.

Toggweiler, J.R., Dixon, K., Broecker, W.S., 1991. The Peru Upwelling and the Ventilation of the South-Pacific Thermocline. Journal of Geophysical Research-Oceans, 96(C11): 20467-20497.

Tominaga, M., M. Lyle, and N.C. Mitchell., 2011. Seismic interpretation of pelagic sedimentation regimes in the 18-53 Ma eastern equatorial Pacific: basin-scale sedimentation and infilling of abyssal valleys. Geochem. Geophys. Geosyst., doi:10.1029/2010GC003347.

Treguer, P. et al., 1995. The Silica Balance in the World Ocean - a Reestimate. Science, 268(5209): 375-379.

Trimble, S.M., Baskaran, M., Porcelli, D., 2004. Scavenging of thorium isotopes in the Canada basin of the Arctic Ocean. Earth and Planetary Science Letters, 222(3-4): 915-932.

Tsuchiya, M., Talley, L.D., 1998. A Pacific hydrographic section at 88 degrees W: Water-property distribution. Journal of Geophysical Research-Oceans, 103(C6): 12899-12918.

Van Andel, T.H., 1973. Texture and Dispersal of Sediments in Panama-Basin. Journal of Geology, 81(4): 434-457.

Van der Loeff, M.M.R., Berger, G.W., 1993. Scavenging of Th-230 and Pa-231 near the Antarctic Polar Front in the South-Atlantic. Deep-Sea Research Part I-Oceanographic Research Papers, 40(2): 339-357.

Venchiarutti, C., Jeandel, C., Roy-Barman, M., 2008. Particle dynamics study in the wake of Kerguelen Island using thorium isotopes. Deep-Sea Research Part I-Oceanographic Research Papers, 55(10): 1343-1363.

Venchiarutti, C., van der Loeff, M.R., Stimac, I., 2011. Scavenging of (231)Pa and thorium isotopes based on dissolved and size-fractionated particulate distributions at Drake Passage (ANTXXIV-3). Deep-Sea Research Part Ii-Topical Studies in Oceanography, 58(25-26): 2767-2784.

Vogler, S., Scholten, J., van der Loeff, M.R., Mangini, A., 1998. Th-230 in the eastern North Atlantic: The importance of water mass ventilation in the balance of Th-230. Earth and Planetary Science Letters, 156(1-2): 61-74.

Walsh, I., Fischer, K., Murray, D., Dymond, J., 1988. Evidence for Resuspension of Rebound Particles from near-Bottom Sediment Traps. Deep-Sea Research Part a-Oceanographic Research Papers, 35(1): 59-70.

Winckler, G., Anderson, R.F., Fleisher, M.Q., Mcgee, D., Mahowald, N., 2008. Covariant glacial-interglacial dust fluxes in the equatorial Pacific and Antarctica. Science, 320(5872): 93-96.

Yu, E.F. et al., 2001. Trapping efficiency of bottom-tethered sediment traps estimated from the intercepted fluxes of Th-230 and Pa-231. Deep-Sea Research Part I-Oceanographic Research Papers, 48(3): 865-889.